MAPPING THE TUMOR VASCULOME:
A NOVEL INTERACTIVE 3D VISUALIZATION OF COMPUTATIONALLY DERIVED TUMOR HEMODYNAMICS

by
Laura M. Ekl

A thesis submitted to Johns Hopkins University in conformity with the requirements for the degree of Master of Arts

Baltimore, Maryland
March, 2021

Abstract

Breast cancer is currently the second major cause of death for women in the US (American Cancer Society 2019). New research has highlighted the significance of the tumor ‘vasculome’ in the progression, metastatic potential, and prognosis of breast tumors (Junttila and de Sauvage 2013). The vasculome encompasses an interdependent web of morphological (i.e. diameter, length, microvascular density), functional (i.e., oxygenation, shear stress, flow rate) and other complementary data (e.g., genomic profiles) that characterize a vascular tree. The vasculome shapes the tissue microenvironment, and specifically in cancer, results in the creation of a unique tumor microenvironment (TME). This TME exerts selection pressure on cancer cell populations and profoundly impacts their survival, proliferation, metastatic potential, and response to therapy.

Advances in multiscale imaging and computer modeling have enabled a recent study that characterizes the vasculome in an ensemble of preclinical breast tumors (Stamatelos and Bhargava, et al. 2019). The main objective of this project was to create an interactive web-based platform for 3D visualization of the tumor vasculome, i.e., the morphological and functional parameters generated during the prior study.

PlayCanvas was used to visualize the vasculome data for normal tissue as well as for breast tumor xenografts via an interactive, web-based platform. The 3D visualizations were supplemented by didactic text and illustrations that were created to provide the user with an understanding of the fundamental morphological and hemodynamics concepts addressed. This interactive application enables new insights into the relationships between different vasculome parameters, and how they can shape the TME. This project is a first step towards a novel ‘visual atlas’ that will be used to map the vasculomes of different tumor models and tissue types.

Chairpersons of the Supervisory Committee

Arvind P. Pathak, Ph.D.*, Preceptor*

Associate Professor, Depts. of Radiology, Biomedical and Electrical Engineering

Sidney Kimmel Comprehensive Cancer Center

Institute for NanoBioTechnology

Institute for Computational Medicine

Johns Hopkins University School of Medicine

Lydia Gregg, M.A., C.M.I., F.A.M.I.*, Department Advisor*

Associate Professor & Director of Operations

Department of Art as Applied to Medicine

Jointly appointed in the Department of Radiology and Radiological Science

Johns Hopkins University School of Medicine

Acknowledgments

This project would not have been possible without the immense support given to me by my instructors, classmates, friends, and family.

I express my endless thanks to my faculty advisor, **Lydia Gregg**, for her steadfast guidance and support. In the middle of a pandemic, she was a beacon of intellect, professionalism, and technical expertise.

Boundless gratitude is owed to **Dr. Arvind Pathak**, my thesis preceptor, and **Dr. Akanksha Bhargava**, my primary lab mentor, for answering all of my many questions and allowing me access to their lab resources and immense imaging/bioengineering knowledge.

Endless thanks must be credited to **Russel Adams** from iSO-FORM, LLC for donating his time and knowledge to solving the most complex challenges in this thesis, and being a teacher to me as well.

Thank you to **David Rini**, **Cory Sandone**, **Jennifer Fairman**, **Jeff Day**, **Tim Phelps**, **Juan Garcia**, **Norman Barker**, **Gary Lees**, **Ian Suk**, **Anne Altemus**, **Donald Bliss**, **Mike Linkinhoker**, and **Sarah Poynton**, for imparting the countless lessons and skills necessary to complete this project. I have treasured my time learning from the entire incredible faculty. An enormous thank you to **Dacia Balch** and **Carol Pfeffer** for the endless support you provide to the students in the department.

Thank you to **Joe Holub**, lead programmer at BodyViz, for his continual insight into data visualization and his ability to clearly break down any problem and give logical advice.

Thank you to my classmates, who it seems like just a short time ago were strangers, and are now some of my closest friends: **Emily Slapin Lufkin**, **Emily Wu**, **Emily Cheng**, **Sora Ji**, **Susie Yun**, and **Kurt Esenwein**.

Thank you to my parents, **Randy** and **Maxine**, brother, **Tim**, and sisters, **Emily** and **Catherine**, for your unending love and support from any distance, and to **Jake Wilson** for his golden retriever-esque energy and our many sanity-restoring hikes and climbs.

Finally, thank you to T**he Vesalius Trust for Visual Communication in the Health Sciences** and **National Cancer Institute (NCI)** grants (5R01CA196701-05 and 1 R01CA237597-01A1) for their generous support of this project.

Table of Contents

List of Figures

List of Abbreviations & Symbols

D	Vascular diameter
D_V	Intervessel distance
GUI	Graphical user interface
L	Vascular length
L_V	Vascular length density
µCT	Micro-computed tomography
MRM	Magnetic resonance microscopy
PO_2	Intravascular oxygen tension
Q	Blood flow rate
RBC	Red blood cell, erythrocyte
S_V	Vascular surface area density
τ	Fluid shear stress
TME	Tumor microenvironment
Vel	Blood velocity

Introduction

Cancer is the second-leading cause of death in the United States (Kumar, Abbas, and Aster 2018). In 2019, breast cancer was the most commonly diagnosed new cancer in women, with over 250,000 new cases (American Cancer Society 2019). It was first suggested that tumor growth is driven by angiogenesis, the creation of new blood vessels, by Folkman in his seminal 1971 paper (Folkman 1971), where he also posited that targeting the neo-vascularization of tumors, i.e., anti-angiogenic therapies, could be effective in arresting tumor growth. In the decades since, there have been major advances in the understanding of molecular mechanisms regulating tumor angiogenesis (Folkman 2007, Semenza 2010). Twelve drugs are currently approved for anti-angiogenic therapies and more are in clinical trials (Jain, Martin, and Chaunhan, et al. 2020) for an array of diseases. Therefore, an understanding of the form and function of tumor microvasculature is critical for developing new cancer treatments that target vascular growth as well as for understanding its role in cancer.

The microvasculature of the tumor has a direct effect on proliferating tumor cells. Evolving subpopulations of genetic distinct cells are known to exist within tumors (Bedard, et al. 2013, Gerlinger, et al. 2012, Anderson, et al. 2006). These distinct clonal cell populations and the associated irregular vasculature create unique tumor microenvironments (TME), which represents a complex and heterogenous landscape in terms of the distribution of oxygen, nutrients, and therapies (Junttila and de Sauvage 2013).

It is critical to develop new tools to map and visualize the spatially and temporally heterogenous TME. Recent advances in multi-scale imaging, i.e., complementary imaging at multiple spatial scales, and computational modeling, have resulted in the morphological characteristics and hemodynamics being modeled and assessed for an entire ensemble of breast tumor xenografts for the first time (Stamatelos and Bhargava, et al. 2019). The present project leverages the data from the 2019 study ‘Tumor Ensemble-Based Modeling and Visualization of Emergent Angiogenic Heterogeneity in Breast Cancer’ (Stamatelos and Bhargava, et al. 2019). This study examined the spatio-temporal heterogeneity in the vascular morphology, emergent hemodynamics, and intravascular oxygenation in a set of eight orthotopic breast tumor xenografts (i.e., a tumor ‘ensemble’) at a high spatial resolution. This study advanced previous research by examining an ensemble of whole-tumors at different stages (21 or 35 days post-inoculation).

Studying an ensemble of tumors enabled the measurement and analysis of inter- and intra-tumor heterogeneity.

The study generated high-fidelity, whole-tumor data for an ensemble of tumors derived from 3D multimodality imaging data (μCT and MRI). These datasets were used to measure and visualize the morphology of the vasculature and simulate oxygen heterogeneity in whole tumor microvascular networks **(Fig. 1)**. This analysis showed larger dispersion of tumor hemodynamic indices than indices of normal microvascular morphology, demonstrating that emergent whole-tumor hemodynamics were more heterogenous than would be expected or predicted from

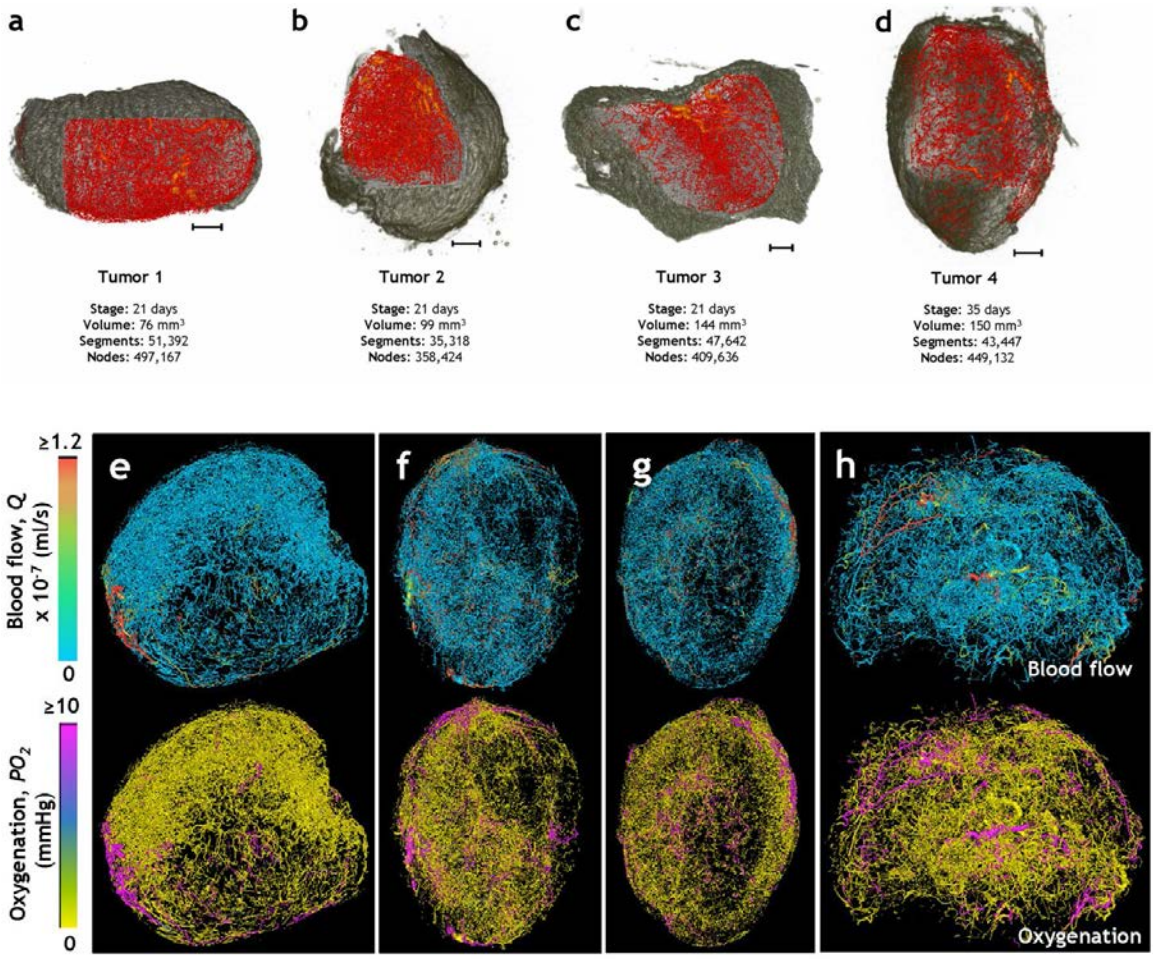

Figure 1. Images adapted with permission from Stamatelos and Bhargava, et. al 2019. Top row: an ensemble of four tumors with the MRI-derived soft tissue and CT-derived blood vessels color coded by vessel diameter. Bottom row: an ensemble of four other tumors with blood vessels color colored by their average blood flow rate (ml/s) (blue) and average intravascular oxygen tension (mm Hg) (gold). *Text not intended to be read.*

underlying variations in microvascular morphology.

The study provided a compelling look at intra-tumor heterogeneity and the establishment of unique microvascular ‘niches’ within each tumor xenograft. They demonstrated that ensemble-based multiparametric data could classify the emergent “angiogenic landscape” better than either morphological or hemodynamic parameters alone.

More broadly, this study provided the foundation of a novel ‘cancer atlas’ and a hybrid image-based framework for investigators to examine other tissues and diseases.

The microcirculation in healthy tissues

The microcirculation (synonymous with microvasculature) in humans comprises the smallest vessels of the circulatory system, i.e., blood vessels with a diameter of less than 100 μm such as the arterioles, capillaries, and venules, as well as associated micro-lymphatic vessels (Costanzo 2018, Jackson 2010). This project focuses on blood and blood vessels and leaves lymphatic vessels for future study.

As descsribed by Jackson, the microcirculation is the “business end” of the circulatory system, responsible for many of the critical functions of the larger cardiovascular system: solute exchange; delivery and extravasation of immune cells; regulation of peripheral vascular resistance, vascular capacitance, and blood pressure; and allocation of blood in response to metabolic demand (Jackson 2010, Costanzo 2018).

In normal, healthy tissues, the vessels of the microcirculation are well-differentiated and form an organized architecture with dichotomous branching. Fractal analysis has demonstrated that healthy microcirculation blood vessels are optimally designed to provide nutrients via diffusion to all supplied cells (Fukumura, Duda, and Munn 2010).

Arterioles

Arterioles are the smallest arteries, with diameters ranging from 20-100 μm (Kumar, Abbas and Aster 2018). Arterioles continue the three-layer organization found in larger vessels, with an external connective tissue adventitia, an intermedia media heavily invested with smooth muscle cells, and internal intima of connective tissue and endothelial cells. First-order arterioles branch to form second-order arterioles, which continue to branch until a terminal arteriole is given off from which capillaries are supplied. First-order arterioles have smooth muscle arranged in two layers, and all subsequent arterioles have one layer of smooth muscle cells (Jackson 2010).

Small arterioles are the site of greatest vascular resistance in the circulatory system, and where the amount of blood entering capillary beds is regulated (Costanzo 2018, Kumar, Abbas and Aster 2018). Descriptions of precapillary sphincters that play a key role in regulation of blood flow to capillary beds have been found exclusively in the mesenteric circulation (Sakai and Hosoyamada 2013). Proportionally, arterioles have a higher smooth muscle-to-lumen ratio than larger muscular arteries, reflecting their function in creating vascular resistance (Lowrie Jr. 2020). The smooth muscle cells in arterioles are tonically active and extensively innervated by sympathetic fibers, allowing for precise control of vascular resistance and flow (Costanzo 2018, Kumar, Abbas and Aster 2018). As a result, blood flow becomes smooth instead of pulsatile within the arterioles (Kumar, Abbas and Aster 2018). Arterioles are also permeable to oxygen and carbon dioxide dissolved in the blood and contribute to gas exchange in tissues (Jackson 2010).

Capillaries

A terminal arteriole gives rise to 1-20 capillaries (Jackson 2010). Capillaries are the smallest and most numerous vessels in the circulatory system. The primary function of these tiny vessels is to exchange fluid, nutrients, dissolved gases, hormones, immune cells, and waste products between the blood and extravascular compartment. The morphology of capillaries is highly specialized to facilitate rapid solute exchange.

Capillaries are slightly smaller than a red blood cell (5-8 μm) and can be a few hundred microns to 1000 μm in length (Pries and Secomb 2003, Costanzo 2018, Kumar, Abbas and Aster 2018, Jackson 2010). They lack the typical three-lamina structure of larger blood vessels and are composed of a single continuous layer of endothelial cells usually surrounded by a complete basal lamina.

Capillaries are supported by pericytes, which are contractile smooth muscle-like cells. Unlike the smooth muscle cells, however, pericytes do not form a complete layer around capillaries (Kumar, Abbas and Aster 2018, Lowrie Jr. 2020, Jackson 2010). Also, unlike smooth muscle cells in larger vessels, the pericytes of capillaries are enclosed by the endothelial cell basement membrane. Pericytes participate in angiogenesis and vascular remodeling, help regulate vascular permeability, and control local vascular resistance (Jackson 2010).

In capillaries, RBCs flow single-file and at their slowest velocity in the circulatory system, allowing more time for exchange. They are deformed into a parachute or jellyfish-like shape by

fluid and shear stresses within the capillary (Jeong, et al. 2006, Chien 1987). This deformation increases the surface area of the RBC, which is thought to facilitate gas transport (Jeong, et al. 2006).

Based on their ultrastructure and permeability, capillaries can be classified into three types, continuous, fenestrated, and discontinuous (i.e., sinusoidal), where continuous capillaries are the least permeable and discontinuous capillaries are the most permeable (Kumar, Abbas and Aster 2018). For the purposes of this thesis, 'normal capillaries' will refer to continuous capillaries (i.e., those with a continuous sheath of endothelial cells surrounded by a complete basement membrane). Continuous capillaries are the most common type of capillary and are found in skeletal muscle, the skin, and the nervous system.

Capillaries are the primary site of gas, nutrient, metabolic waste, heat, hormone, and fluid exchange. While capillaries have the smallest individual diameters of any vessel, as a group, they have the largest vessel surface area, corresponding to their main function of solute exchange (Costanzo 2018, Lowrie Jr. 2020). Blood flow rate is lowest in the capillaries, allowing time for solute diffusion to occur (Kumar, Abbas and Aster 2018). Gases dissolved in the blood such as O2 and CO2 are able to diffuse directly across the endothelial cell membranes. Transport of substances like water, ions, glucose, and amino acids occurs through junctions between endothelial cells or through large clefts in fenestrated capillaries. Large molecules like proteins are transported across capillary walls via endocytosis (Costanzo 2018). Finally, hydrostatic and osmotic pressure gradients influence plasma and interstitial fluid transport in and out of capillaries.

Although the structure and organization of capillary beds varies greatly depending on the tissue supplied, capillary beds are highly regulated and organized (Corliss, et al. 2019). **In healthy tissue, all cells are located within the diffusion distance of oxygen: ~100-200 µm.** Often when cells experience hypoxia due to poor perfusion- or diffusion-limited oxygen transport, they can secrete cytokines that trigger angiogenesis to provide a new blood supply. This is a phenomenon frequently observed in solid tumors (Folkman 1971, Jain 1988).

Not all capillaries are completely perfused with blood at all times. Blood is preferentially directed to capillary beds where metabolic demand is high (e.g., the stomach after eating, or

skeletal muscle during exercise) by upstream arteries and arterioles (Costazo 2018).

Venules

Capillaries eventually merge to form post-capillary venules, which then drain into collecting venules, muscular venules with 1-2 complete layers of smooth muscle cells, and small veins. Post-capillary venules have a slightly larger diameter (X-Y μm) than capillaries, and while they are similarly devoid of smooth muscle, they are covered in a nearly complete layer of pericytes (Jackson 2010, Costanzo 2018). These vessels have the weakest inter-endothelial junctions of all vessel types and are the primary site of immune cell adhesion and migration (Kumar, Abbas and Aster 2018, R. K. Jain 1988). Water and dissolved solutes continue to be exchanged in the post-capillary and collecting venules (Jackson 2010).The presence of one or two layers of smooth muscle cells indicates a higher-order venule (Jackson 2010).

Venules usually run in parallel with corresponding arterioles, allowing exchange of gases and vasoactive substances (Jackson 2010).

Venules and veins contain less elastic tissue than arteries of corresponding order, which contributes to their large vascular capacitance (Costanzo 2018, Kumar, Abbas and Aster 2018). In fact, the majority of blood in the cardiovascular system (about two-thirds of all blood) is contained in the venules and small veins (Costanzo 2018).

As the cardiovascular system is driven by a pressure gradient, venules and veins have the lowest blood pressure. Veins are also more prone to external compression and penetration by tumors because of their thinner walls (Kumar, Abbas, and Aster 2018).

Tumor microcirculation

Neovascularization

Tumors form new vessels through a variety of mechanisms ranging from vasculogenesis, to angiogenesis, and host vessel co-option (Jain et. al., 2020). The formation of new blood vessels is necessary for tumors to grow larger than a volume of 1-2 mm^3 (i.e., the diffusion limit of oxygen and nutrients that supply the tumor tissues) (Folkman 1971). Tumors are not immediately angiogenic, instead, an angiogenic switch, is turned from off to on (Carmeliet and Jain 2000, Hanahan and Weinberg 2011, Bouck, Stellmach and Hsu 1996). Angiogenesis then occurs pathologically and tumors can increase in size. Pathologic angiogenesis is classified as one of the ten “Hallmarks of Cancer” (Hanahan and Weinberg 2011).

A tumor's ability to vascularize directly affects its own survival and growth, as well as its ability to metastasize. The new vascular bed in tumors also provides a route for immune cells and the delivery of therapeutic agents (Corliss, et al. 2019, Kumar, Abbas, and Aster 2018, Carmeliet and Jain 2000). So, it is critical to study angiogenesis and identify areas of neovascularization and high microvessel density count in patients (Folkman 1971).

Morphology of the tumor microcirculation

Tumor vessels are typically immature and leaky, with abnormally large gaps between endothelial cells, more trans-endothelial channels, abnormal pericyte coverage, and discontinuous basement membranes (Hashizume, et al. 2000, Corliss, et al. 2019, Jain, Martin and Stylianopoulos 2014, Gould and Linninger 2015). Tumor vessels display irregular and larger-than-normal intervessel distances (Baish, et al. 2011).

Tumor microcirculations are known to contain arterio-venous shunts, where capillary beds are bypassed by vessels with large diameters and high flows (R. K. Jain 1988).

Abnormal tumor vessel geometry (e.g., tortuosity, branching patterns) increases the geometric resistance to blood flow. Plasma leaking out of vessels between immature endothelial cells increases hematocrit and blood viscosity, increasing viscous resistance. These increased geometric and viscous resistances cause blood flow and velocity to be heterogenous and lower than that in comparable vessels (R. K. Jain 1988, Jain, Martin and Chaunhan, et al. 2020, Sevick and Jain 1989a, Sevick and Jain 1989b).

Blood flow is further disrupted by abnormal plasma skimming effects, or the proportional separation of plasma and RBCs at vascular branch points (Gould and Linninger 2015). Normal vessels display a proportional separation of RBCs into daughter branches based on the relative size of each daughter vessel (Gould and Linninger 2015). In tumor vessels, there is irregular separation of hematocrit into daughter branches (Jain 1988).

Increased mechanical pressure, both from dividing tumor cells and increased interstitial pressure from fluid leakage, can intermittently collapse blood and lymphatic vessels, cutting off tumor tissues from oxygen and limiting waste clearance. Angiogenesis may not be able to keep up or be organized enough to sustain all parts of a tumor. Necrosis can occur if cells are located at distances greater than the diffusion distance of oxygen (~160 μm from the nearest vessel)

(Thomlinson and Gray, 1955). Hypoxic areas exist heterogeneously in the majority of human solid cancers (Fakhrejahani and Toi 2012). These areas pose a unique challenge to treatment.

Effects of the tumor microcirculation on cancer therapies

The spatial and temporal heterogeneity innate to tumor microvasculature disrupts delivery and decreases efficacy of cancer therapeutics. Inadequate vascularization or transient perfusion of tumor tissues by irregular microvasculature prevents or hinders delivery of cytotoxic agents to tumor cells at their effective concentrations. Cancer cells in hypoxic TMEs show a decrease in proliferation, rendering chemotherapy, which targets proliferating cells, less effective. Hypoxic areas in tumors also have almost no oxygen available to be converted into damaging free radicals by conventional radiation therapies (Jain 2020).

Antiangiogenic treatments and anti-vascular therapies target the blood vessels in the tumor, aiming to starve the tumor by disrupting their vasculature. This presents a paradox, as tumor vessels are progressively destroyed, the delivery of complementary therapies (e.g., chemo- or radiation-therapy) are disrupted for the previously described reasons. Despite these challenges, a range of recently approved antiangiogenic therapies have been employed for treating a variety of cancers (Jain et al 2020).

'Normalization' of the tumor vessels is a relatively new idea in cancer therapy, that involves therapeutic-induced maturing of tumor blood vessels, reduction in vessel tortuosity, and pruning of extraneous vessels, resulting in the enhanced delivery of cancer therapies (R. K. Jain 2005, R. K. Jain 2001).

Tumor microenvironment & clonal selection

Genetically unique subpopulations of cells exist within tumors (Bedard, et al. 2013, Gerlinger, et al. 2012). These cell subpopulations proliferate in an unconstrained manner, compete for resources, and accumulate mutations in alignment with Darwinian selection (Norwell 1976). Abnormal tumor microvasculature and hemodynamics puts selection pressure on tumor cells for more aggressive and metastatic cancer cells, with greater drug resistance (Norwell 1976). Research has investigated the selection pressures for nutrients/space (Fearon and Vogelstein, 1990), and for invasion/metastasis (Liotta/Kohn, 2003), although the exact mechanism of

selection is still being debated (Anderson et al 2006; Ramaswamy et al., 2003).

Hemodynamics

Hemodynamics is the study of the specialized fluid dynamics that apply to blood flow in the circulatory system, based on the concepts of pressure, resistance, flow, and capacitance (Costanzo 2018, Badeer 2001). Blood flow through the circulatory system deviates from the assumptions made in Poiseuille's equation for fluid flow in a tube that require the fluid to be Newtonian, tubes to be rigid, and flow to be constant, and so cannot be described by conventional hydrodynamics. Hemodynamics is closely related to the field of hemorheology, which is the study of the flow and deformation properties of blood and its formed elements, and describes characteristics like blood viscosity, red blood cell aggregation and deformability, and fluid shear forces (Baskurt and Meiselman 2003). While there are several concepts discussed in this project that might be considered hemorheology, for the purposes of this project, all of the simulated parameters will be referred to as 'hemodynamic' parameters.

Studying the abnormal hemodynamics found in tumors is a powerful tool for elucidating the inner workings of tumors and can provide invaluable insight into the delivery of therapeutics, cancer progression, and metastatic potential.

Overview of relevant hemodynamic concepts

The hemodynamic concepts covered in this project are described below. The features of microcirculation are broadly organized into morphological parameters, which describe the geometry of blood vessels, and functional parameters, which describe the physiology of blood vessels. Taken together, these parameters make up the 'vasculome' of the tissue being studied.

- **Morphological Parameters**
    - **Vascular length (L)**: the sum of the length of the line segments that make up a vessel or segment. A vessel is bounded where it joins another vessel or gives off a branch. The unit for vascular length is μm.
    - **Vascular diameter (D)**: the average diameter of a vessel in μm. In tumor vessels, the diameter can vary along the length of the vessel, necessitating an average diameter be calculated.
    - **Intervessel distance (D_V)**: the distance in μm, between any point in the tissue to the nearest blood vessel. This is an indirect measure of oxygen and nutrient diffusion

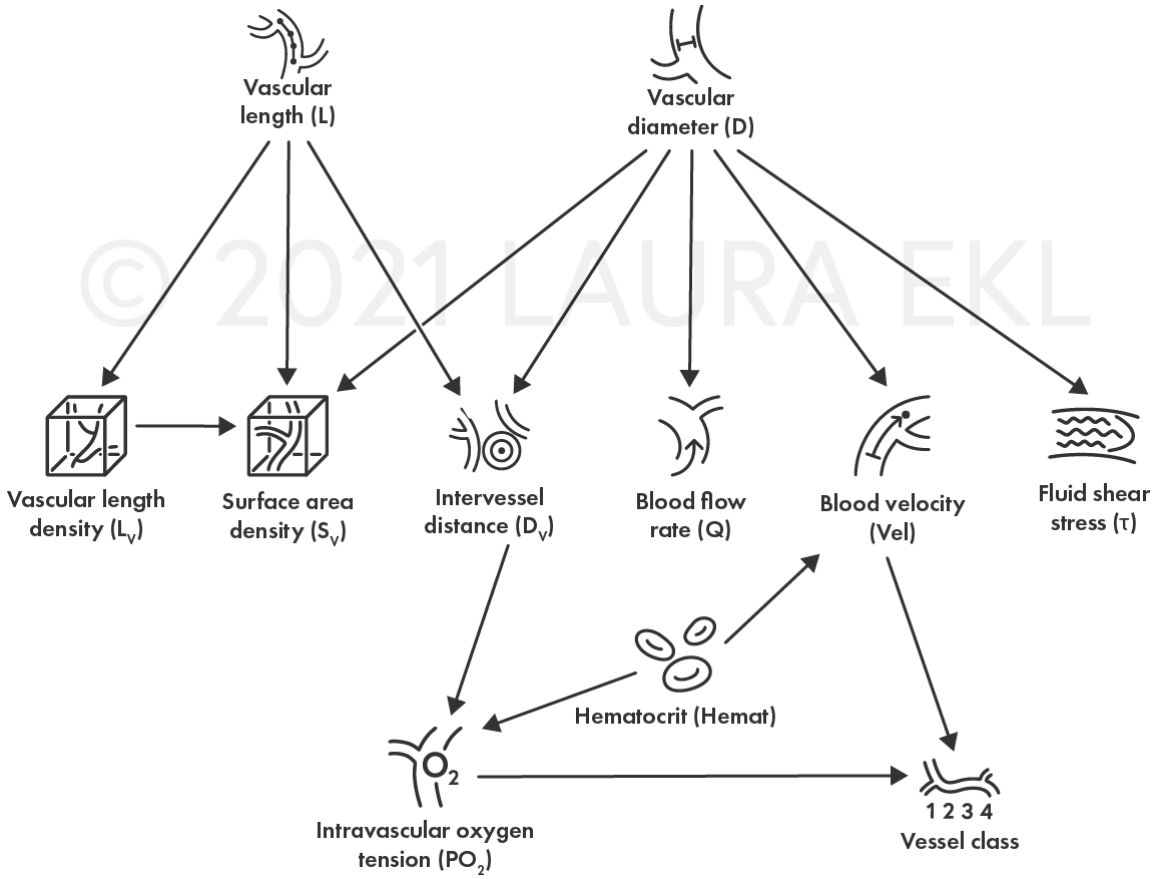

Figure 2. Vasculome definition diagram. Inter-relationships and dependencies between the morphological and functional parameters that the constitute the vasculome.

distance and a rough estimate of vascular density.

- **Vascular length density (L_V)**: the average length of the vessels within a unit volume of tissue. The units for L_V are mm/mm^3. Length density is an estimate of vascular density.
- **Vascular surface area density (S_V)**: the average surface area of the vessels within a unit volume of tissue, the units for which are mm^2/mm^3. Surface area density is an estimate of vascular density, and more accurate than L_V because it accounts for the vessel caliber.

- **Functional parameters**
  - **Blood flow rate (Q)**: the volume of blood flowing past a specific point per second, the units for which are ml/s.
  - **Blood flow velocity (Vel)**: the linear speed of blood flow, i.e., the distance that blood travels per second, the units for which are in mm/s.

- **Intravascular oxygen tension (PO_2)**: a measure of the partial pressure of oxygen within the blood vessels, the units for which are mm Hg.
- **Hematocrit (Hemat):** the fractional volume of RBCs in a volume of blood, expressed as a percentage.
- **Fluid shear stress (τ):** the frictional force that results from adjacent fluid layers moving at different speeds, the units for which are dyne/cm^2.
- **Vessel class:** a vessel classification (1-4) assigned based on the intravascular PO_2, velocity, and diameter of the blood vessel. Each vessel class describes the overall functionality of the blood vessel (ranging from being able to deliver O_2, to not being able to deliver O_2, or being a vascular shunt) (Stamatelos and Bhargava, et al. 2019).

These parameters are collectively quantified to describe the vasculome in tumors, and are tightly interrelated by the equations and mathematical relationships that underpin them **(Fig. 2)**.

Tumor visualization platform currently available

The Human Tumor Atlas Network (https://humantumoratlas.org/) is a project supported by the National Cancer Institute (NCI) that aims to map the cellular components of multiple cancer types at different stages of progression (e.g. pre-cancerous, treatment resistant etc.) (Rozenblatt-Rosen 2020). It is supported by institutions and organizations that aim to collect data describing tumors. However, this is primarily geared towards cancer genomics and global statistics and does not touch on the vascular components of solid tumors.

Didactic considerations

Teaching hemodynamics

An understanding of foundational hemodynamic concepts is imperative to learning about the function of the normal circulation and tumor physiology. Therefore, hemodynamics is a fundamental class for undergraduate and graduate students in nursing and medicine, mechanical, materials, and biomedical engineering, and medical biophysics. Teaching hemodynamics presents unique challenges due to the interdisciplinary nature of the topic (Dunsworth, Murphy, and Wu 2020). Students may not be familiar with the aspects of the cardiovascular system that deviate from Poiseuille‘s assumptions – i.e., pulsatile flow from a heartbeat, soft pipes as the vessels, and branching structure of vessels (Dunsworth, Murphy, and Wu 2020). A limited number of interactive teaching platforms for hemodynamics have been developed, but these

are primarily geared at teaching hemodynamics in terms of critical care (Hessinger, et al. 2008, Dunsworth, Murphy and Wu 2020). Therefore, there is a need for new educational tools that cover hemodynamics in terms of the tumor microcirculation.

Applied theories

Learning theories of instructional design provide a framework describing the most effective practices to educate a learner about a complex topic. Several learning theories were considered when designing this project:

- **Sweller's Cognitive Load Theory** – advocates reducing learners cognitive load by avoiding split-attention and redundancy (Sweller 1988, Sweller, Ayres, and Kalyuga 2011).
- **Reigeluth's Elaboration Theory** – presenting instruction in order of increasing complexity for optimal learning (Reigeluth and Stein 1983, Reigeluth 1979, Reigeluth 1992).
- **Cognitive Theory of Multimedia Learning** – a set of principles describing effective strategies for designing optimal learning experiences (Clark and Mayer 2016).

Thesis Objectives

The goal of this thesis was to create an interactive, web-based 3D visualization of measured and simulated tumor vasculome data in order to provide a comprehensive overview of the heterogenous tumor microvasculature by completing the following objectives:

- Create a reproducible workflow that leverages multiscale imaging data and simulated hemodynamics to develop virtual 3D models corresponding to the tumor vasculome.
- Visualize the following morphologic and hemodynamic components of the vasculomes in 3D space: blood vessel diameter and length, intervessel distance, vascular length density, vascular surface area density, blood flow rate, flow velocity, hematocrit, vessel shear stress, intravascular oxygen tension, and vessel class.
- Communicate the fundamental definitions of hemodynamic parameters within the context of metastasis, cancer progression, and treatment resistance with didactic text and animations.
- Utilize best practices for web accessibility, usability, and data dissemination to allow researchers to interact with the vasculomes via an interactive online application. The web-based interface will allow researchers to display tumors in 3D space, overlay variables of interest, rotate, pan, and zoom into each tumor. The site will integrate didactic content to highlight TME features of interest, such as hypoxic areas indicating treatment resistance as

well as describe key concepts in tumor hemodynamics.

Audience

The primary audience of this project is cancer researchers who are studying tumor heterogeneity. Secondary audiences include graduate and undergraduate students and biomedical trainees that are learning hemodynamic concepts and cancer biology fundamentals, as well as those who can use this didactic resource to teach such topics.

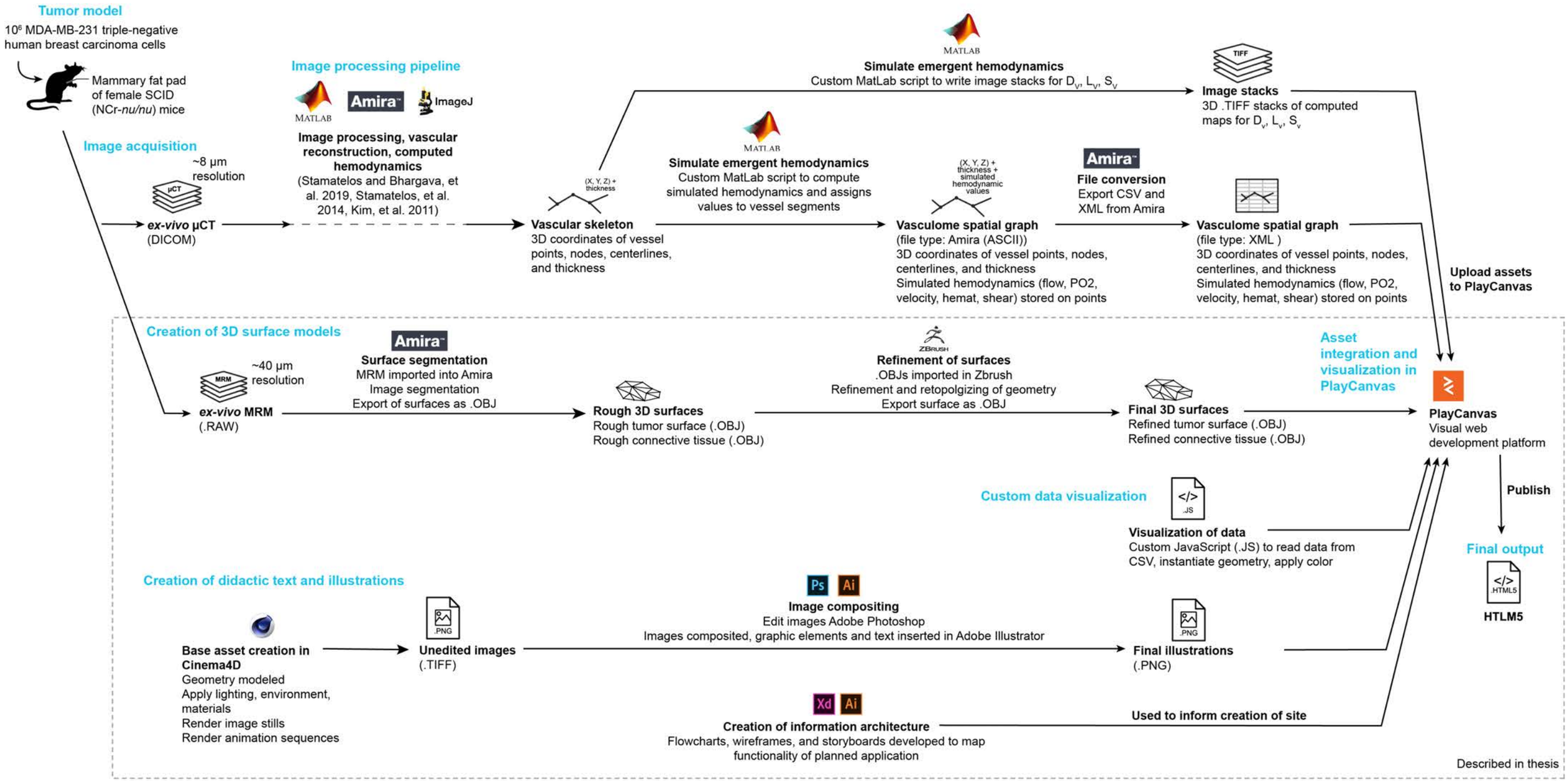

Figure 3. Workflow overview. Overview of software and data types employed from the experimental model and project.

Materials & Methods

An overview of the data types and software used in this project is provided in **Fig. 3**.

Review of Literature

Research and conversations with members of the Pathak Lab yielded a comprehensive document including the name, symbol, unit, definition, significance, formula, and references for each of the didactic sections **(Appendix A)**. The definitions and formulas informed the creation of the sketches and illustrations that accompanied the text. Two novel formulas were written for vessel length and vessel diameter.

Sources and types of data

Multiscale imaging datasets were acquired using magnetic resonance microscopy (MRM) and micro-computed tomography (μCT) from eight breast tumor xenografts and processed as described in Stamatelos and Bhargava, et al. 2019. The image-based microvascular morphology derived from the μCT data was processed in Amira and Matlab to construct a mathematical 'spatial graph' describing the blood vessel network as 3D points connected by line segments, with parameters associated at each point. 3D image stacks were also generated in Matlab to describe three of the morphological parameters. All datasets were provided by the thesis preceptor, Dr. Arvind Pathak.

Imaging data

The ex-vivo MRM of the soft tissues (~40 μm resolution) was shared as a RAW file with dimensions 395x467x337 pixels **(Fig. 4)**. This dataset was later used to derive the surfaces of the surrounding tissue and compute the tumor volume.

Vasculome spatial graph

The bulk of the vasculome data, including most morphological and functional parameters, was stored as an Amira spatial graph data type. A graph refers to a set of lines in 3D space connecting points. Nodes are the points that define the start or end of a vessel segment, where the vessel segment branches or joins another vessel. A segment refers to a complete blood vessel, which is composed of one or more lines **(Fig. 5)**.

A spatial graph can store multiple values at each point (i.e. can store the values for several parameters at one Cartesian coordinate), and can also store several graphs that may work together to define geometry. In this case, three graphs (describing nodes, segments, and points)

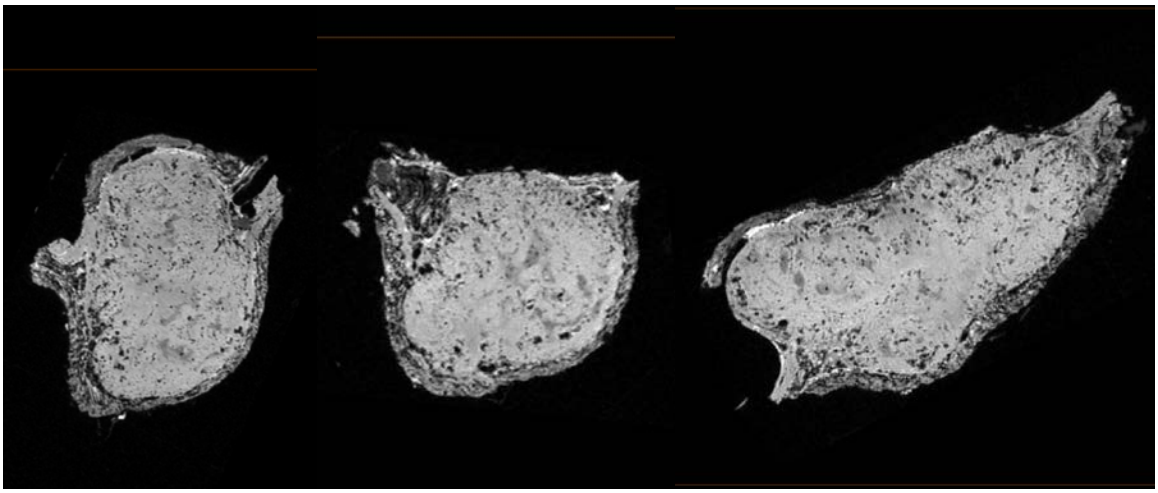

Figure 4. Soft tissue data from a breast tumor xenograft acquired using MRM. Orthogonal views visualized in Amira. Left to right: xy, xy, yz planes.

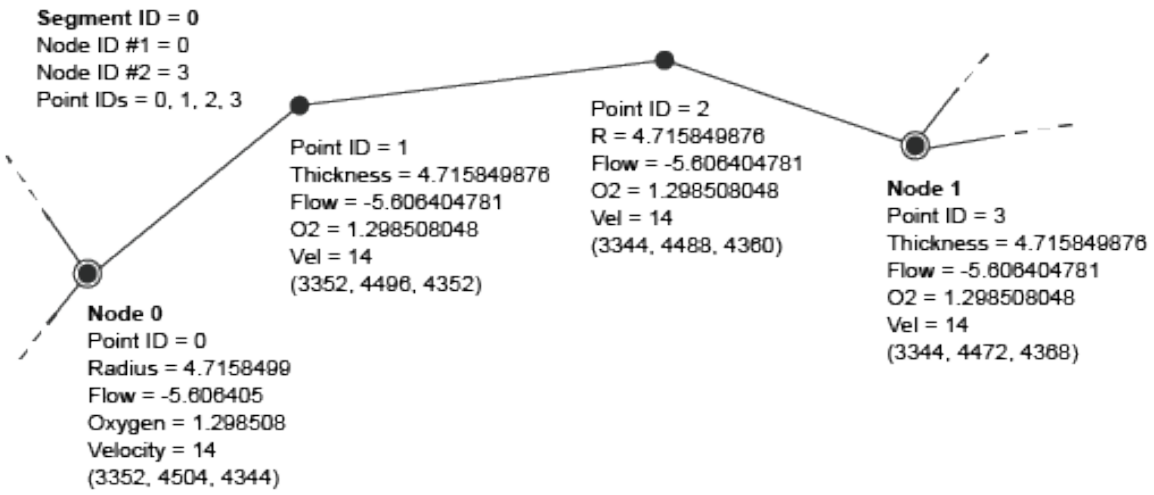

Figure 5. Representation of the blood vessel geometry as a spatial graph. Schematic representation of a single blood vessel as stored in the spatial graph format (data corresponds to the tumor xenograft shown in **Fig. 6**. This vessel corresponds to lines 2-5 on the middle image (Points sheet). Node 0 is the same as Point 0, and Node 1 is the same as Point 3.

	Node ID	X Coord	Y Coord	Z Coord	Coordination Number
2	0	3352	4504	4344	1
3	1	3344	4472	4368	1
4	2	3352	4504	4344	1
5	3	3392	4552	4384	1
6	4	3360	4520	4328	1
7	5	3352	4504	4344	1
8	6	3344	4472	4368	1
9	7	3312	4408	4360	1
10	8	3400	4576	4376	1

Nodes | Points | Segments | +

Figure 6.1. Vasculome spatial graph spreadsheet. The overall structure of the tumor vessels and their associated morphological (radius) and functional (flow, oxygenation, velocity) parameters are described. Nodes sheet, listing a Node ID and the associated Cartesian coordinate of that node. A node is a boundary point of the blood vessel.

	Point ID	Radius	Flow	Oxygenation	Velocity	X Coord	Y Coord	Z Coord
2	0	4.71584988	-5.6064048	1.29850805	14	3352	4504	4344
3	1	4.71584988	-5.6064048	1.29850805	14	3352	4496	4352
4	2	4.71584988	-5.6064048	1.29850805	14	3344	4488	4360
5	3	4.71584988	-5.6064048	1.29850805	14	3344	4472	4368
6	4	7.07427979	-6.151794	1.29877603	4.4842658	3352	4504	4344
7	5	7.07427979	-6.151794	1.29877603	4.4842658	3376	4504	4352
8	6	7.07427979	-6.151794	1.29877603	4.4842658	3384	4504	4352
9	7	7.07427979	-6.151794	1.29877603	4.4842658	3392	4496	4360
10	8	7.07427979	-6.151794	1.29877603	4.4842658	3400	4496	4360

Nodes | Points | Segments | +

Figure 6.2. Vasculome spatial graph spreadsheet. Points sheet, giving a Point ID, and the associated radius, flow, oxygenation, and velocity values, and listing the Cartesian coordinate.

	Segment ID	Node ID #1	Node ID #2	Point IDs
2	0	0	1	0,1,2,3
3	1	2	3	4,5,6,7,8,9,10,11,12,13,14,15,16,17,18,19,20,21,22,23,24,25,26,27,28
4	2	4	5	29,30,31
5	3	6	7	32,33,34,35,36,37,38,39
6	4	8	9	40,41,42,43,44
7	5	10	11	45,46,47,48,49,50,51,52,53,54,55
8	6	12	13	56,57,58,59,60,61,62,63
9	7	14	15	64,65,66,67
10	8	16	17	68,69,70,71,72,73,74,75

Nodes | Points | Segments | +

Figure 6.3. Vasculome spatial graph spreadsheet. Segments sheet, listing a Segment ID, the start node (Node ID #1) and end node (Node ID #2), and the points that are included in each segment. A segment is a complete blood vessel as bounded by two Nodes, and it can be made up of multiple connected points.

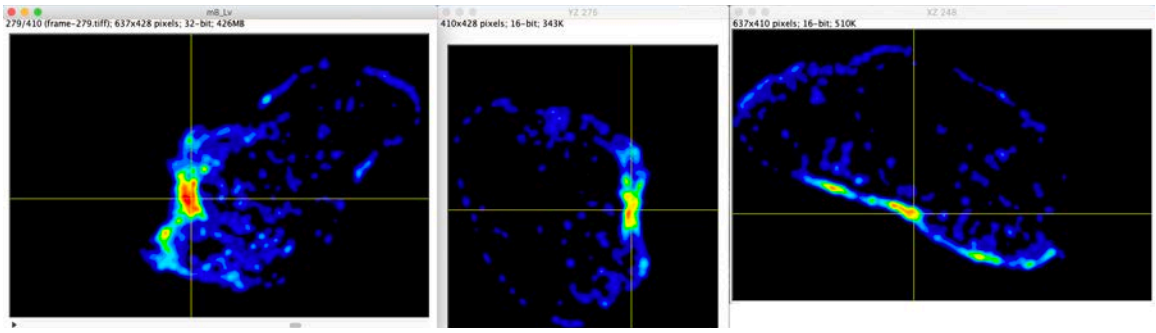

Figure 7. Vascular length density. The 3D .tiff stack containing representative (i.e. from sample #m8). L_V data visualized in orthogonal views in ImageJ. A standard 16-color look up table has been applied. *Text not intended to be read.*

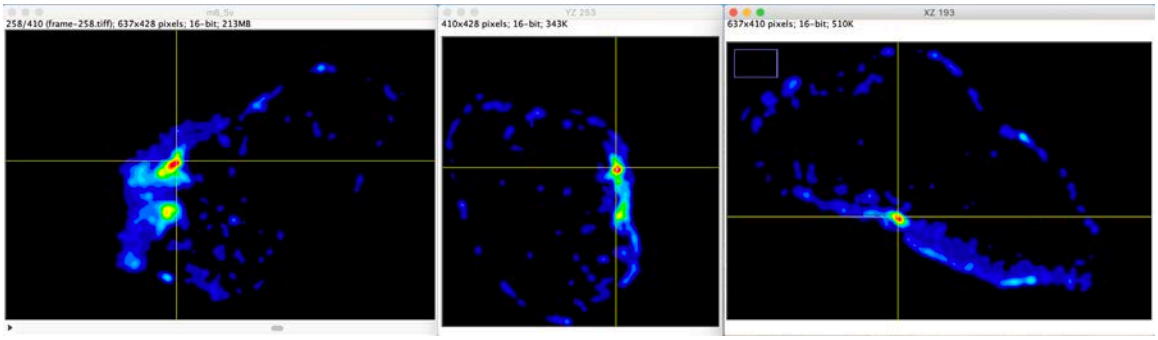

Figure 8. Vascular surface area density. The 3D .tiff stack containing representative (i.e. from sample #m8) S_V data visualized in orthogonal views in ImageJ. A standard 16-color look up table has been applied. *Text not intended to be read.*

were used to describe the vasculome **(Figs. 6.1-6.3)**.

Computed morphological data in 3D .tiff stacks

Three of the morphological parameters (intervessel distance, D_V; vascular length density L_V; and surface area density, S_V) could not be stored at specific points and nodes because by nature these measures apply to the tissue volume as a whole and are reflections of broader TME conditions. Vascular length density (L_V) **(Fig. 7)** and surface area density (S_V) **(Fig. 8)** were shared as 3D .tiff stacks, each at a resolution of 637x428x410 pixels. (Intervessel distance was not shared as part of this project.) These stacks were used in the wireframing process to describe a future feature of the site.

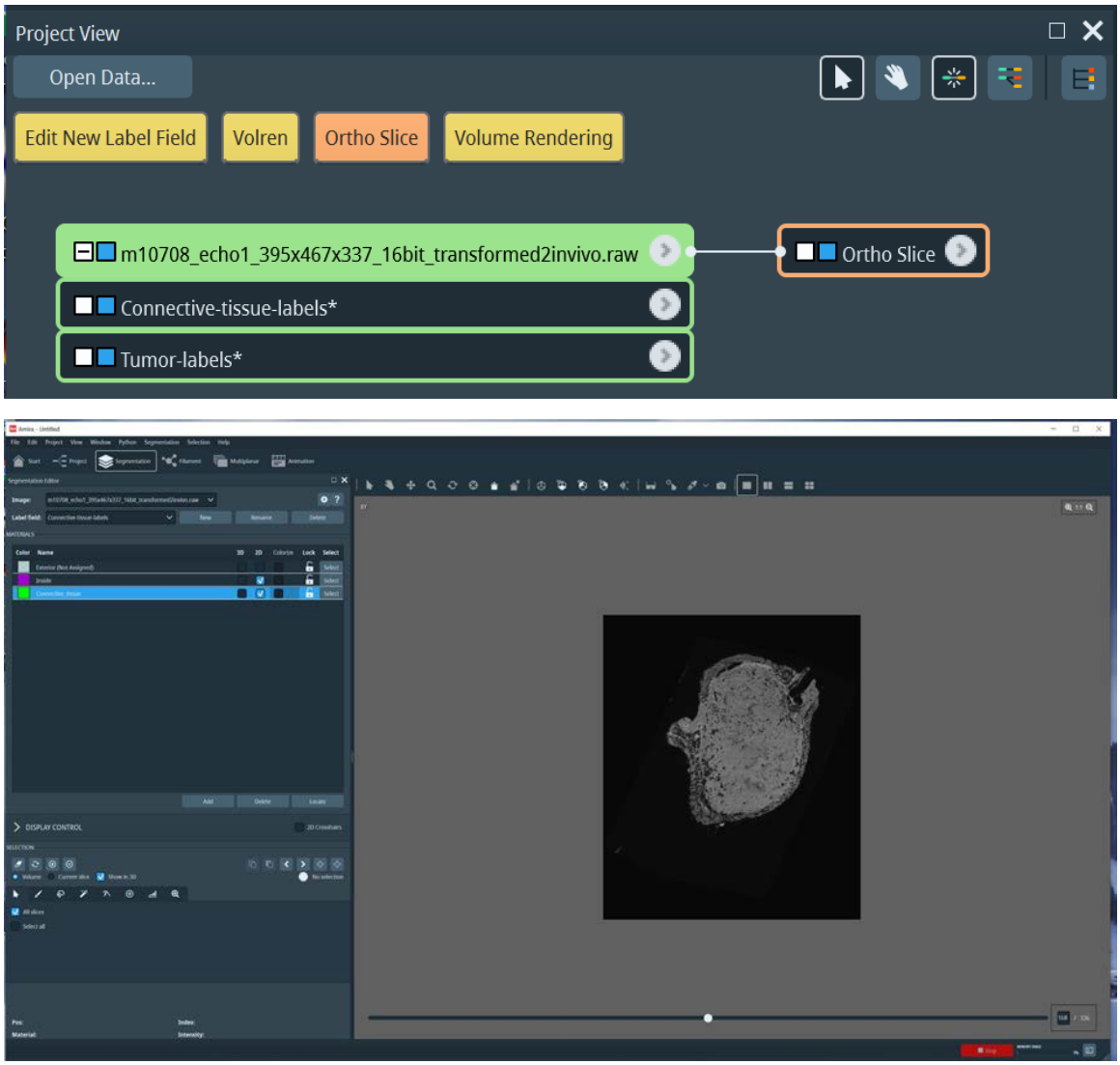

Figure 9. Surface segmentation. Top: two labels on the data object in the Amira Project panel. Bottom: a new material in Segmentation tab. *Text not intended to be read.*

Software

A range of software packages were utilized to complete this project. Thermo Scientific™ Amira™ Software was used to segment the MRM dataset and export .obj files of the soft tissue and tumor surfaces. Pixologic Zbrush® was used to smooth, retopologize, and optimize these .obj files. Cinema4D® was used to model, light, texture, animate, and render the vasculome illustrations. These renders were edited in Adobe Photoshop®. The final illustrations were laid out and combined with text and graphic elements in Adobe Illustrator®. Adobe XD® and Illustrator were used to create wireframes of the web layouts. The PlayCanvas web platform was used to create the visualizations of the vasculome and to build interactivity.

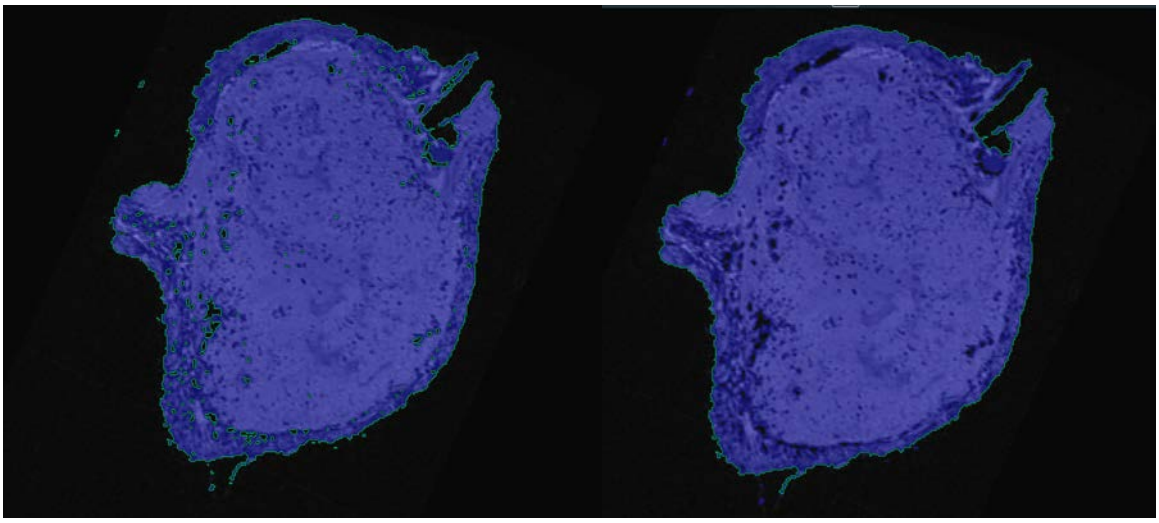

Figure 10. Refinement of surface segmentation. Left: selection yielded by *Threshold* function. Right: segmentation after *Fill holes* and *Remove island* functions.

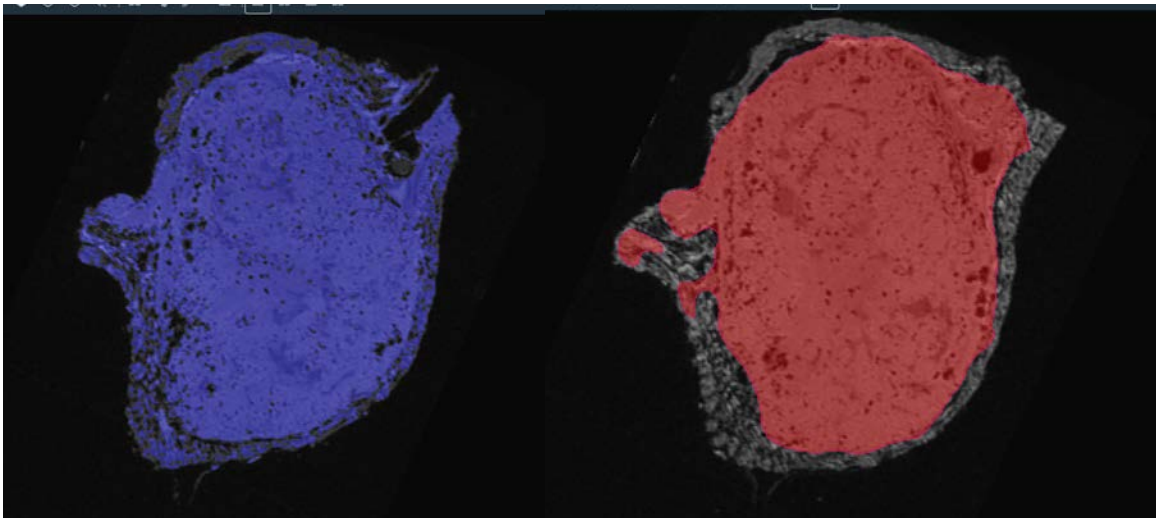

Figure 11. Tumor surface segmentation. Left: segmentation yielded by *Threshold* filter only. Right: refined segmentation of inner tumor surface.

Generation of tumor surfaces

Segmentation of tumor tissue

The soft tissue surfaces (surface of total tissue sample, and surface of tumor within tissue sample) were derived from magnetic resonance microscopy (MRM) data (~40 µm resolution). The files were shared as RAW files with a resolution of 395x467x337 (no specific unit, i.e., 'unscaled').

The tumor MRM was imported into Amira. Two labels were created on the data object to store

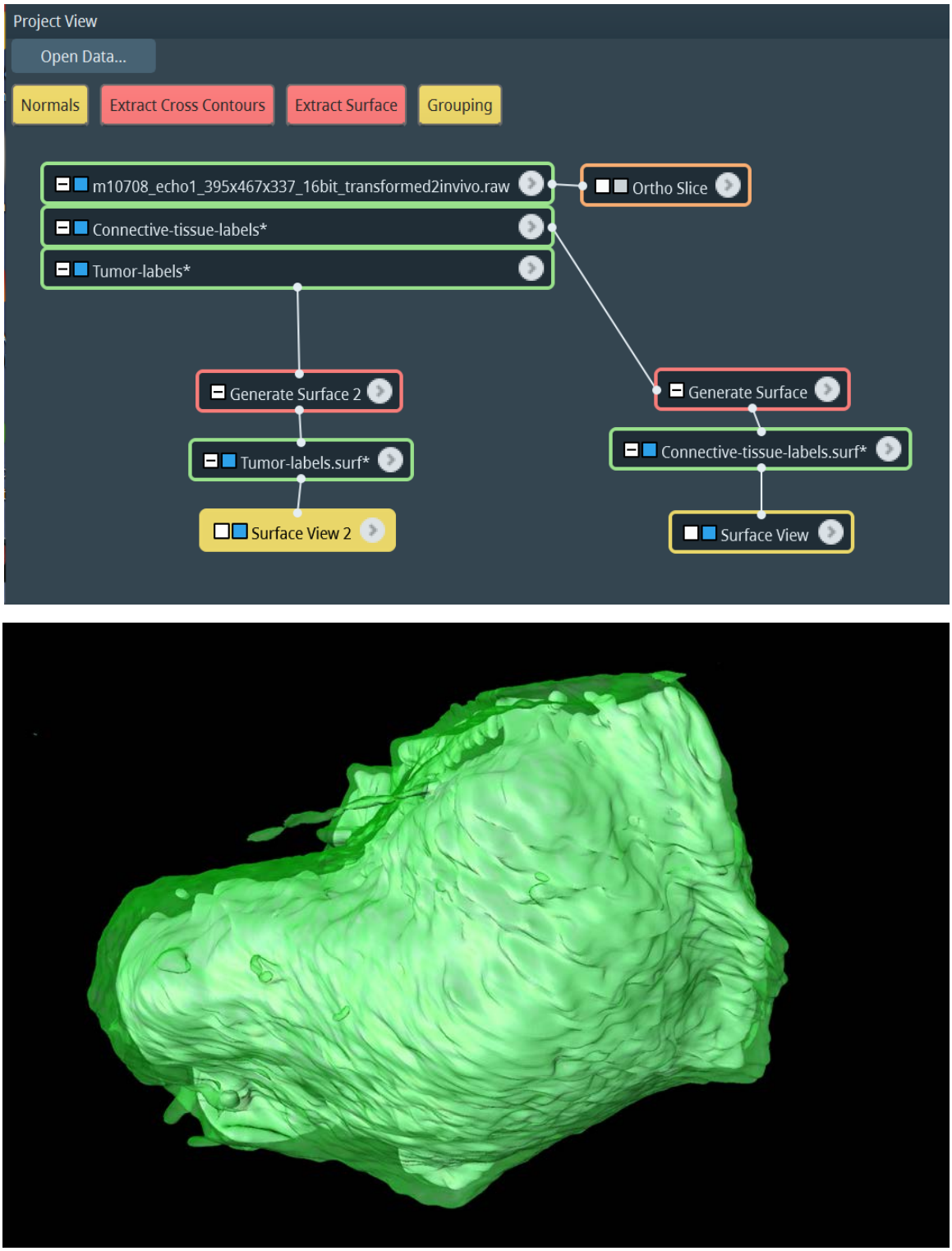

Figure 12. Exporting surface .objs from Amira. Top: project view after segmentation of both surfaces. Bottom: inner tumor and outer soft tissue surfaces visualized in Amira prior to export.

Figure 13. Surface .objs refined in Zbrush. Top row: soft tissue surface as imported into Zbrush from Amira (left), and after refinement (right). Bottom row: tumor tissue surface as imported into Zbrush from Amira (left) and after refinement (right).

the soft tissue and tumor tissue segmentations, respectively. The first label (soft tissue) was selected and a new Material was created and renamed in the Segmentation Tab **(Fig. 9)**.

A *Threshold* filter was used to fill the majority of the soft tissue. This selection was refined with iterations of the *Fill holes* and *Remove island* commands **(Fig. 10)**.

This segmentation process was repeated with the inner surface of the tumor mass. The paintbrush segmentation tool and *Smooth* functions were also used to further refine the automatic threshold errors within areas of low contrast between the tumor tissue and surrounding soft tissue **(Fig. 11)**.

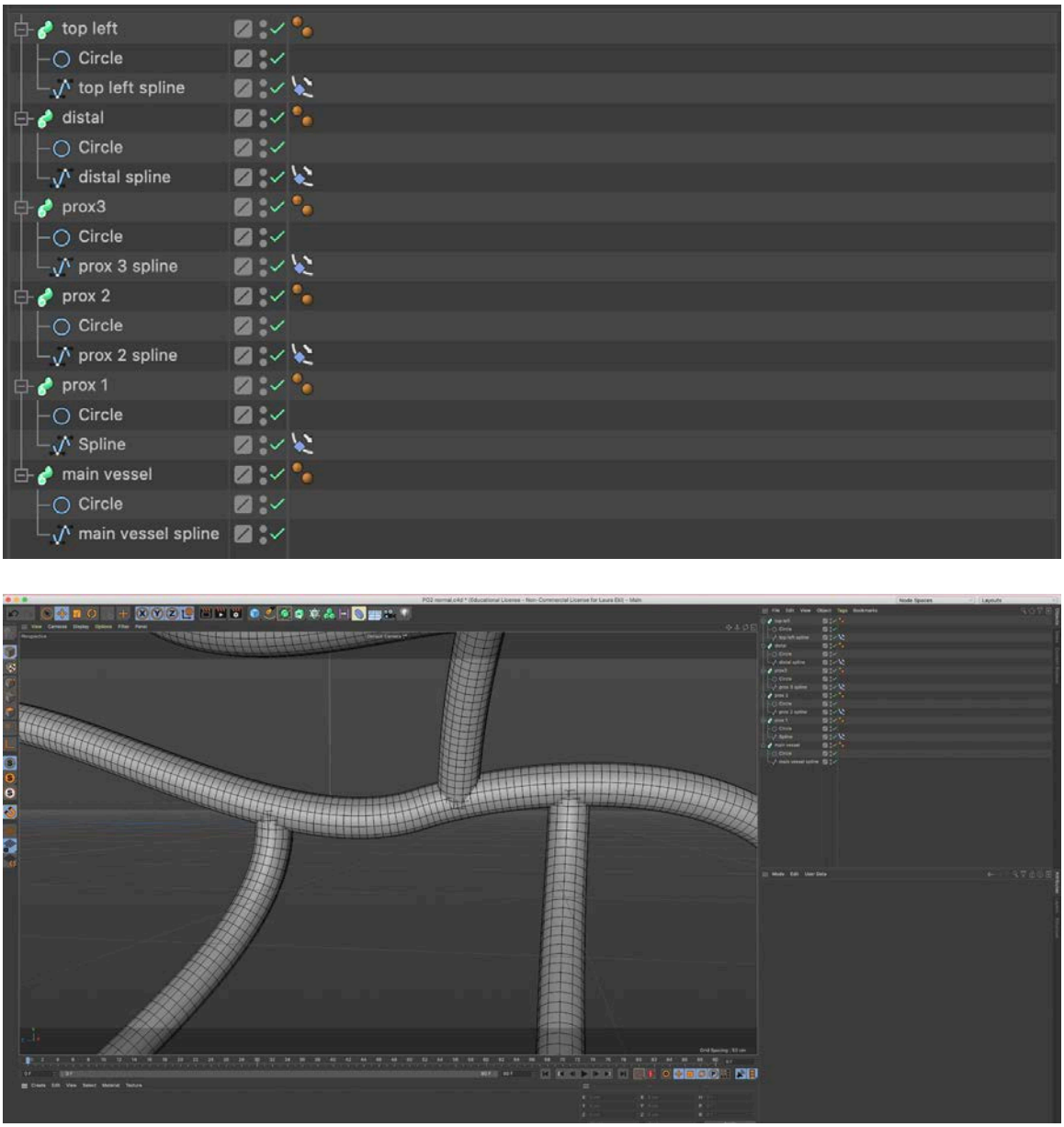

Figure 14. Healthy vessel base geometry. Top: sweep objects. Bottom: sweep objects, paths with Align to Spline tags. *Text not intended to be read.*

After both surfaces had been segmented and refined, they were exported as .obj files from the Project tab **(Fig. 12)**.

Refining surfaces in Zbrush

The two surfaces that were exported from Amira were imported into Zbrush as two new subtools. *Polish* and *Polish by Features* deformations were applied. The smooth brush was used for remaining rough areas.

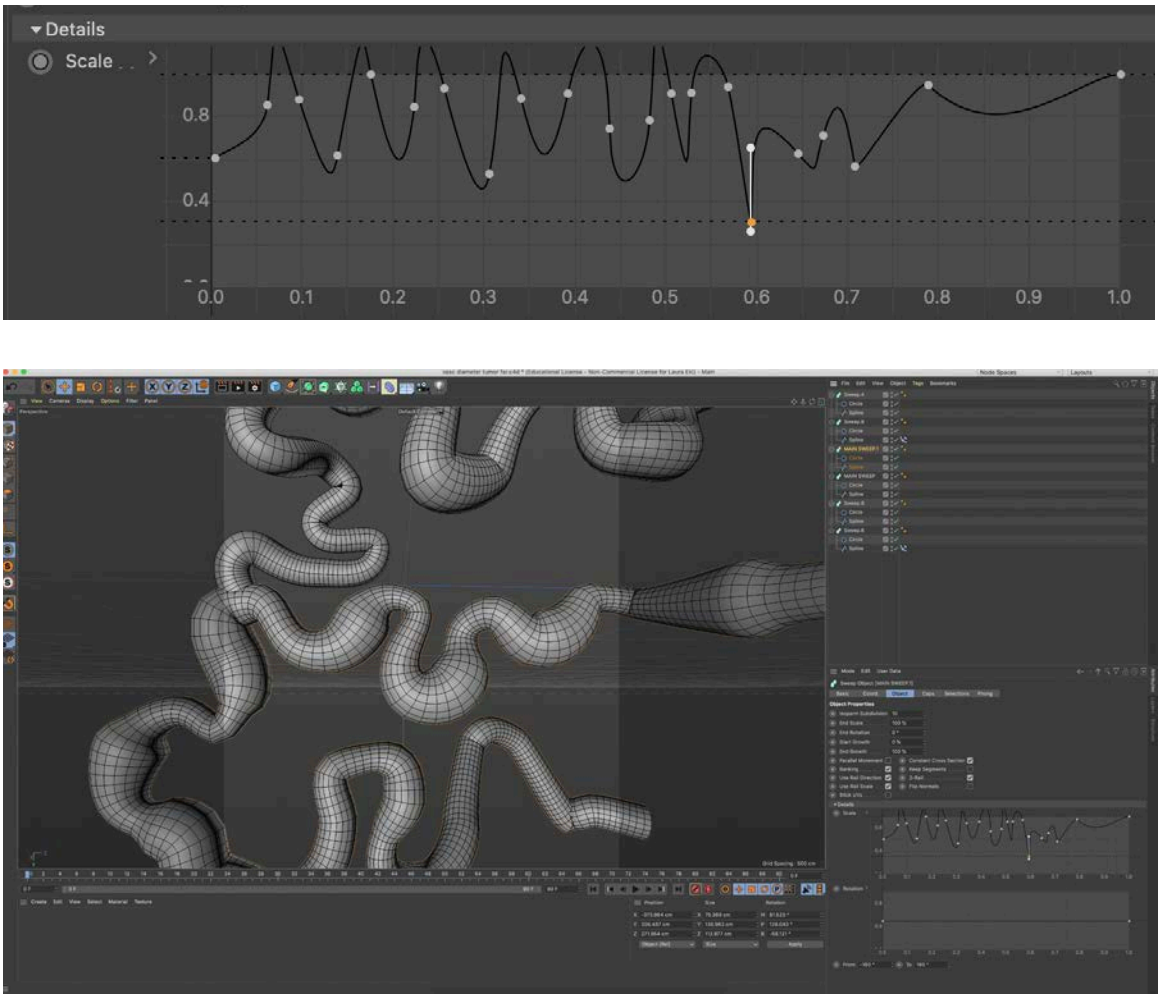

Figure 15. Tumor vessel base geometry. Top: sweep objects with diameter of sweep adjusted. Bottom: tumor vessels with uneven diameters. *Text not intended to be read.*

After smoothing, *Zremesh* was applied to the meshes with a target point count of 100k points **(Fig. 13)**.

Each final mesh was exported as an .obj using the Subtools plugin panel to be used in PlayCanvas.

Didactic content development

Content aggregation and synthesis

The didactic content complementing the interactive visualization focused on the parameters included in the primary paper, in addition to the term ‘vasculome’ itself (Stamatelos and Bhargava, et al. 2019). This amounted to 10 didactic sections (vasculome, vessel length, vessel diameter, intervessel distance, vascular length density, vascular surface area density, blood flow rate,

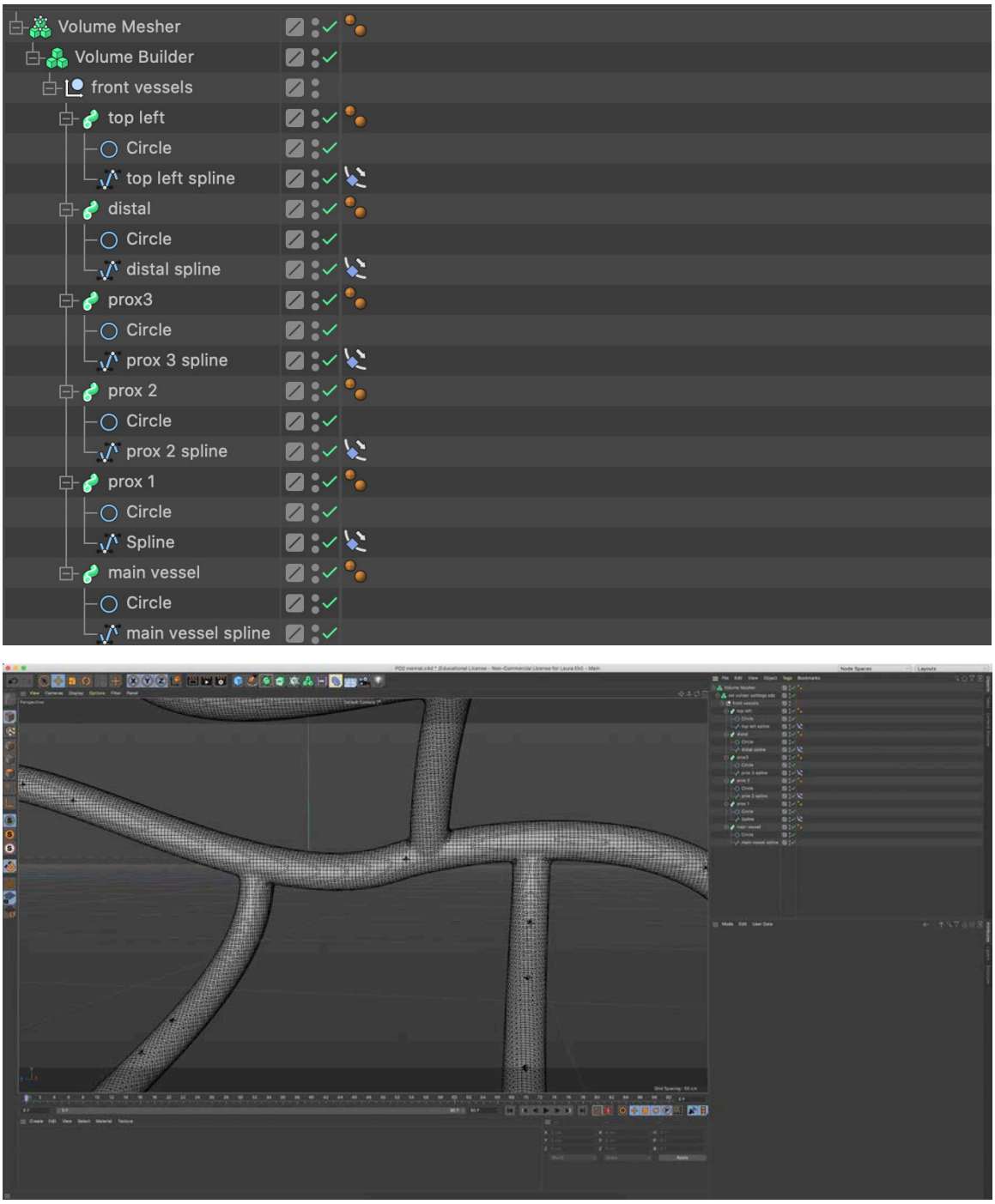

Figure 16. Remeshed vessel geometry. Top: sweep objects in Volume builder and mesher. Bottom: remeshed object. *Text not intended to be read.*

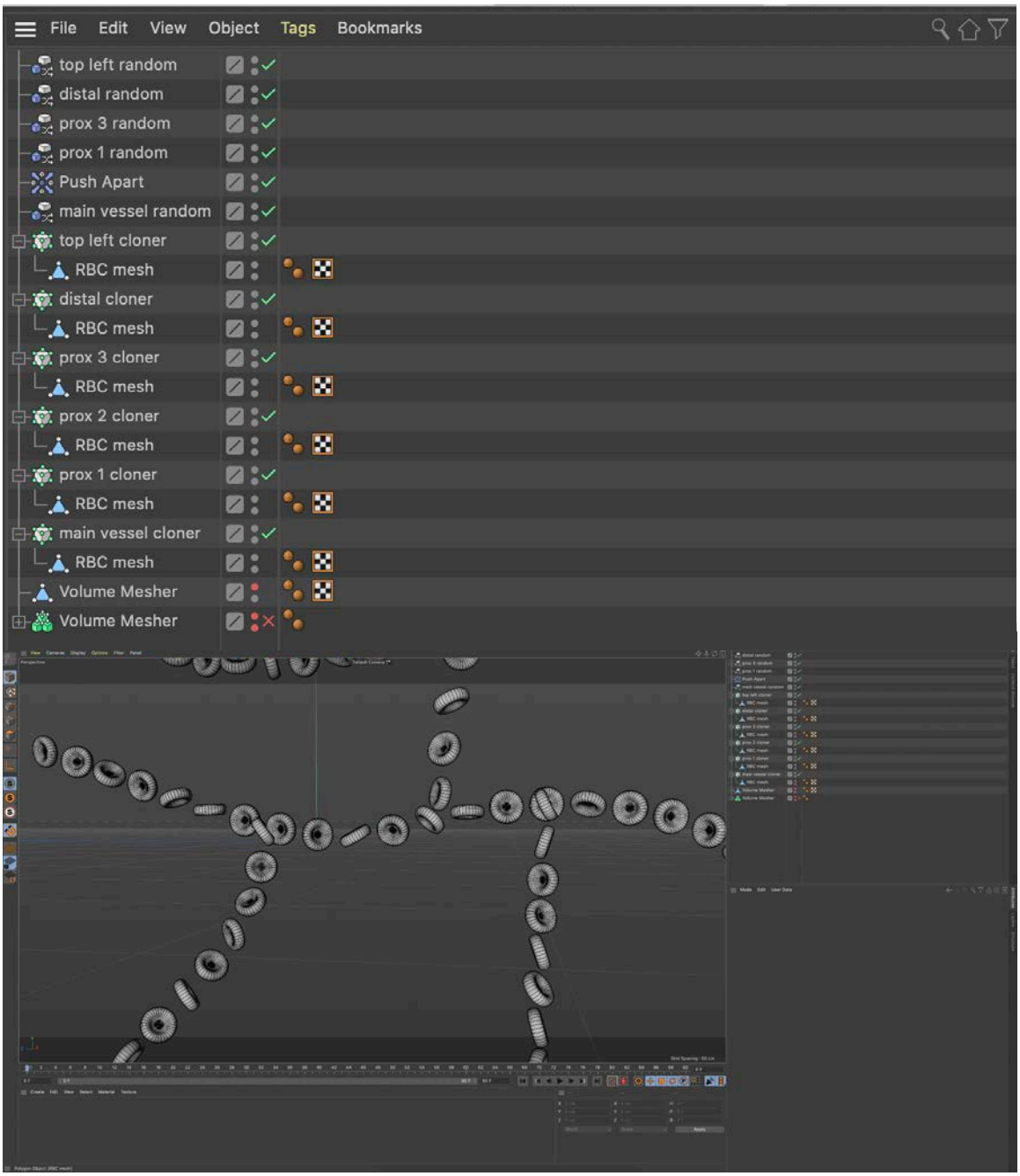

Figure 17. RBC cloners. Top: objects panel with Cloners and MoGraph effectors. Bottom: RBCs in scene. *Text not intended to be read.*

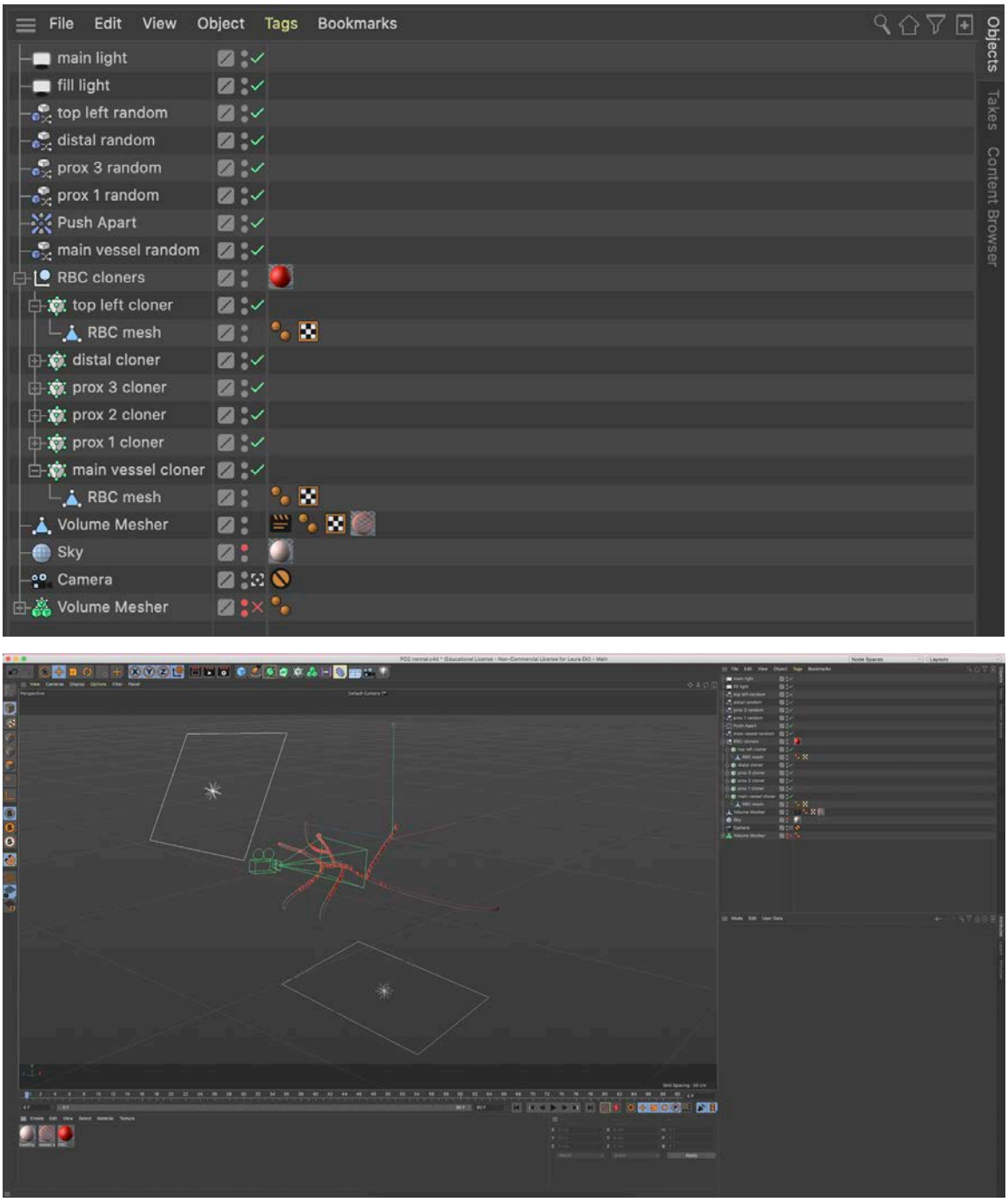

Figure 18. C4D environment. Top: object manager. Bottom: C4D scene with vessels, RBCs, lights, materials, sky (not shown), and camera. *Text not intended to be read.*

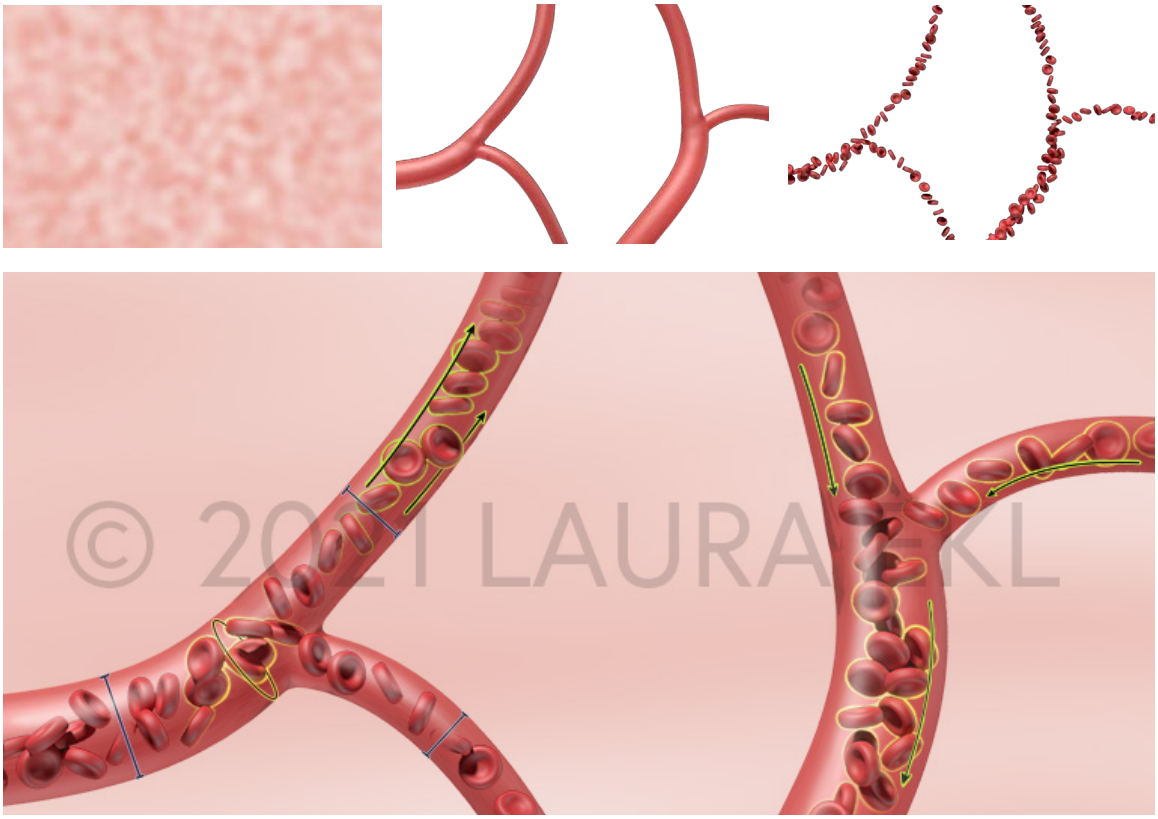

Figure 19. Photoshop edits. Top: individual renders from C4D (left to right: background, blood vessels, RBCs). Bottom: composited image ready for application of text in Illustrator.

intravascular oxygen tension, hematocrit, and fluid shear stress).

For every section, the symbol and unit, a precise definition, a formula (when applicable), a visual representation, and relevant references were given. Two *de novo* formulas were written (vessel length and vessel diameter). Iterative rounds of review resulted in the final didactic content **(Appendix A)**. All sections were treated as illustrations.

Didactic illustrations

The text and formula for each section was used to define the components of each illustration. The illustrations were designed to be 960px wide with a variable height depending on the content to fit into the didactic window. Iterations of sketches and storyboards were reviewed with the didactic text to ensure accuracy.

The normal and tumor vessel scene for the illustrations were built in Cinema4D. Generally, the models were built at a scale of 1 cm = 1 μm to maintain relative scale regarding the sizes of arterioles, capillaries, and red blood cells. Blood vessels were created by defining splines and

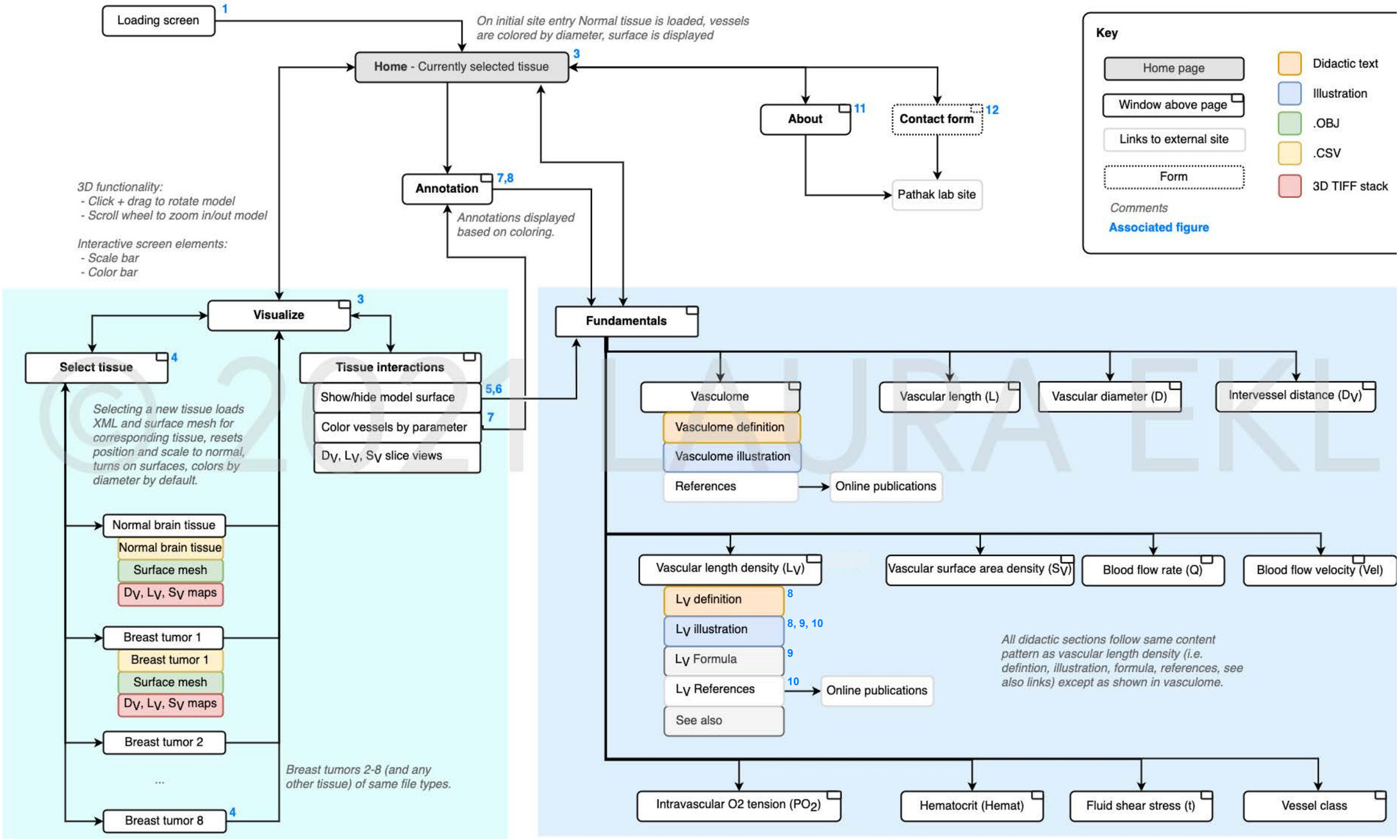

Figure 20. Flowchart. Information architecture diagram mapping overall interactivity of the 3D visualization platform.

using the Align to Spline tag to ensure splines were adjacent **(Fig. 14)**. Sweeps applied to base vessel splines with circle spline primitives ranging from radius = 3.5 cm for the smallest capillaries to radius = 10+ cm for arterioles and veins **(Fig. 14)**. For tumor vessels with uneven diameters, the radius profile of the sweep was adjusted **(Fig. 15)**.

Vessels close to the camera were placed into a Volume Builder with an SDS Smooth surface, then Volume Mesher. The Volume Mesher structure is converted to a mesh with the Current State to Object command to generate a continuous surface with no joints **(Fig. 16)**.

A simple RBC was created from a Cube primitive and a subdivision surface was applied. The same splines used in the vessel sweeps were used to as the target object to clone RBC models along. MoGraph Random and Push Apart Effectors were applied to the RBC cloners to add variation to the RBCs within the vessels **(Fig. 17)**. The cloners were expanded using the Current State to Object command.

Two area lights with soft shadows were applied to every file. A Sky object was added, and one of two Materials was applied to the Sky object to represent healthy or tumor tissue. A camera was added and Physical Depth of Field was enabled, the F-stop adjusted in the Properties panel **(Fig. 18)**.

The Render Settings were defined to a custom resolution based on the final illustration size. The renders produced by C4D were imported into Photoshop, where hue/saturation, lighting, and blurs were adjusted. Graphic elements were added if needed. The edited images were saved as .pngs **(Fig. 19)**.

These .png files were then imported and placed into the final Illustrator file. Text and remaining graphic elements were added. The final illustrations were exported from Illustrator.

Interactive 3D web-based application

Summary of interactivity

The web-based interactive resource was designed with the bulk of the functionality organized into two components: the interactive 3D visualization of the tissue vasculome (normal or tumor), and the accompanying didactic text and illustrations explaining the vasculome parameters.

The visualization assets and didactic components were organized into a flowchart describing the overall content and functionality of each element of the site **(Fig. 20)**. The flowchart was modified based on feedback about the hierarchy, functionality, and content of the visualization

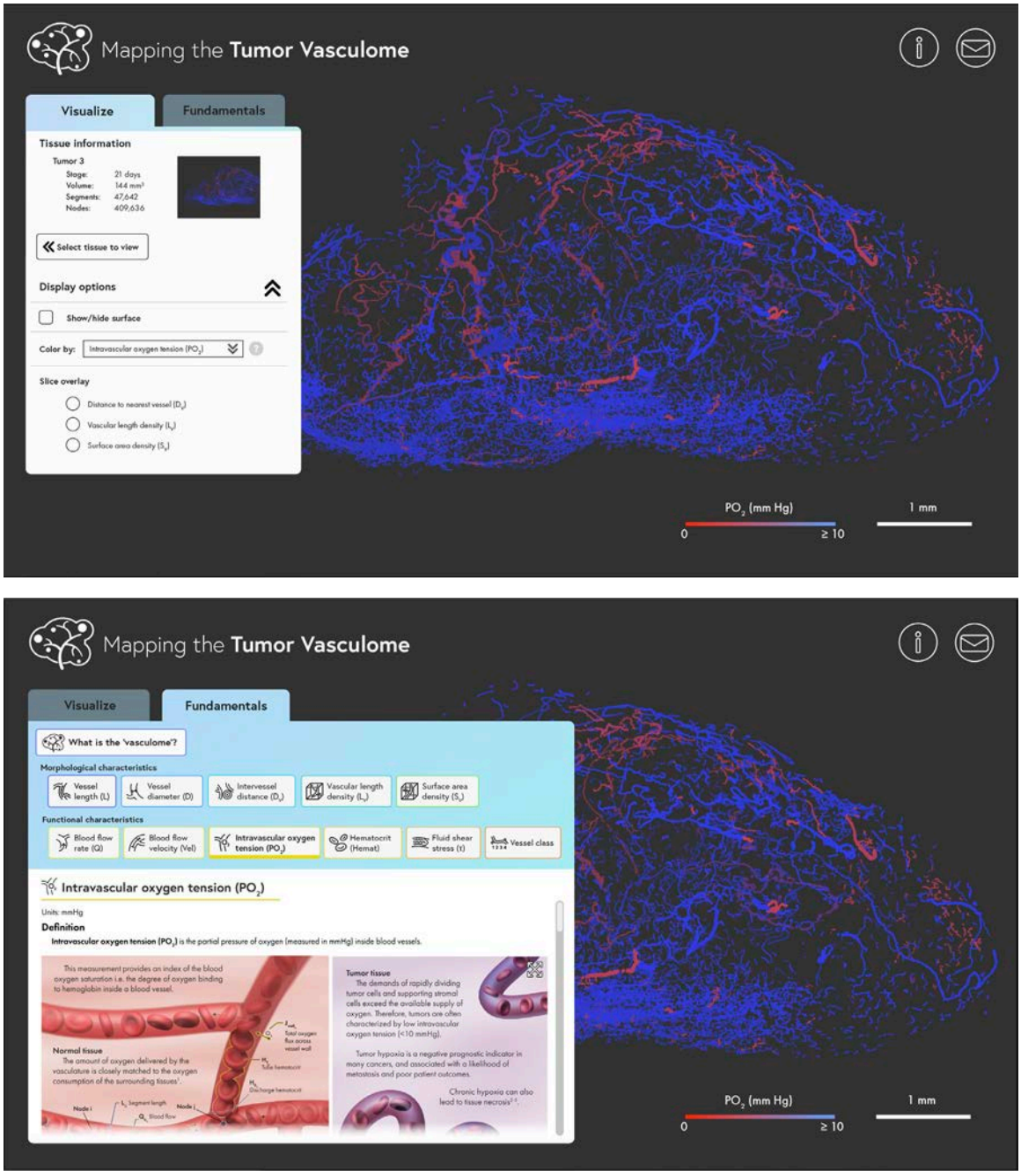

Figure 21. Final wireframes. The user interface shown for the two major modes of the visualization platform. Most of the content is consolidated into a single window on the left with tabs to allow navigation between sections. Top: options shown for visualization of vasculome. Bottom: didactic section open. *Text within image not intended to be read.*

Icons

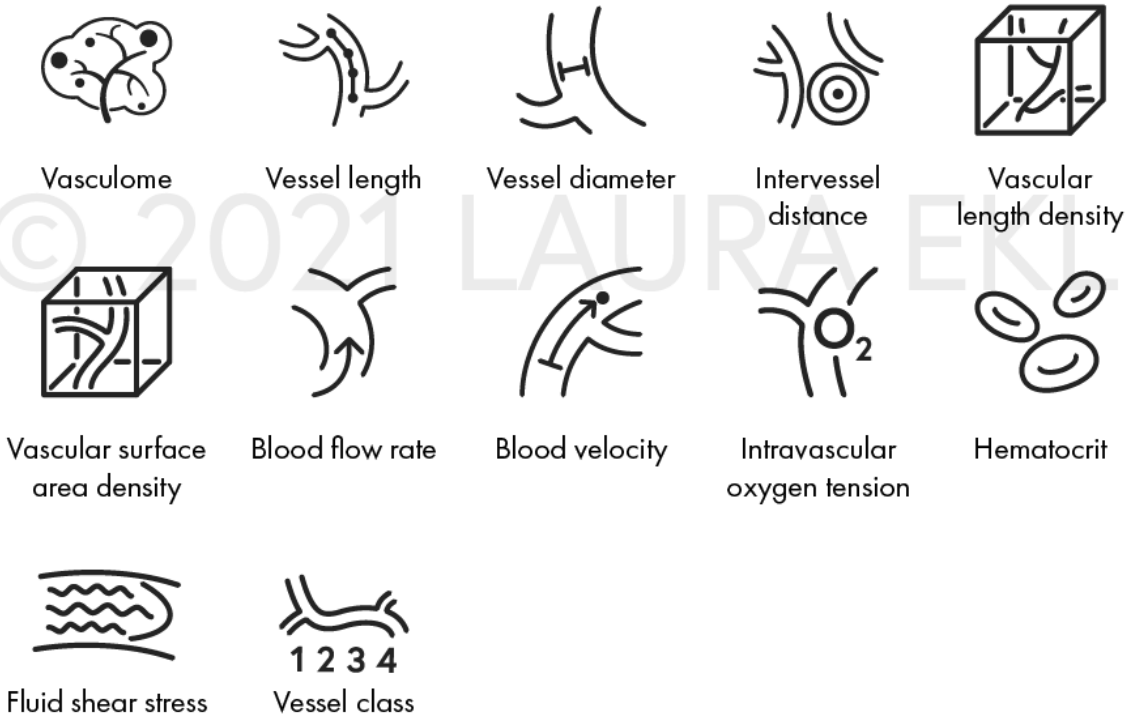

Button styles

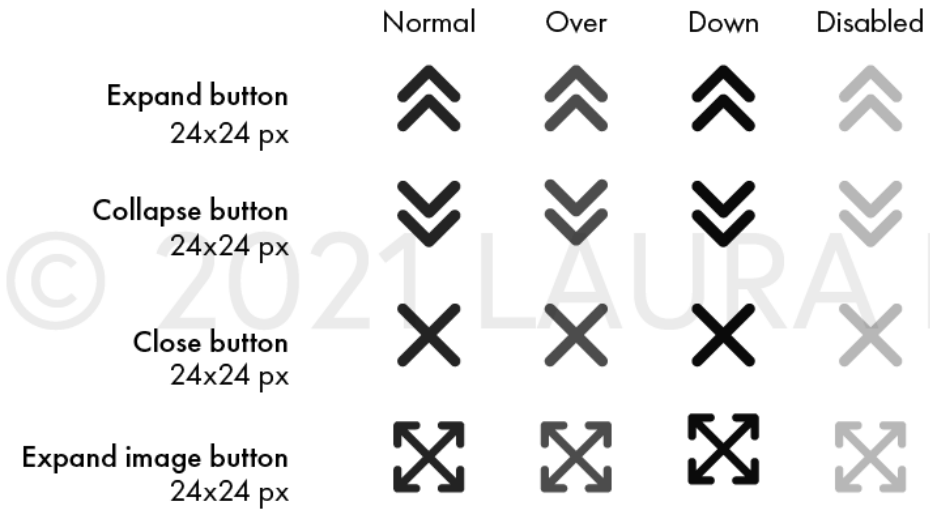

Figure 22. Icon and button samples.

and didactic segments provided by Drs. Pathak and Bhargava.

User interface design

Preliminary grayscale wireframes were developed during the planning stages to organize content and map interactivity. These wireframes were built in Adobe XD and reviewed by members of the Pathak Lab. Usability testing with this group facilitated identification of areas where overall layout, design, navigation, and content could be improved.

Following modifications to the interface and site functionality resulting from ongoing feedback, final high-fidelity full-color wireframes were created in Adobe Illustrator to serve as a guide when developing the graphical user interface (GUI) in PlayCanvas **(Fig. 21.)**. Most of the screen space was reserved for the vasculome 3D visualization, and a single floating window on the left contained the options for visualization and the didactic content. This organization conserved space and provided a single location for the user to access the content on the site. Additional screen elements included an interactive scale bar, interactive color bar, and buttons for an About and Contact section. A dark-colored background was chosen to increase contrast between the color-coded vessels.

A style guide was developed to define the text sizes and features, button states, menu styles, and colors. Typefaces were based on the current Pathak Lab website (Europa and Futura-PT) to maintain brand continuity. Standard buttons were designed, including the typical mail icon for the Contact section, and the lower-case “i” for the information section. A site logo was designed, and icons were created to identify each of the 12 vasculome parameters **(Fig. 22)**.

Visualization of vasculome data in PlayCanvas web platform

Interactive visualization of the vasculome data was accomplished in the web platform PlayCanvas. PlayCanvas (https://playcanvas.com/) is a free editing environment for WebGL design of interactive web content. The platform is entirely web-hosted and designed to be plugin-free, enabling access on any browser or mobile device. The authoring platform runs as HTML5 and interactivity can be added with custom JavaScript code.

To visualize the vasculome data stored in the .csv file, a new PlayCanvas project and scene were created, custom JavaScript (.js) code was written to visualize the vasculome .csv data, 3D interactions (rotation, zoom) were defined, and a simple GUI were developed by iSO-FORM, LLC, a medical illustration media company based in Ames, IA.

On initialization, the custom .js code loads the vasculome .csv data file from a link, and a loading screen is displayed. The custom script optimized the data in the .csv file to reduce the number of displayed points. Once the .csv file is loaded into memory, the file was parsed line by line to extract the location, thickness, O_2, and flow rate data. For each line of data, a 3D object (i.e. cubes) is instantiated at the XYZ location in the file. The 3D object is scaled to match the thickness value and assigned color based on the vasculome parameter (e.g. O_2, flow rate) value.

For each line of the .csv file that was parsed, the follow code was executed:

```
var scale = this.file.data[i].thickness*0.01;
var pos = new pc.Vec3(this.file.data[i].x*0.01, this.file.data[i].y*0.01, this.file.
data[i].z*0.01);
var o2Color = new pc.Color(255*o2percentNormalized, 0,
255-(255*o2percentNormalized));
var newModel = this.app.root.addChild(this.template);
newModel.setLocalScale(scale, scale, scale);
newModel.setPosition(pos);
newModel.meshInstances[0].setParameter('material_color', [o2Color, o2Color, o2Color]);
```

Lighting and shadows were disabled in the scene to reduce render time. The graphical user interface was coded in Javascript by iSO-FORM to allow for switching between two variables (PO_2 and flow) and navigation between visualize and fundamental tabs.

Hosting on the web

The interactive HTML5 package can be downloaded from PlayCanvas and re-hosted on the user server.

Results

Information architecture and wireframes

A flowchart **(Fig. 20)** was created to organize the major interactions and content of the website. Media types included text, images (.png), animation (.mp4), 3D models (.obj), spatial arrays (.csv), and computed hemodynamic maps (3D .tif).

A series of low-fidelity wireframes **(Fig. 23.1-23.12)** were created from selected user interaction pathways within the flowchart. Numbers on the flowchart correspond to the numbers on the storyboards. Selected sections include the following pages: Loading screen (1), home screen (2), tissue selection menu (3), breast tumor 8 loaded (4), show/hide the model surface (5), recolor vessels by oxygen tension (6), slice viewer (7), annotation (8), length density didactic section (9), about window (10), contact form (11).

A series of application interfaces were created to mockup the final user interaction and graphical user interface **(Fig. 24.1-24.15)**.

Didactic illustrations and formulas

Illustrations were created to supplement the text, formulas, and references for each didactic section. Sketches were created for each illustration **(Appendix A)**. The illustrations were integrated into the 3D interactive of the final web application **(Fig 25.1-25.10)**.

Two formulas were written to describe the calculations used to determine vascular length and vascular diameter specifically for the data in the spatial graph format (**Appendix A**).

Visual style

Icons, button styles, and colors were defined in a style guide to maintain consistency and guide development of web application **(Fig. 26.1-26.5)**.

Three-Dimensional Model

A 3D model of the soft tissue surfaces was created in Amira and refined in Zbrush **(Fig. 27, 28)**. Materials were later applied in PlayCanvas.

Interactive application

Selected components of the full PlayCanvas-based interactive application were completed, including visualization of normal brain and breast tumor tissue, switching between variable displays, annotation functionality, and didactic window. The application allows users to interact

with the visualization on a desktop computer, tablet, or mobile phone through click-to-rotate and zoom functionality.

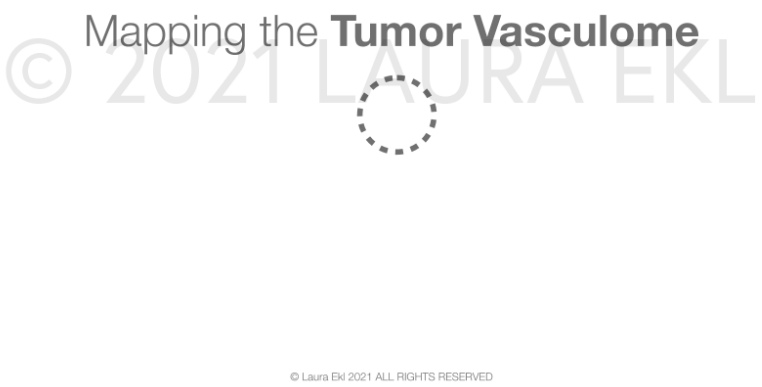

Figure 23.1. Storyboards. Application pre-loader.

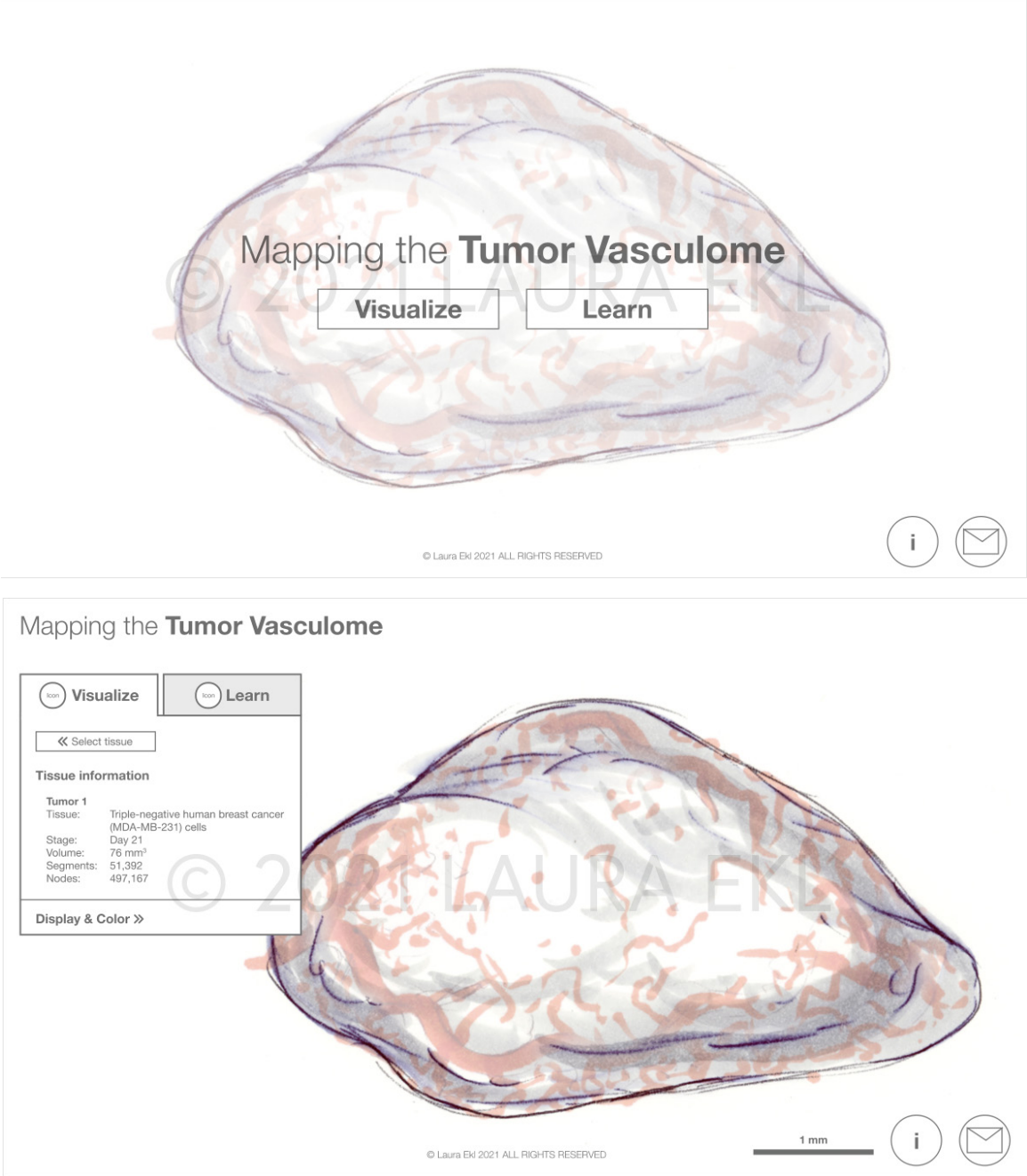

Figure 23.2-.3. Storyboards. Application storyboards. Top: landing page. Bottom: tumor tissue visualization.

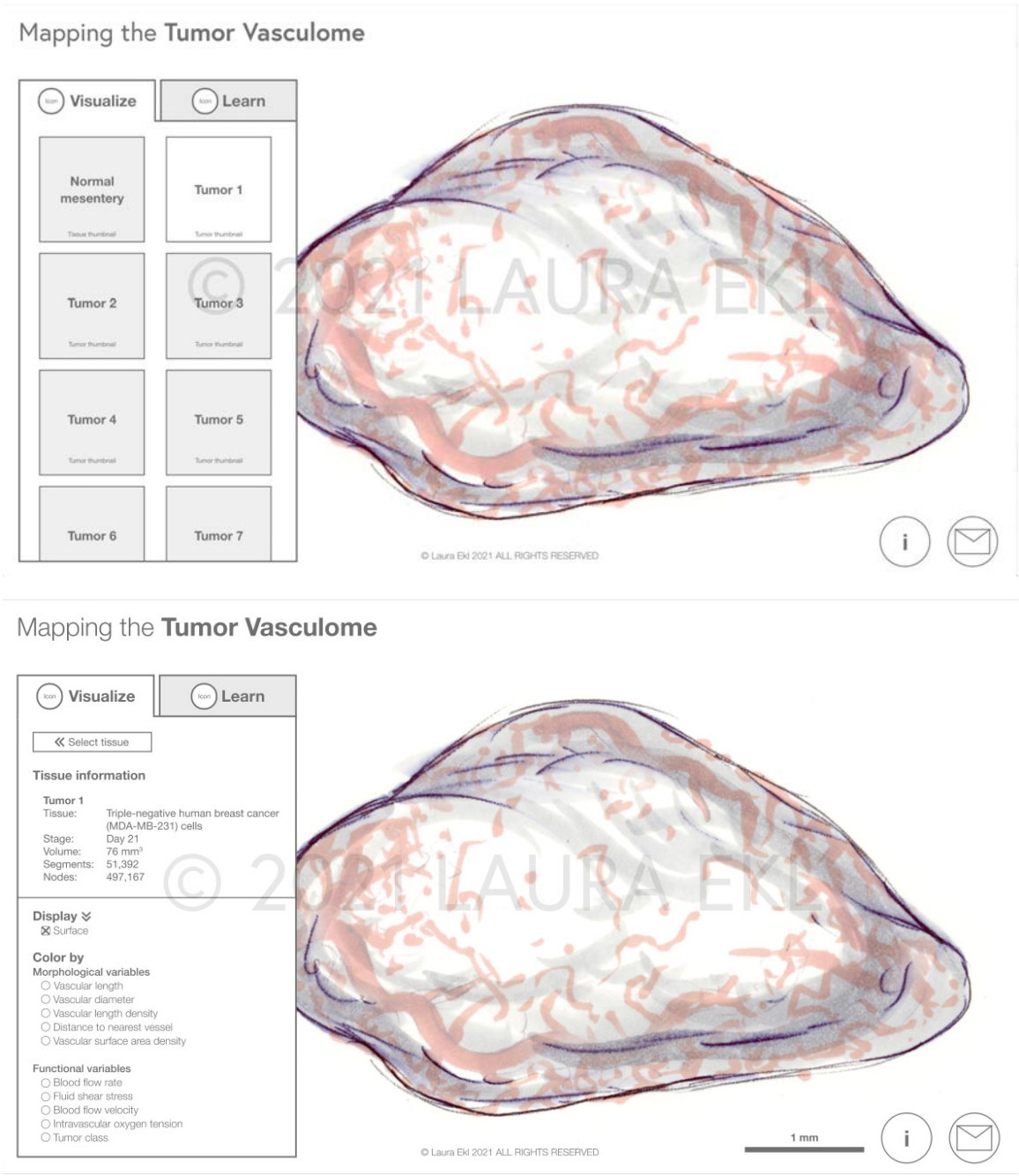

Figure 23.4-.5. Storyboards. Application storyboards. Top: select tissue menu. Bottom: visualization graphical user interface. *Text within image not intended to be read.*

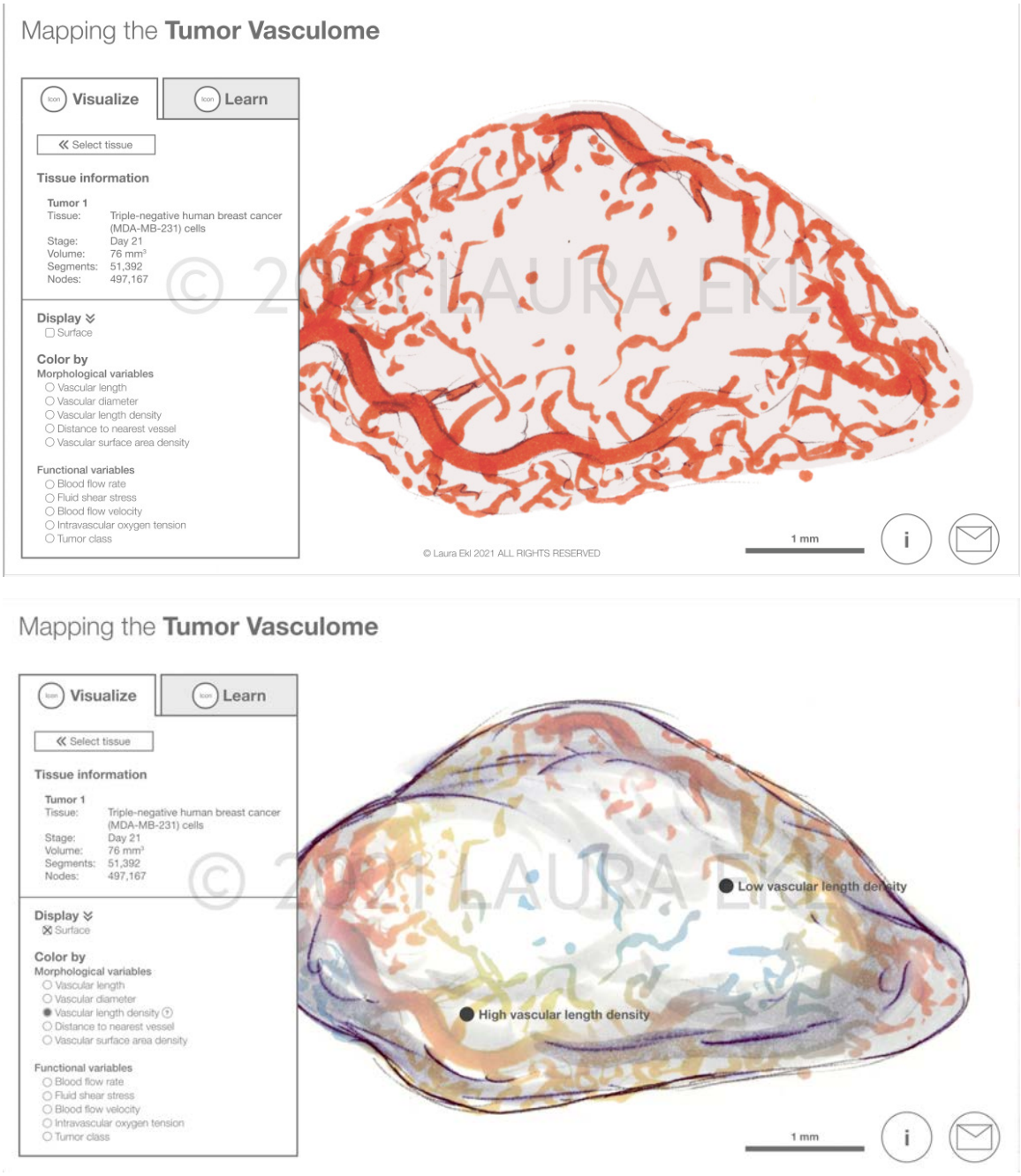

Figure 23.6-.7. Storyboards. Application storyboards. Top: tumor surface disabled. Bottom: color vessels by L_v, annotations displayed. *Text within image not intended to be read.*

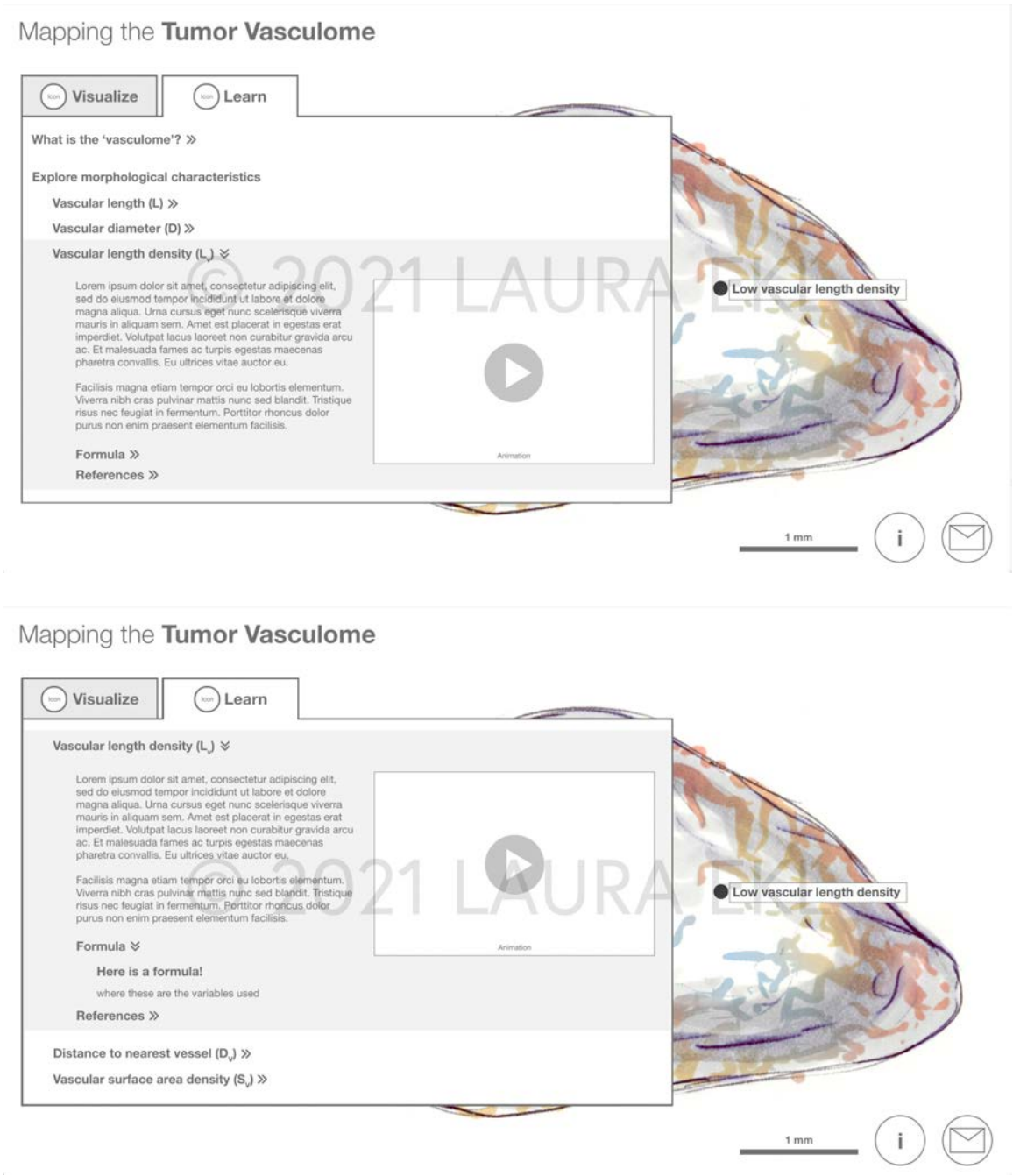

Figure 23.8-.9. Storyboards. Application storyboards. Top: annotation selected and linked didactic content displayed. Bottom: didactic menu formula section. *Text within image not intended to be read.*

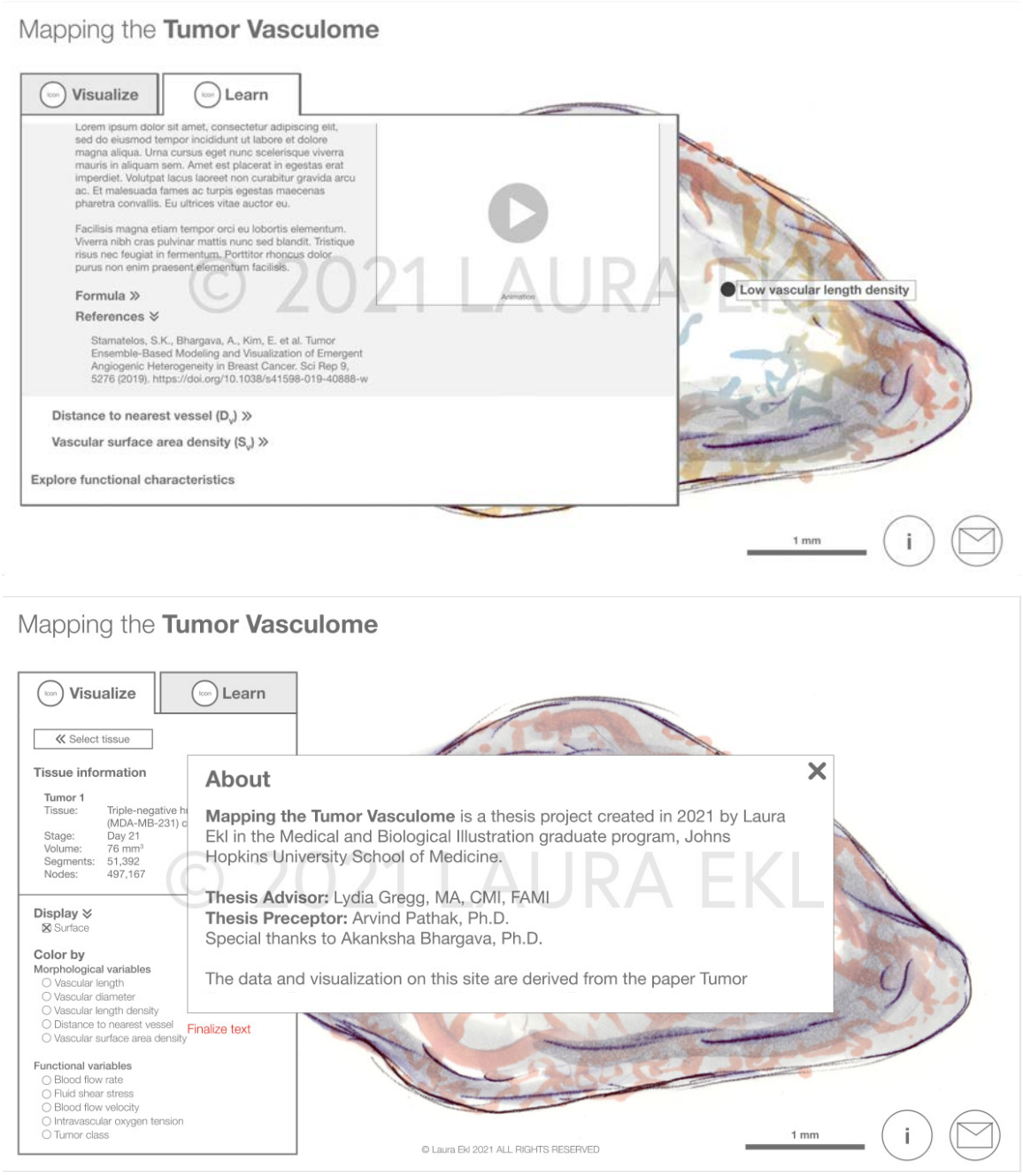

Figure 23.10-.11. Storyboards. Application storyboards. Top: didactic menu references section. Bottom: about window. *Text within image not intended to be read.*

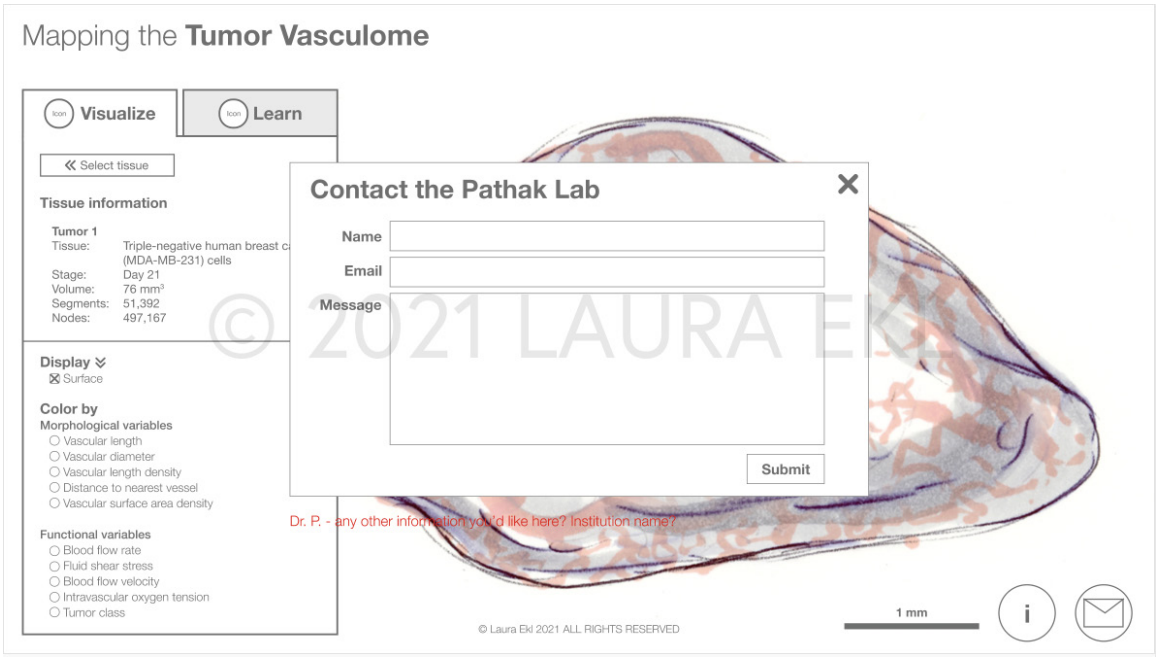

Figure 23.12. Storyboards. Application storyboards. Contact form. *Text within image not intended to be read.*

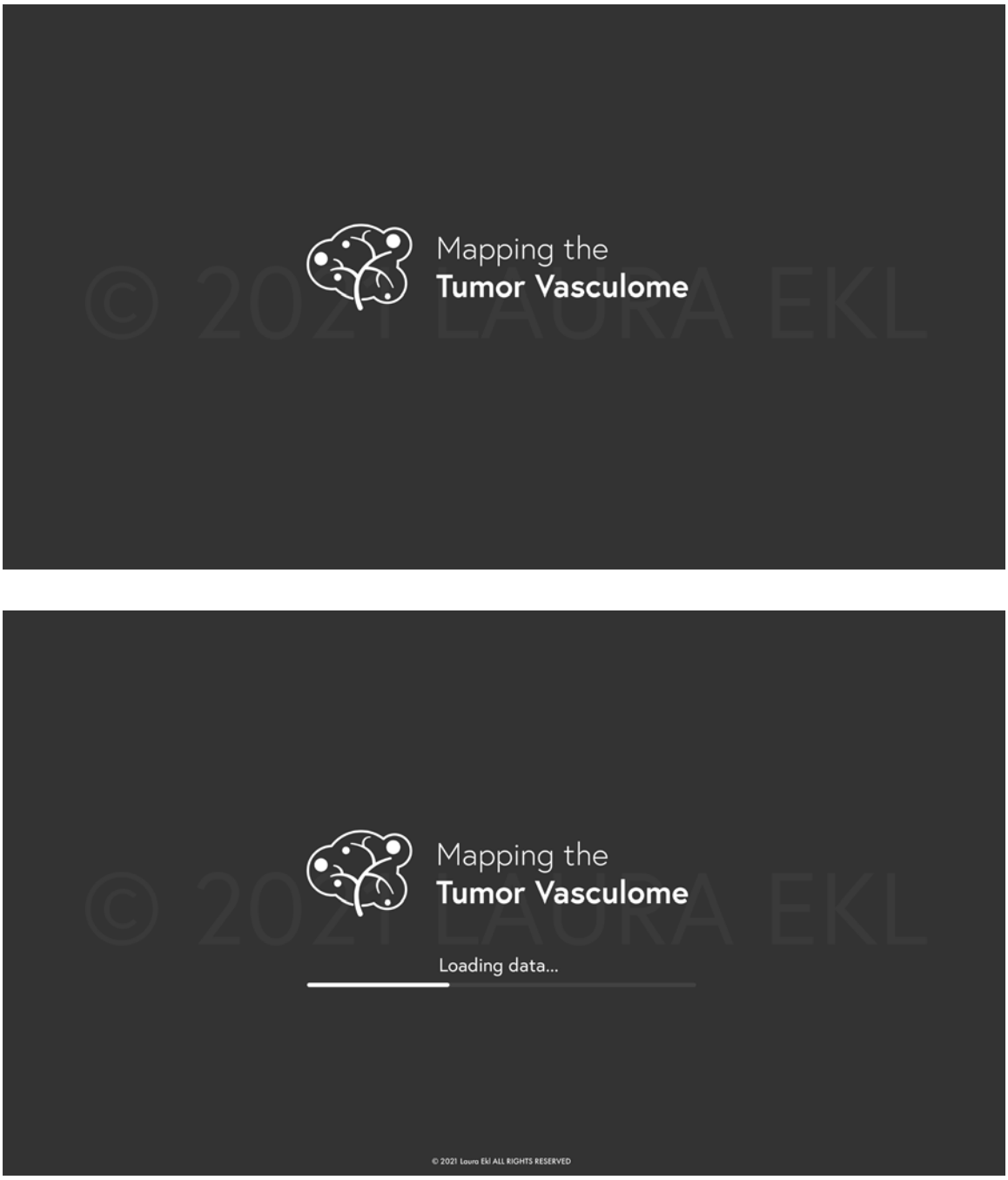

Figure 24.1-.2. Application interfaces. Top: splash page. Bottom: pre-loader. *Text within image not intended to be read.*

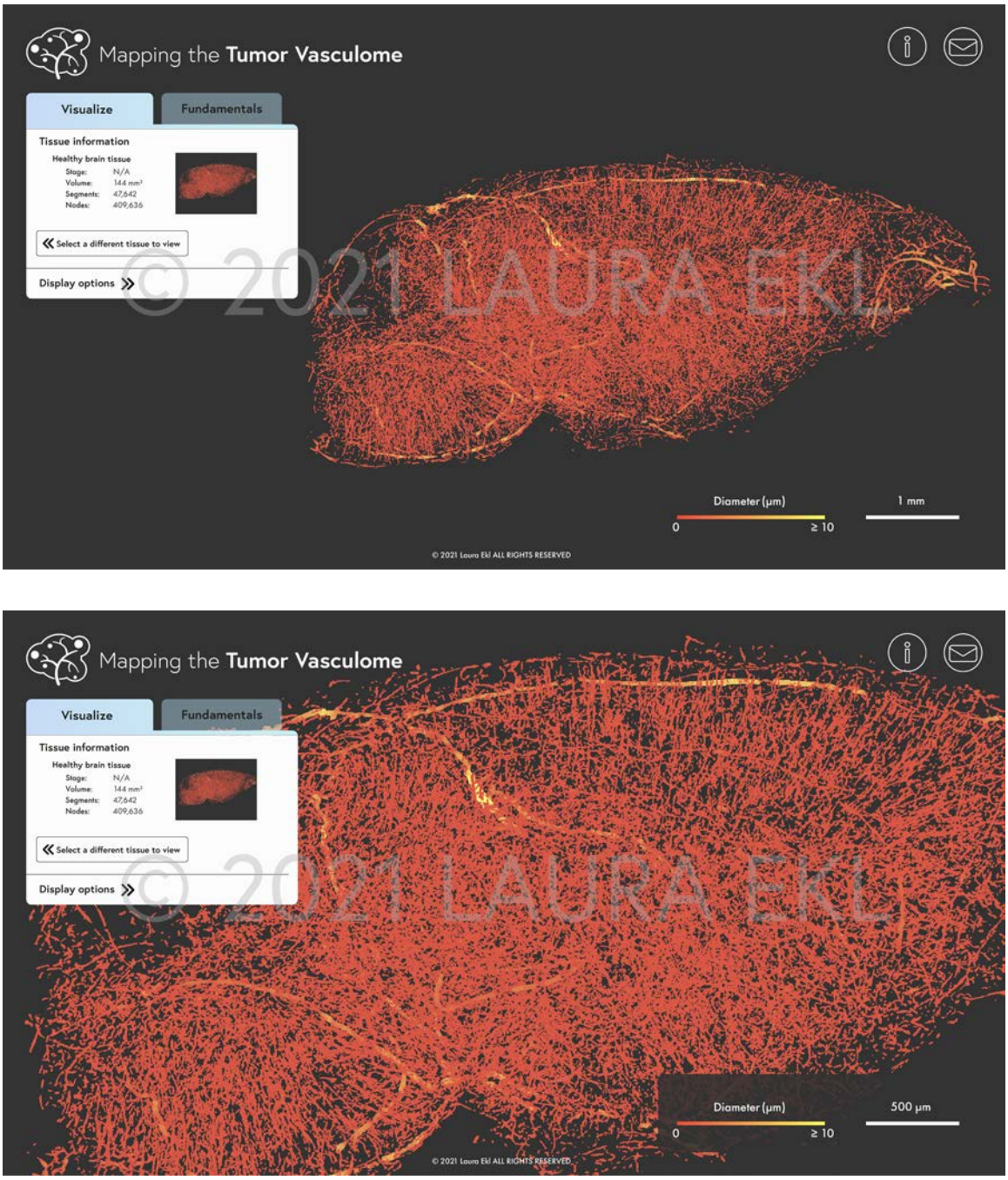

Figure 24.3-.4. Application interfaces. Top: normal murine brain vasculome displayed on entrance to site. Bottom: zoom functionality. *Text within image not intended to be read.*

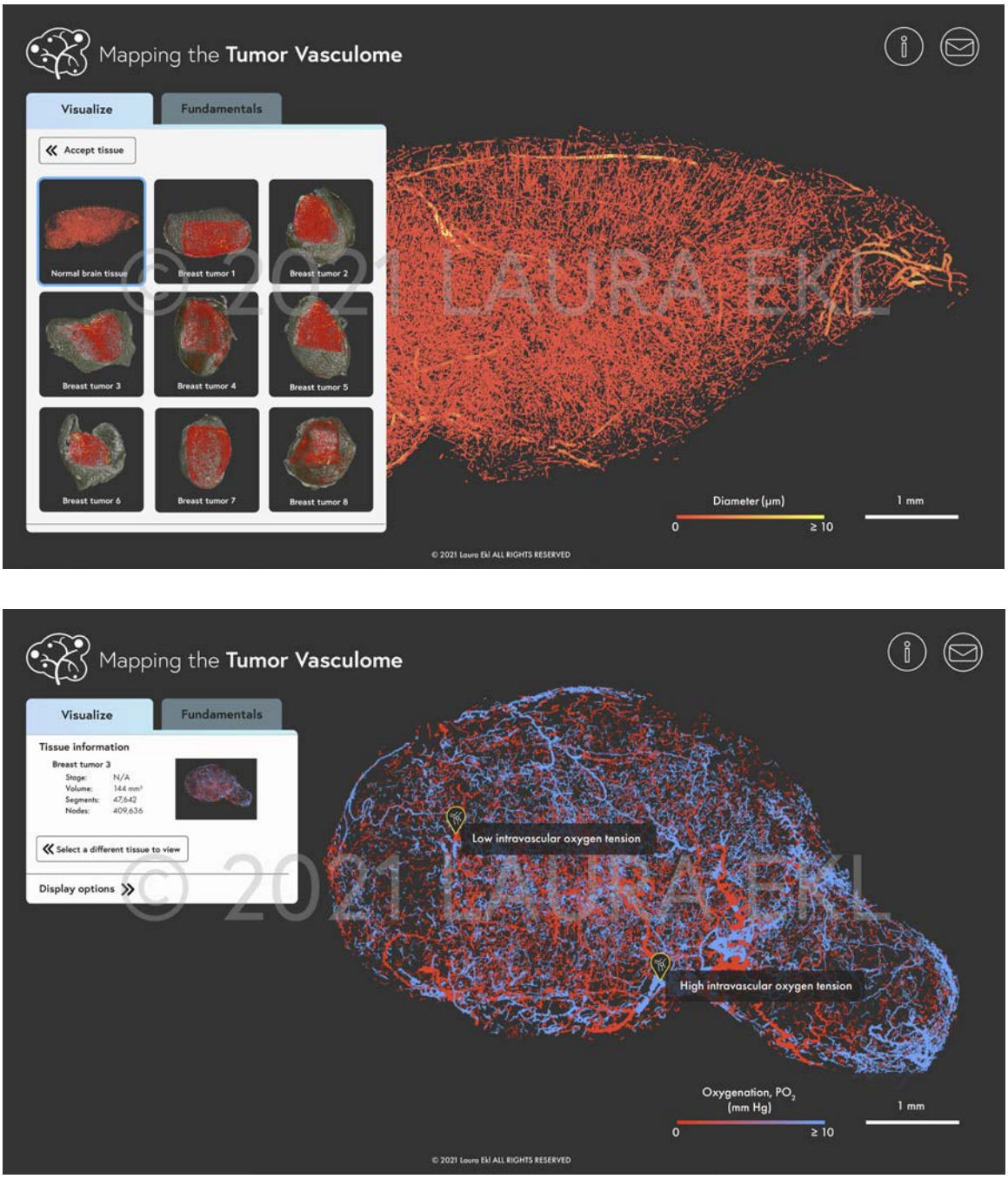

Figure 24.5-.6. Application interfaces. Top: select tissue window. Bottom: tumor tissue selected and annotations displayed. *Text within image not intended to be read.*

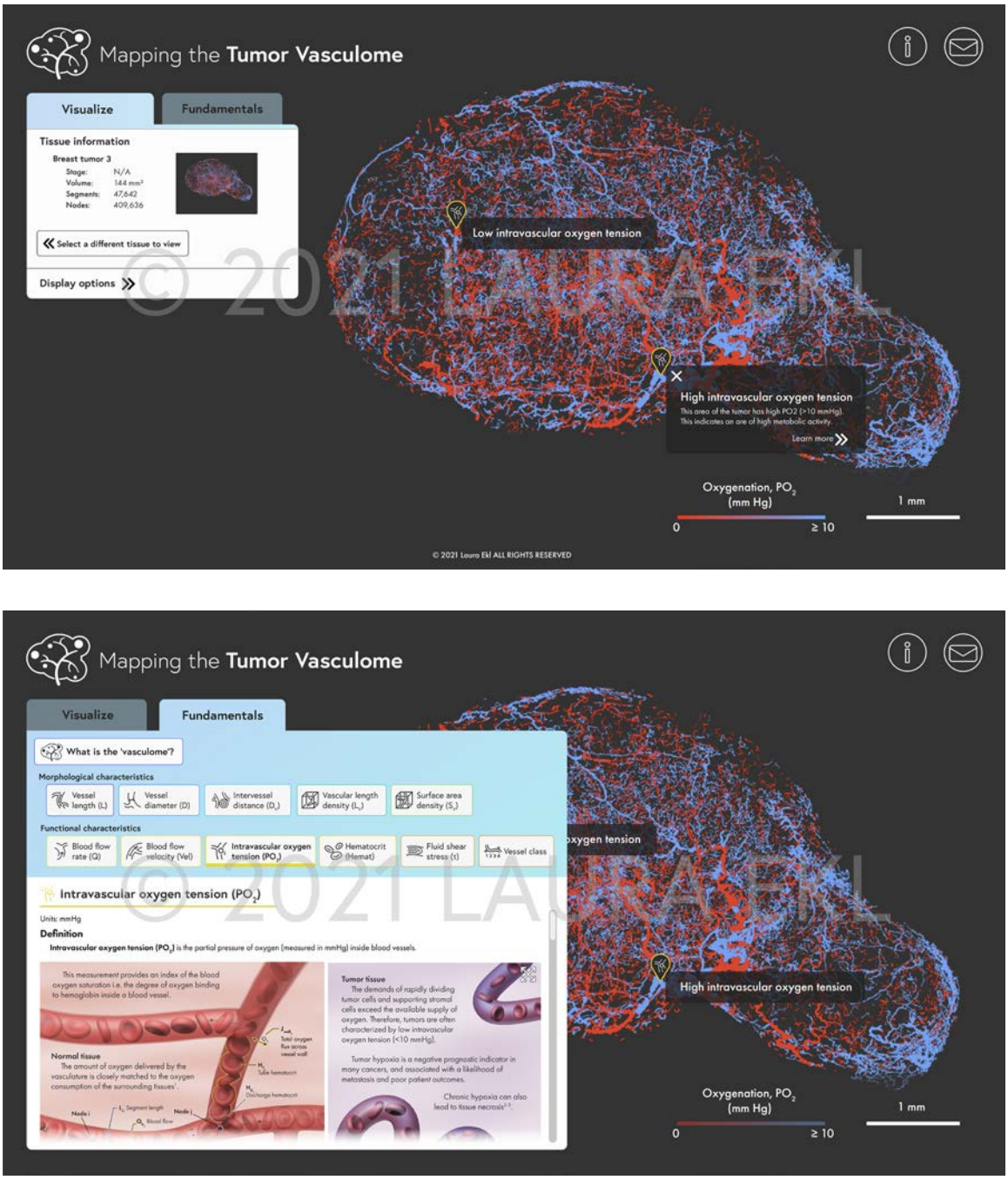

Figure 24.7-.8. Application interfaces. Top: annotation selected. Bottom: link to didactic section. *Text within image not intended to be read.*

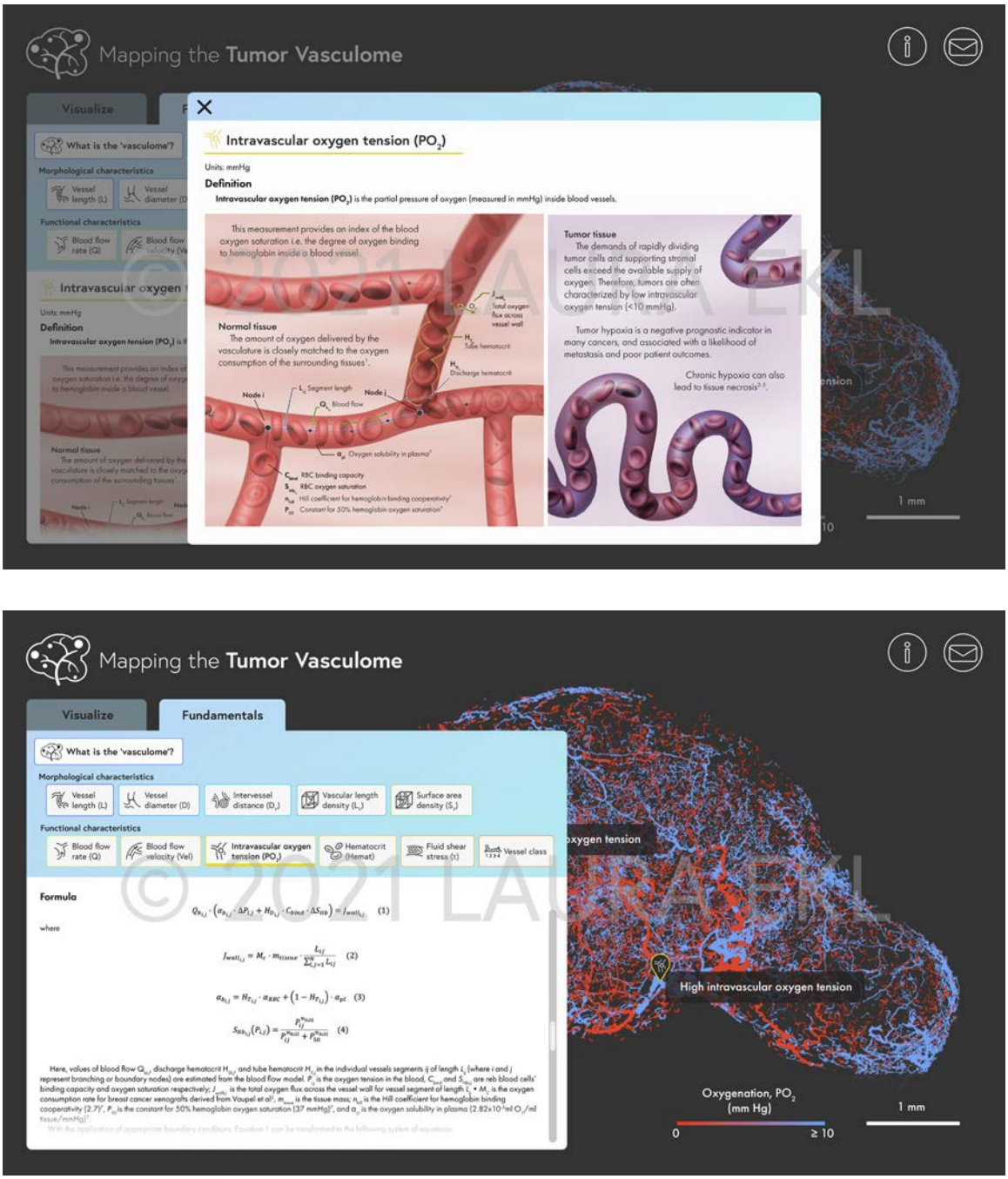

Figure 24.9-.10. Application interfaces. Top: illustration expanded. Bottom: didactic formula section. *Text within image not intended to be read.*

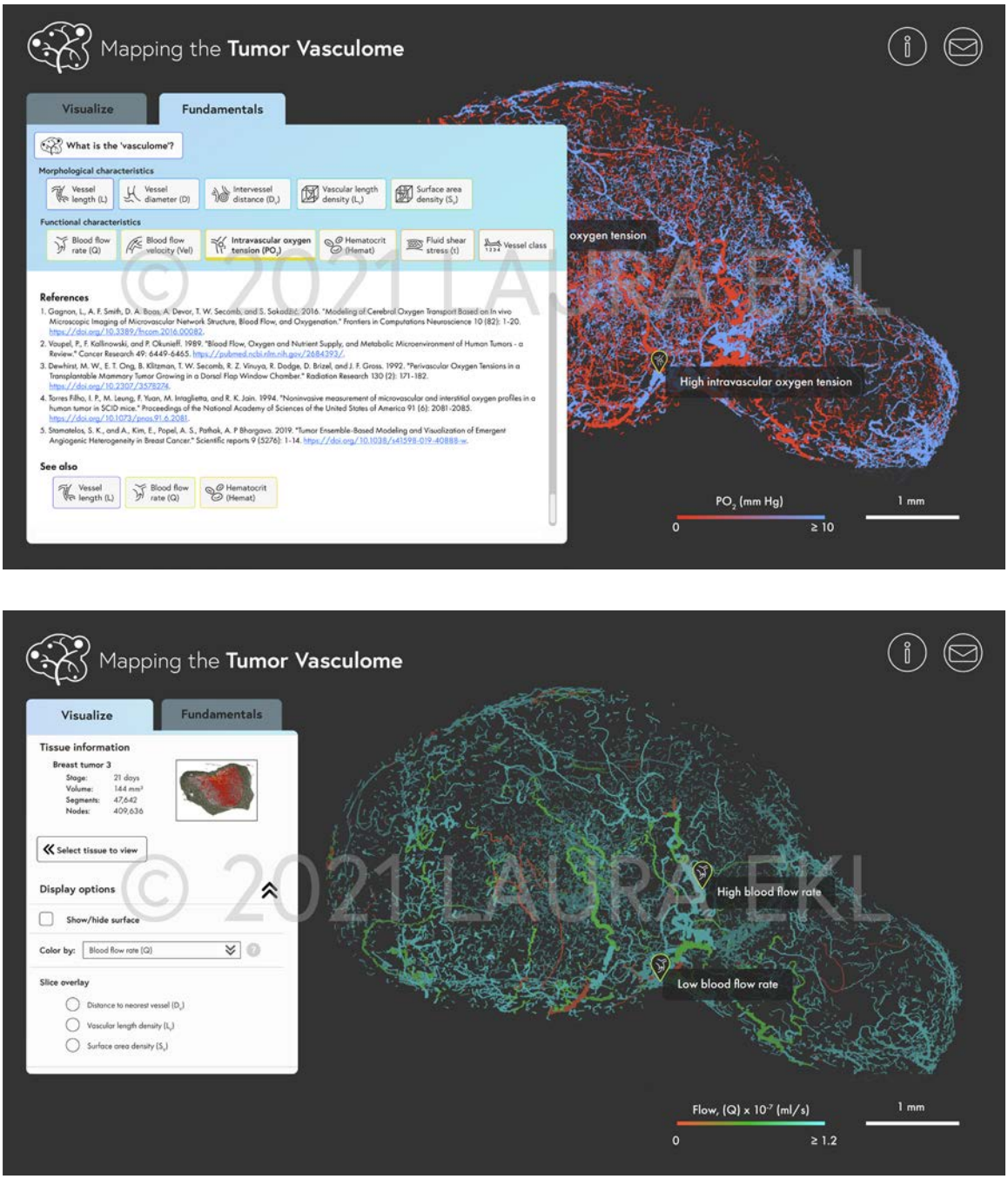

Figure 24.11-.12. Application interfaces. Top: didactic references section with hyperlinks, linked didactic content. Bottom: switch variable display. *Text within image not intended to be read.*

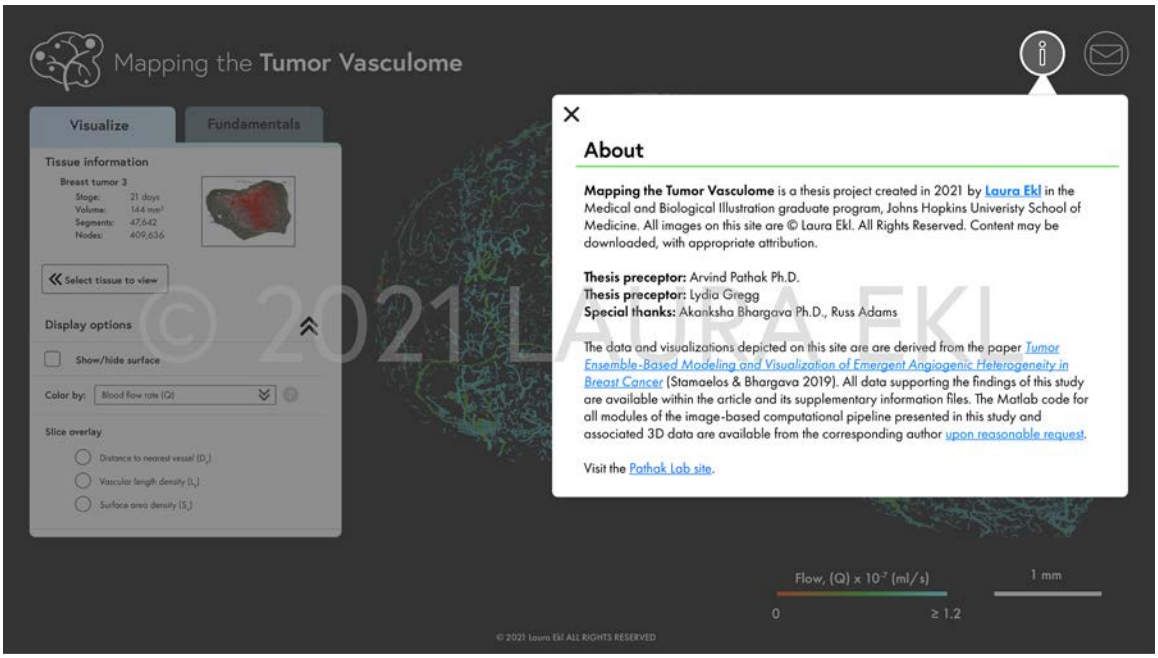

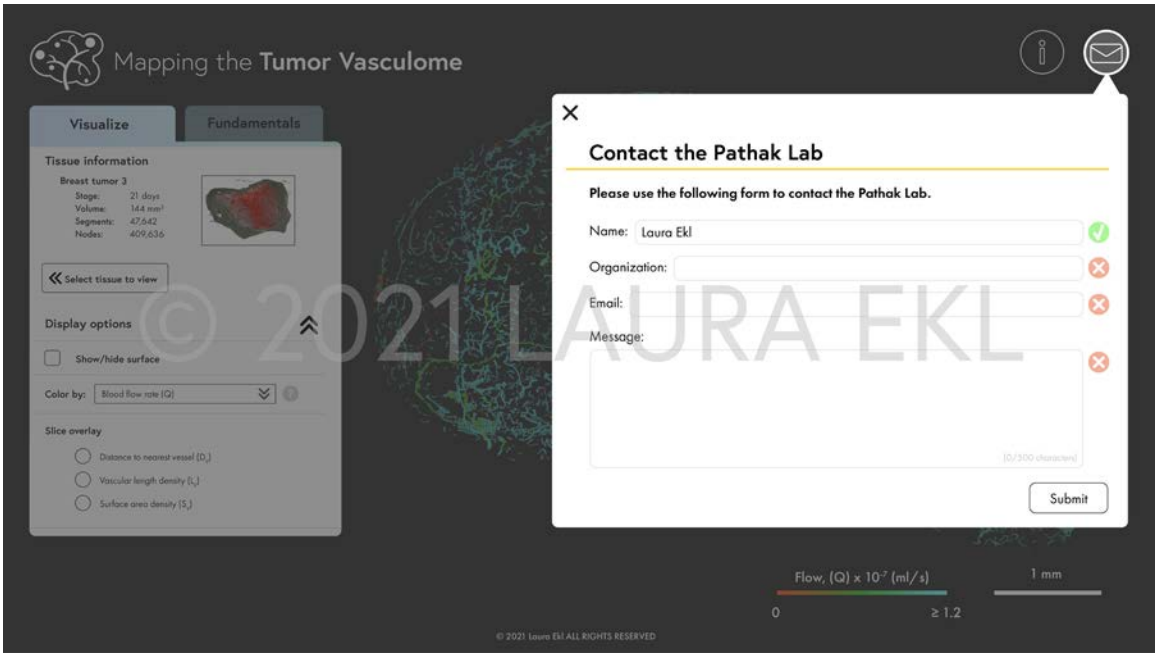

Figure 24.13-.14. Application interfaces. Top: about window. Bottom: switch variable display. *Text within image not intended to be read.*

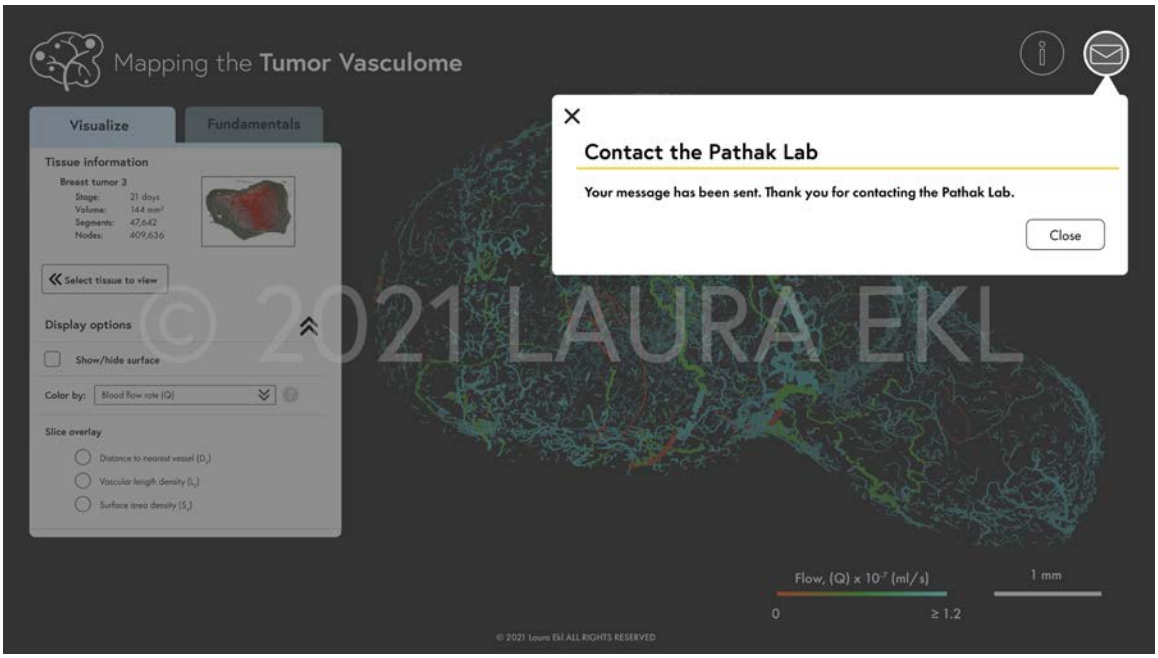

Figure 24.15. Application interfaces. Contact form received message. *Text not intended to be read.*

Vasculome

Definition

'Vasculome' refers to the complete set of characteristics that define the microvascular components of a tissue. The vasculome includes both morphological parameters of the blood vessels, such as vessel length, diameter, and distance to the nearest vessel, as well as functional characteristics, like blood flow velocity, hematocrit, oxygenation, and shear stress.

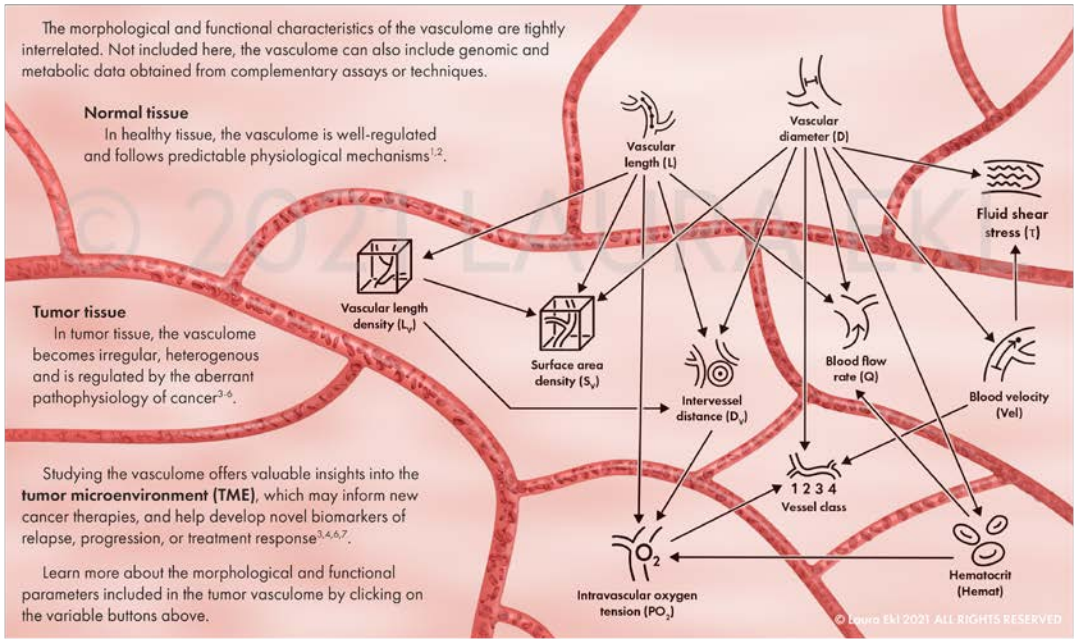

References

1. Popel, A. S., and P. C. Johnson. 2005. "Microcirculation and Hemorheology." *Annual Review of Fluid Mechanics* 37: 43-69. https://doi.org/10.1146/annurev.fluid.37.042604.133933.
2. Pries, A. R., T. W. Secomb, P. Gaehtgens, and J. F. Gross. 1990. "Blood flow in microvascular networks. Experiments and simulation." *Circulation research* 67 (4): 826-834. https://doi.org/10.1161/01.res.67.4.826.
3. Jain, R. K. 1988. "Determinants of Tumor Blood Flow: A Review." *Cancer Research* 48 (10): 2641-2658. https://pubmed.ncbi.nlm.nih.gov/3282647/.
4. Vaupel, P., F. Kallinowski, and P. Okunieff. 1989. "Blood Flow, Oxygen and Nutrient Supply, and Metabolic Microenvironment of Human Tumors - a Review." *Cancer Research* 49: 6449-6465. https://pubmed.ncbi.nlm.nih.gov/2684393/.
5. Konerding, M.A., W. Malkusch, B. Klapthor, C. van Ackern, E. Fait, S. A. Hill, C. Parkins, D. J. Chaplin, M. Presta, and J. Denekamp. 1999. "Evidence for characteristic vascular patterns in solid tumours: quantitative studies using corrosion casts." *British Journal of Cancer* 80 (5/6): 724-732. https://doi.org/10.1038/sj.bjc.6690416.
6. Stamatelos, S. K., and A., Kim, E., Popel, A. S., Pathak, A. P Bhargava. 2019. "Tumor Ensemble-Based Modeling and Visualization of Emergent Angiogenic Heterogeneity in Breast Cancer." *Scientific reports* 9 (5276): 1-14. https://doi.org/10.1038/s41598-019-40888-w.
7. Pathak, A. P., M. F. Penet, and Z. M. Bhujwalla. 2010. "MR Molecular Imaging of Tumor Vasculature and Vascular Targets." *Advances in Genetics* (69): 1-30. https://doi.org/10.1016/S0065-2660(10)69010-4.
8. Stamatelos, S. K., E. Kim, A. P. Pathak, and A. S. Popel. 2014. "A bioimage informatics based reconstruction of breast tumor microvasculature with computational blood flow predictions." *Microvascular research* 91: 8-21. https://doi.org/10.1016/j.mvr.2013.12.003.

Figure 25.1. Didactic window. Vasculome illustration in window with accompanying text. *Text in image not intended to be read; full text included in Appendix A.*

Vessel length (L)

Unit: μm

Definition

Vessel length (L) is defined as the distance between the end points of a blood vessel.

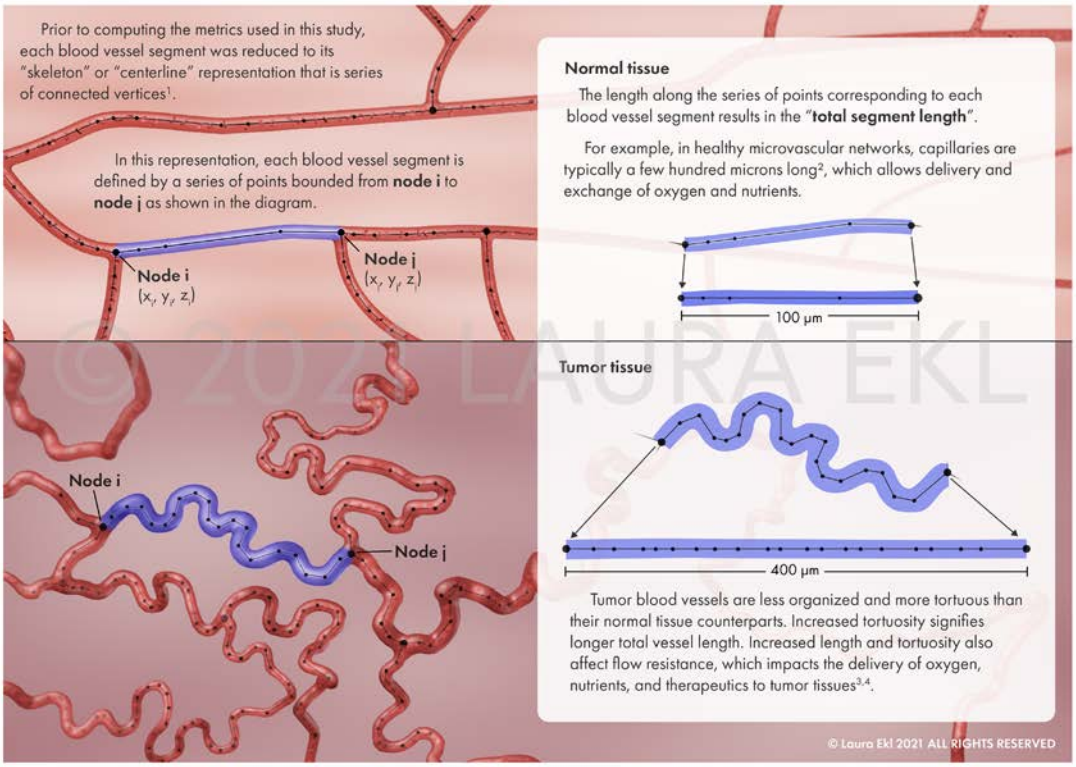

Formula

$$L_{ij} = \sum_{k=i}^{j} \sqrt{(x_{k+1} - x_k)^2 + (y_{k+1} - y_k)^2 + (z_{k+1} - z_k)^2}$$

where L_{ij} is the length of the segment from nodes i to j, and nodes i and j are defined by the Cartesian points (x_i, y_i, z_i), (x_j, y_j, z_j).

References

1. Stamatelos, S. K., E. Kim, A. P. Pathak, and A. S. Popel. 2014. "A bioimage informatics based reconstruction of breast tumor microvasculature with computational blood flow predictions." *Microvascular research* 91: 8-21. https://doi.org/10.1016/j.mvr.2013.12.003.
2. Pries, A. R., and T. W. Secomb. 2003. "Rheology of the microcirculation." *Clinical Hemorheology and Microcirculation* (IOS Press) 29 (3-4): 143-148. https://europepmc.org/article/med/14724335.
3. Hilmas, D. E., and E. L. Gillette. 1974. "Morphometric analyses of the microvasculature of tumors during growth and after x-irradiation." *Cancer* 33: 103-110. https://doi.org/10.1002/1097-0142(197401)33:1<103::AID-CNCR2820330116>3.0.CO;2-7.
4. Stamatelos, S. K., and A., Kim, E., Popel, A. S., Pathak, A. P Bhargava. 2019. "Tumor Ensemble-Based Modeling and Visualization of Emergent Angiogenic Heterogeneity in Breast Cancer." *Scientific reports* 9 (5276): 1-14. https://doi.org/10.1038/s41598-019-40888-w.

See also

Intervessel distance (D_v) | Vascular length density (L_v) | Surface area density (S_v)

Figure 25.2. Didactic window. Vessel length illustration in window with accompanying text. *Text in image not intended to be read; full text included in Appendix A.*

Vessel diameter (D)

Unit: μm

Definition

Vessel diameter (D) is calculated by doubling the radius of the blood vessel, measured orthogonally from the centerline to either side of the vessel lumen.

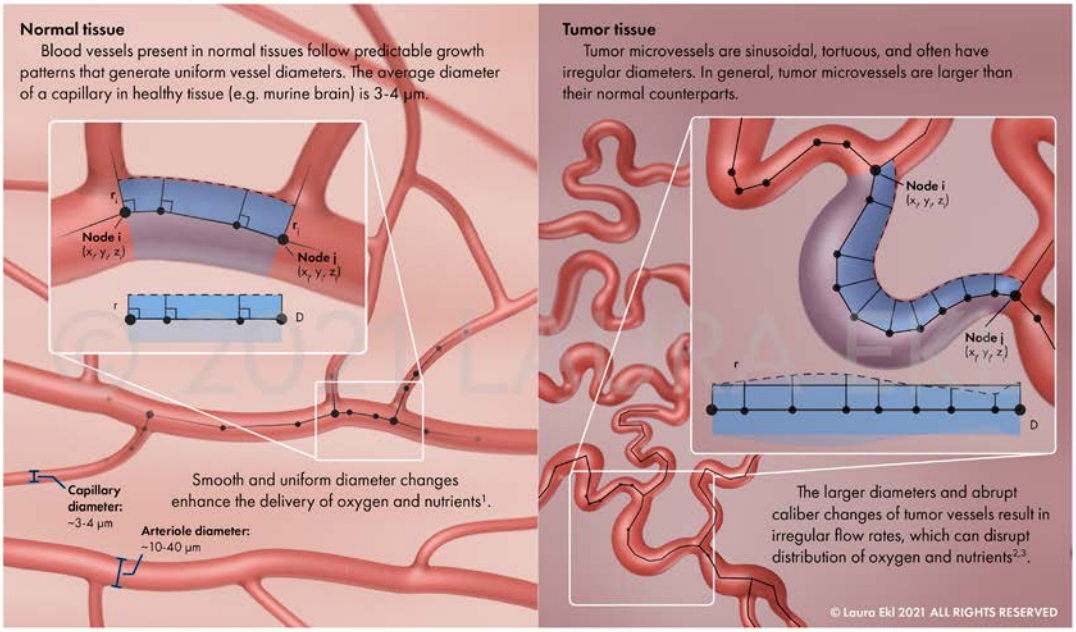

Formula

$$D_{ij} = \frac{2}{j-i+1}\sum_{k=i}^{j} r_k$$

where D_{ij} is blood vessel diameter, r_k is the radius at a point k within the segment bounded from nodes i to j[3,4].

References

1. Quintana, D. D., S. E. Lewis, Y. Anantula, J. A. Garcia, S. N. Sarkar, J. Z. Cavendish, C. M. Brown, and J. W. Simpkins. 2019. "The cerebral angiome: High resolution MicroCT imaging of the whole brain cerebrovasculature in female and male mice." *Neuroimage* 202 (116109): 1-17. https://doi.org/10.1016/j.neuroimage.2019.116109.
2. Leunig, M., F. Yuan, M. D. Menger, Y. Boucher, A. E. Goetz, K. Messmer, and R. K. Jain. 1992. "Angiogenesis, Microvascular Architecture, Microhemodynamics, and Interstitial Fluid Pressure during Early Growth of Human Adenocarcinoma LSI74T in SCID Mice." *Cancer Research* 52 (23): 6553-6560. https://pubmed.ncbi.nlm.nih.gov/1384965/.
3. Stamatelos, S. K., and A., Kim, E., Popel, A. S., Pathak, A. P Bhargava. 2019. "Tumor Ensemble-Based Modeling and Visualization of Emergent Angiogenic Heterogeneity in Breast Cancer." *Scientific reports* 9 (5276): 1-14. https://doi.org/10.1038/s41598-019-40888-w.
4. Stamatelos, S. K., E. Kim, A. P. Pathak, and A. S. Popel. 2014. "A bioimage informatics based reconstruction of breast tumor microvasculature with computational blood flow predictions." *Microvascular research* 91: 8-21. https://doi.org/10.1016/j.mvr.2013.12.003.

See also

Intervessel distance (D_v) | Surface area density (S_v) | Blood flow rate (Q) | Blood flow velocity (Vel) | Fluid shear stress (τ) | Vessel class (1 2 3 4)

Figure 25.3. Didactic window. Vessel diameter illustration in window with accompanying text. *Text in image not intended to be read; full text included in Appendix A.*

Intervessel distance (D_v)

Unit: µm

Definition

Intervessel distance or the **distance to the nearest blood vessel (D_v)** is the 3D Euclidian distance (µm) between a point in the tissue to the nearest blood vessel. Intervessel distance is an indirect measure of the efficacy of extravascular transport of nutrients.

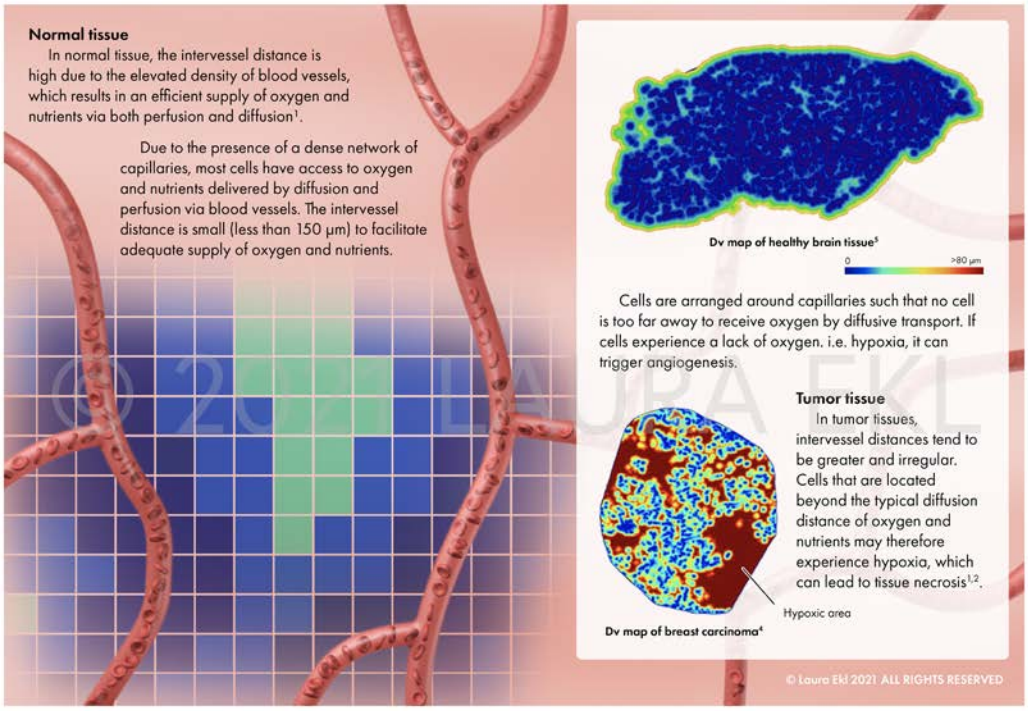

Formula

$$R = \frac{1}{\sqrt{\pi \cdot L_D}}$$

where R is the extravascular diffusion distance and L_D is the vascular length density as described in the next section[3,4].

References

1. Konerding, M.A., W. Malkusch, B. Klapthor, C. van Ackern, E. Fait, S. A. Hill, C. Parkins, D. J. Chaplin, M. Presta, and J. Denekamp. 1999. "Evidence for characteristic vascular patterns in solid tumours: quantitative studies using corrosion casts." *British Journal of Cancer* 80 (5/6): 724-732. https://doi.org/10.1038/sj.bjc.6690416.
2. Baish, J W, T Stylianopoulos, R. M. Lanning, W. S. Kanoun, D. Fukumura, L. L. Munn, and R. K. Jain. 2011. "Scaling rules for diffusive drug delivery in tumor and normal tissues." *Proceedings of the National Academy of Sciences of the United States of America* 108 (5): 1799-1803. https://doi.org/10.1073/pnas.1018154108.
3. Stamatelos, S. K., E. Kim, A. P. Pathak, and A. S. Popel. 2014. "A bioimage informatics based reconstruction of breast tumor microvasculature with computational blood flow predictions." *Microvascular research* 91: 8-21. https://doi.org/10.1016/j.mvr.2013.12.003.
4. Stamatelos, S. K., and A., Kim, E., Popel, A. S., Pathak, A. P, Bhargava. 2019. "Tumor Ensemble-Based Modeling and Visualization of Emergent Angiogenic Heterogeneity in Breast Cancer." *Scientific reports* 9 (5276): 1-14. https://doi.org/10.1038/s41598-019-40888-w.
5. Bhargava, A., Monteagudo, B., Aggarwal, M., Pathak, A. 2020. "A Novel Vascular Fiducials-based Approach (VASFID) for Co-registering Multiscale Imaging Data for Microcirculation Systems Biology." *The FASEB Journal* 34 (S1): 1. https://doi.org/10.1096/fasebj.2020.34.s1.06756.

See also

Vessel length (L) | Vessel diameter (D) | Vascular length density (L_v) | Intravascular oxygen tension (PO_2)

Figure 25.4. Didactic window. Intervessel distance illustration in window with accompanying text. *Text in image not intended to be read; full text included in Appendix A.*

Vascular length density (L_V)

Unit: mm/mm³

Definition

Vascular length density (L_V) is defined as the average length of blood vessels within a unit volume of tissue. Therefore, vascular length density has units of mm/mm³.

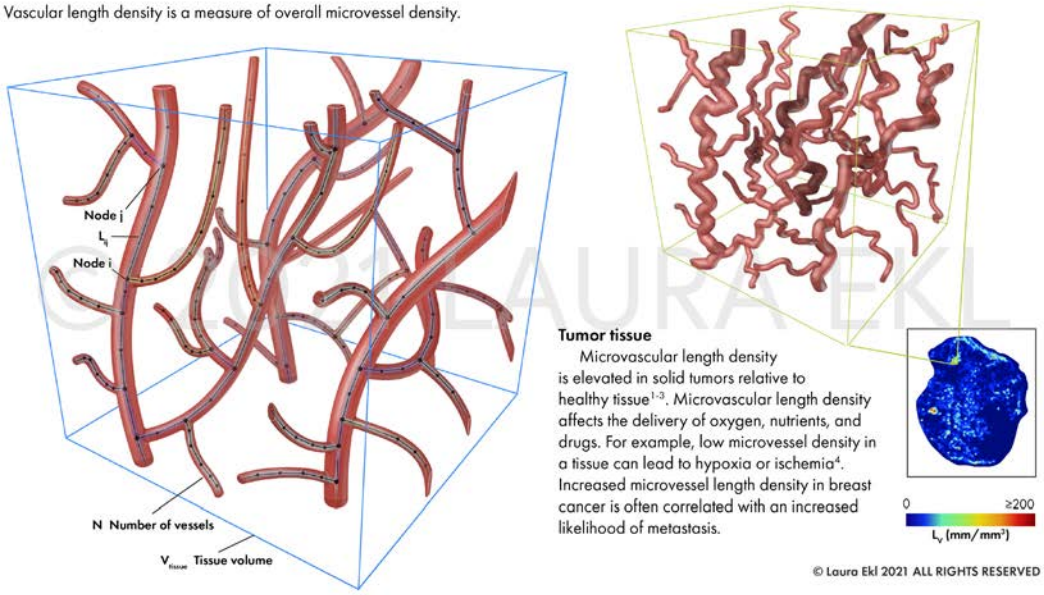

Formula

$$L_D = \frac{1}{V_{tissue}} \sum_{i,j=1}^{N} L_{ij}$$

where L_D is vascular length density (mm/mm³), V_{tissue} is volume of the tissue (mm³), N is the number of vessels, and L_{ij} is the vessel segment length (mm)[3,5].

References

1. Hilmas, D. E., and E. L. Gillette. 1974. "Morphometric analyses of the microvasculature of tumors during growth and after x-irradiation." *Cancer* 33: 103-110. https://doi.org/10.1002/1097-0142(197401)33:1<103::AID-CNCR2820330116>3.0.CO;2-7.
2. Forster, J. C., W. M. Harriss-Phillips, M. J. J. Douglass, and E. Bezak. 2017. "A review of the development of tumor vasculature and its effects on the tumor microenvironment." *Hypoxia* 5: 21-32. https://doi.org/10.2147/HP.S133231.
3. Stamatelos, S. K., and A., Kim, E., Popel, A. S., Pathak, A. P Bhargava. 2019. "Tumor Ensemble-Based Modeling and Visualization of Emergent Angiogenic Heterogeneity in Breast Cancer." *Scientific reports* 9 (5276): 1-14. https://doi.org/10.1038/s41598-019-40888-w.
4. Hasan, J., R. Byers, and G. C. Jayson. 2002. "Intra-tumoural microvessel density in human solid tumours." *British Journal of Cancer* 86 (10): 1566 – 1577. https://doi.org/10.1038/sj.bjc.6600315.
5. Stamatelos, S. K., E. Kim, A. P. Pathak, and A. S. Popel. 2014. "A bioimage informatics based reconstruction of breast tumor microvasculature with computational blood flow predictions." *Microvascular research* 91: 8-21. https://doi.org/10.1016/j.mvr.2013.12.003.

See also

Vessel length (L) | Surface area density (S_V)

Figure 25.5. Didactic window. Vascular length density illustration in window with accompanying text. *Text in image not intended to be read; full text included in Appendix A.*

Vascular surface area density (S_V)

Unit: mm/mm³

Definition

Vascular surface area density (S_V) is the average surface area of the blood vessel in a unit volume of tissue. Therefore, the units for vascular surface area density are mm² per mm³.

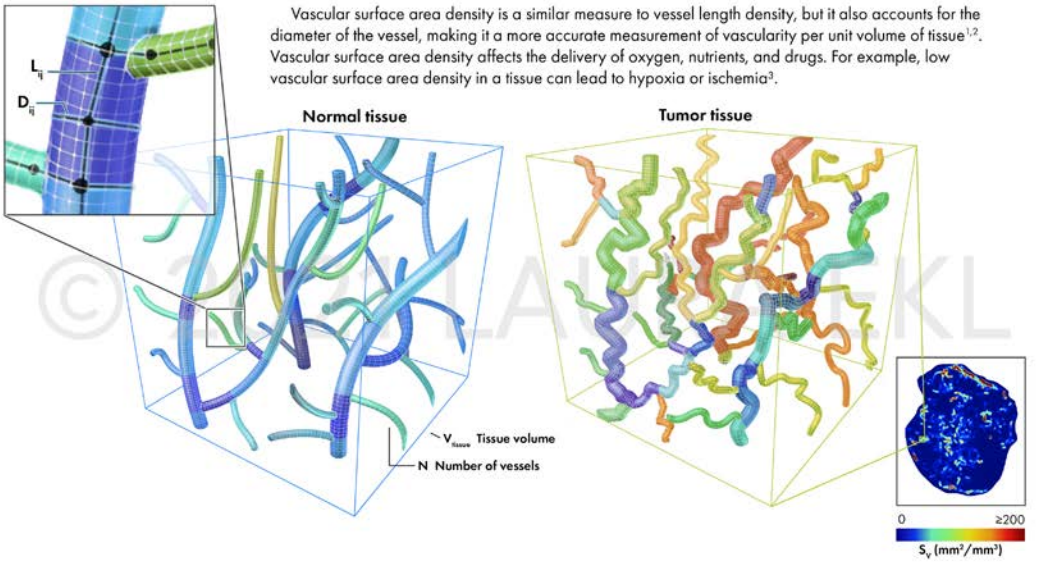

Vascular surface area density is a similar measure to vessel length density, but it also accounts for the diameter of the vessel, making it a more accurate measurement of vascularity per unit volume of tissue[1,2]. Vascular surface area density affects the delivery of oxygen, nutrients, and drugs. For example, low vascular surface area density in a tissue can lead to hypoxia or ischemia[3].

Formula

$$S_D = \frac{1}{V_{tissue}} \sum_{i,j=1}^{N} \pi \cdot D_{ij} \cdot L_{ij}$$

where S_D is vascular surface density (mm²/mm³), V_{tissue} is volume of the tissue (mm³), N is the number of vessels, D_{ij} is the diameter of the segment between nodes i and j, L_{ij} is the length of the segment between nodes i and j (mm)[2,4].

References

1. Forster, J. C., W. M. Harriss-Phillips, M. J. J. Douglass, and E. Bezak. 2017. "A review of the development of tumor vasculature and its effects on the tumor microenvironment." *Hypoxia* 5: 21-32. https://doi.org/10.2147/HP.S133231.
2. Stamatelos, S. K., and A., Kim, E., Popel, A. S., Pathak, A. P Bhargava. 2019. "Tumor Ensemble-Based Modeling and Visualization of Emergent Angiogenic Heterogeneity in Breast Cancer." *Scientific reports* 9 (5276): 1-14. https://doi.org/10.1038/s41598-019-40888-w.
3. Hasan, J., R. Byers, and G. C. Jayson. 2002. "Intra-tumoural microvessel density in human solid tumours." *British Journal of Cancer* 86 (10): 1566 – 1577. https://doi.org/10.1038/sj.bjc.6600315.
4. Stamatelos, S. K., E. Kim, A. P. Pathak, and A. S. Popel. 2014. "A bioimage informatics based reconstruction of breast tumor microvasculature with computational blood flow predictions." *Microvascular research* 91: 8-21. https://doi.org/10.1016/j.mvr.2013.12.003.

See also

Vessel length (L) | Vessel diameter (D) | Vascular length density (L_V)

Figure 25.6. Didactic window. Vascular surface area density illustration in window with accompanying text. *Text in image not intended to be read; full text included in Appendix A.*

Blood flow rate (Q)

Unit: ml/s

Definition

Blood flow rate (Q) is a measure of the volume of blood flowing per unit time (e.g. measured in ml/s) within a blood vessel segment.

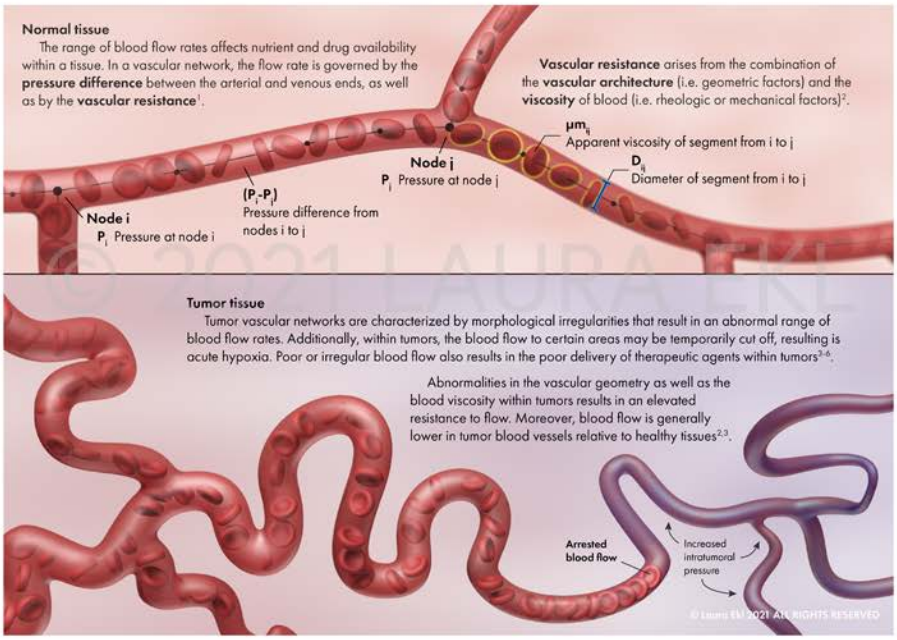

Formula

$$Q_{ij} = G_{ij} \cdot (P_i - P_j)$$

where Q_{ij} is the blood flow rate of the segment between nodes i and j, G_{ij} is the hydraulic conductance of a segment, and (P_i-P_j) is the pressure drop from nodes i to j.

$$G_{ij} = \frac{\pi \cdot D_{ij}^{4}}{128 \cdot \mu_{ij} \cdot L_{ij}}$$

G_{ij} can be further defined, where D_{ij} is the diameter of the segment from nodes i to j, μ_{ij} is the apparent viscosity of the segment from nodes i to j, and L_{ij} is the length of the segment from nodes i to j.

$$\sum_{i,j=1}^{N} Q_{ij} = 0$$

where N is the number of vessel segments, and Q_{ij} is the flow rate between nodes i and j.

References

1. Gagnon, L., A. F. Smith, D. A. Boas, A. Devor, T. W. Secomb, and S. Sakadžić. 2016. "Modeling of Cerebral Oxygen Transport Based on In vivo Microscopic Imaging of Microvascular Network Structure, Blood Flow, and Oxygenation." *Frontiers in Computations Neuroscience* 10 (82): 1-20. https://doi.org/10.3389/fncom.2016.00082.
2. Jain, R. K. 1999. "Transport of Molecules, Particles, and Cells in Solid Tumors." *Annual review of biomedical engineering* 1 (1): 241-263. https://doi.org/10.1146/annurev.bioeng.1.1.241.
3. Leunig, M., F. Yuan, M. D. Menger, Y. Boucher, A. E. Goetz, K. Messmer, and R. K. Jain. 1992. "Angiogenesis, Microvascular Architecture, Microhemodynamics, and Interstitial Fluid Pressure during Early Growth of Human Adenocarcinoma LS174T in SCID Mice." *Cancer Research* 52 (23): 6553-6560. https://pubmed.ncbi.nlm.nih.gov/1384965/.
4. Jain, R. K. 1988. "Determinants of Tumor Blood Flow: A Review." *Cancer Research* 48 (10): 2641-2658. https://pubmed.ncbi.nlm.nih.gov/3282647/.
5. Torres Filho, I. P., M. Leung, F. Yuan, M. Intaglietta, and R. K. Jain. 1994. "Noninvasive measurement of microvascular and interstitial oxygen profiles in a human tumor in SCID mice." *Proceedings of the National Academy of Sciences of the United States of America* 91 (6): 2081-2085. https://doi.org/10.1073/pnas.91.6.208.
6. Stamatelos, S. K., and A., Kim, E., Popel, A. S., Pathak, A. P Bhargava. 2019. "Tumor Ensemble-Based Modeling and Visualization of Emergent Angiogenic Heterogeneity in Breast Cancer." *Scientific reports* 9 (5276): 1-14. https://doi.org/10.1038/s41598-019-40888-w.
7. Stamatelos, S. K., E. Kim, A. P. Pathak, and A. S. Popel. 2014. "A bioimage informatics based reconstruction of breast tumor microvasculature with computational blood flow predictions." *Microvascular research* 91: 8-21. https://doi.org/10.1016/j.mvr.2013.12.003.

See also

Vessel length (L) | Vessel diameter (D) | Hematocrit (Hemat)

Figure 25.7. Didactic window. Blood flow rate illustration in window with accompanying text. *Text in image not intended to be read; full text included in Appendix A.*

Intravascular oxygen tension (PO_2)

Units: mmHg

Definition

Intravascular oxygen tension (PO_2) is the partial pressure of oxygen (measured in mmHg) inside blood vessels.

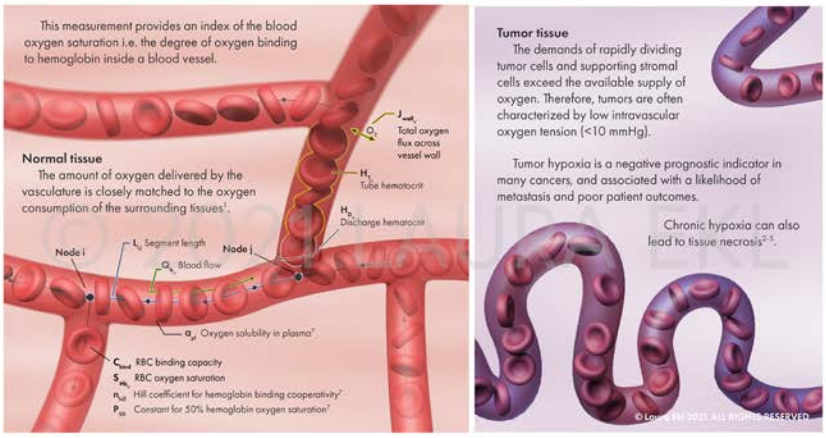

Formula

$$Q_{b_{i,j}} \cdot \left(\alpha_{b_{i,j}} \cdot \Delta P_{i,j} + H_{D_{i,j}} \cdot C_{bind} \cdot \Delta S_{Hb}\right) = J_{wall_{i,j}} \quad (1)$$

where

$$J_{wall_{i,j}} = M_c \cdot m_{tissue} \cdot \frac{L_{ij}}{\sum_{i,j=1}^{N} L_{ij}} \quad (2)$$

$$\alpha_{b_{i,j}} = H_{T_{i,j}} \cdot \alpha_{RBC} + \left(1 - H_{T_{i,j}}\right) \cdot \alpha_{pl} \quad (3)$$

$$S_{Hb_{i,j}}(P_{i,j}) = \frac{P_{ij}^{n_{hill}}}{P_{ij}^{n_{hill}} + P_{50}^{n_{hill}}} \quad (4)$$

Here, values of blood flow $Q_{b_{ij}}$, discharge hematocrit $H_{D_{ij}}$, and tube hematocrit $H_{T_{ij}}$ in the individual vessels segments ij of length L_{ij} (where i and j represent branching or boundary nodes) are estimated from the blood flow model. P_{ij} is the oxygen tension in the blood, C_{bind} and $S_{Hb_{ij}}$ are reb blood cells' binding capacity and oxygen saturation respectively; $J_{wall_{ij}}$ is the total oxygen flux across the vessel wall for vessel segment of length $L_{ij} \cdot M_c$ is the oxygen consumption rate for breast cancer xenografts derived from Vaupel et al[2], m_{tissue} is the tissue mass; n_{hill} is the Hill coefficient for hemoglobin binding cooperativity (2.7)[7], P_{50} is the constant for 50% hemoglobin oxygen saturation (37 mmHg)[7], and α_{pl} is the oxygen solubility in plasma (2.82×10^{-5}ml O_2/ml tissue/mmHg)[7].

With the application of appropriate boundary conditions, Equation 1 can be transformed to the following system of equations:

$$(D_{int} + S_{int}) \cdot P_{int} = (D_{bound} + S_{bound}) \cdot P_{bound} + J_{wall} \quad (5)$$

where, D_{int} and S_{int} are the sparse matrices containing the transport coefficients for dissolved and bound oxygen derived from Equation 1 for branching nodes; P_{int} is the oxygen tension vector for branching nodes; D_{bound} and S_{bound} are the vectors of intravascular transport coefficients for boundary segments; P_{bound} is the oxygen partial pressure vector for boundary segments. This system is solved for oxygen tension (P_{int}) at all branching nodes and then S_{Hb} values are updated based on Equation 4.

References

1. Gagnon, L., A. F. Smith, D. A. Boas, A. Devor, T. W. Secomb, and S. Sakadžić. 2016. "Modeling of Cerebral Oxygen Transport Based on In vivo Microscopic Imaging of Microvascular Network Structure, Blood Flow, and Oxygenation." Frontiers in Computations Neuroscience 10 (82): 1-20. https://doi.org/10.3389/fncom.2016.00082.
2. Vaupel, P., F. Kallinowski, and P. Okunieff. 1989. "Blood Flow, Oxygen and Nutrient Supply, and Metabolic Microenvironment of Human Tumors - a Review." Cancer Research 49: 6449-6465. https://pubmed.ncbi.nlm.nih.gov/2684393/.
3. Dewhirst, M. W., E. T. Ong, B. Klitzman, T. W. Secomb, R. Z. Vinuya, R. Dodge, D. Brizel, and J. F. Gross. 1992. "Perivascular Oxygen Tensions in a Transplantable Mammary Tumor Growing in a Dorsal Flap Window Chamber." Radiation Research 130 (2): 171-182. https://doi.org/10.2307/3578274.
4. Torres Filho, I. P., M. Leung, F. Yuan, M. Intaglietta, and R. K. Jain. 1994. "Noninvasive measurement of microvascular and interstitial oxygen profiles in a human tumor in SCID mice." Proceedings of the National Academy of Sciences of the United States of America 91 (6): 2081-2085. https://doi.org/10.1073/pnas.91.6.2081.
5. Stamatelos, S. K., and A., Kim, E., Popel, A. S., Pathak, A. P Bhargava. 2019. "Tumor Ensemble-Based Modeling and Visualization of Emergent Angiogenic Heterogeneity in Breast Cancer." Scientific reports 9 (5276): 1-14. https://doi.org/10.1038/s41598-019-40888-w.

See also

Vessel length (L) | Blood flow rate (Q) | Hematocrit (Hemat)

Figure 25.8. Didactic window. Intravascular oxygen tension illustration in window with accompanying text. *Text in image not intended to be read; full text included in Appendix A.*

Hematocrit (Hemat)

Unit: Percentage

Definition

Hematocrit (Hemat) is the volume of red blood cells (erythrocytes) in a given volume of blood expressed as a percentage.

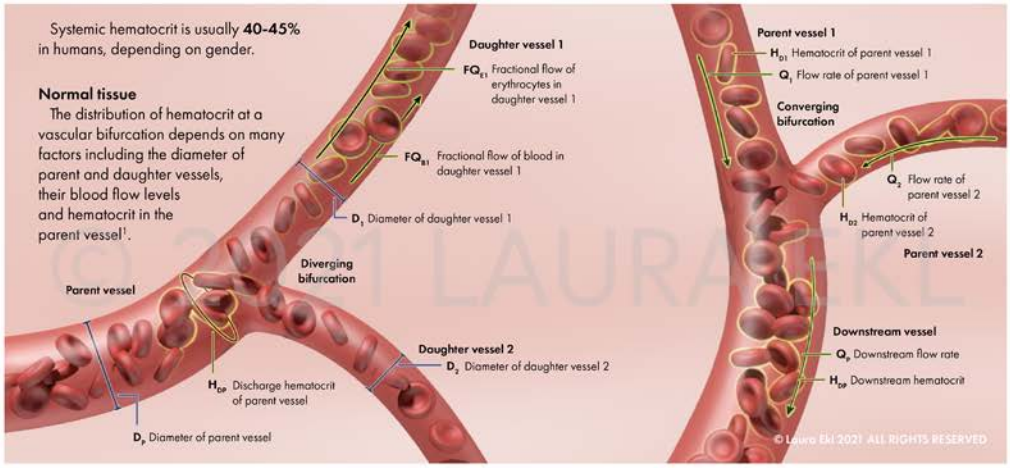

Formula

$$\text{logit}(FQ_{E1}) = A + B \cdot \text{logit}\left(\frac{FQ_{B1} - X_0}{1 - 2 \cdot X_0}\right)$$

$$A = -\frac{6.96 \cdot \ln\left(\frac{D_1}{D_2}\right)}{D_P}$$

$$B = 1 + 6.98 \cdot \left(\frac{1 - H_{DP}}{D_P}\right)$$

$$X_0 = \frac{0.4}{D_P}$$

Logit is the inverse of the sigmoidal logistic function *log(p)-log(1-p)*, where 0<p<1. FQ_{E1} and FQ_{B1} are the fractional flows of erythrocytes and blood in daughter branch 1. D_1, D_2, and D_P are the diameters of the daughter branches and parent segment, respectively. H_{DP} is the discharge hematocrit in the parent segment. A, B, and X_0 are empirically measured constants[2]. Consequently, the hematocrit in daughter branch 1 is calculated according to:

$$H_{D1} = \frac{FQ_{E1} \cdot H_{DP} \cdot Q_P}{Q_1}$$

In a converging bifurcation, downstream hematocrit (H_{DP}) is estimated by downstream flow rate (Q_P) as well as the hematocrits (H_{D1}, H_{D2}) and flow rates (Q_1, Q_2) in the two parent segments:

$$H_{DP} \cdot Q_P = H_{D1} \cdot Q_1 + H_{D2} \cdot Q_2$$

Estimation of updated hematocrit leads to new values for viscosity.

References

1. Popel, A. S., and P. C. Johnson. 2005. "Microcirculation and Hemorheology." *Annual Review of Fluid Mechanics* 37: 43-69. https://doi.org/10.1146/annurev.fluid.37.042604.133933.
2. Stamatelos, S. K., and A., Kim, E., Popel, A. S., Pathak, A. P Bhargava. 2019. "Tumor Ensemble-Based Modeling and Visualization of Emergent Angiogenic Heterogeneity in Breast Cancer." *Scientific reports* 9 (5276): 1-14. https://doi.org/10.1038/s41598-019-40888-w.
3. Stamatelos, S. K., E. Kim, A. P. Pathak, and A. S. Popel. 2014. "A bioimage informatics based reconstruction of breast tumor microvasculature with computational blood flow predictions." *Microvascular research* 91: 8-21. https://doi.org/10.1016/j.mvr.2013.12.003.

See also

Vessel diameter (D) | Blood flow rate (Q) | Intravascular oxygen tension (PO_2) | Fluid shear stress (τ)

Figure 25.9. Didactic window. Hematocrit illustration in window with accompanying text. *Text in image not intended to be read; full text included in Appendix A.*

Shear stress (τ)

Units: dyne/cm²

Definition

Shear stress (τ) is the frictional force experienced by adjacent layers of a fluid due to its motion, expressed in dyne/cm².

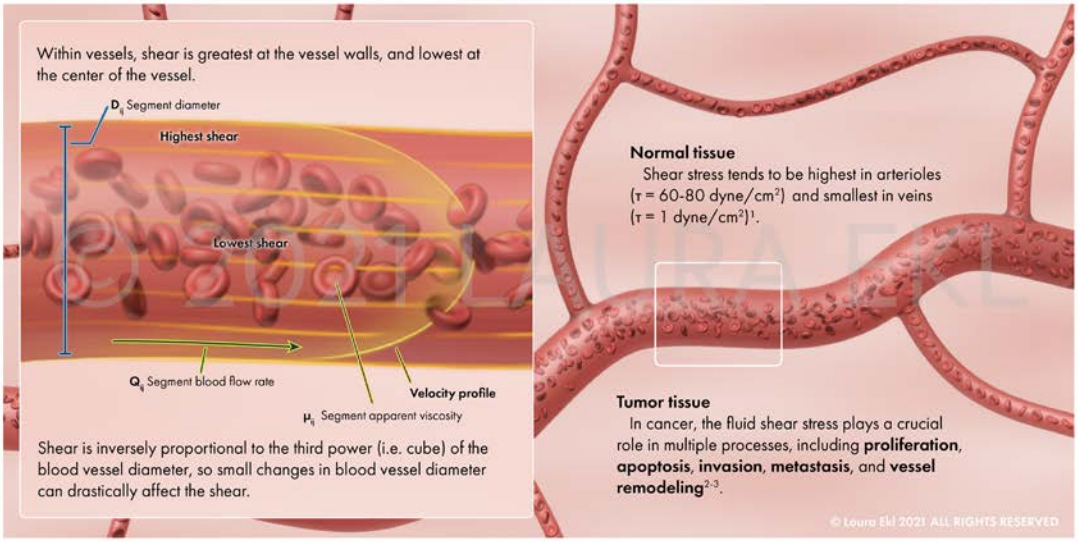

Formula

$$\tau_{ij} = \frac{32 \cdot \mu_{ij} \cdot Q_{ij}}{\pi \cdot {D_{ij}}^3}$$

where τ_{ij} is the wall shear stress, μ_{ij} is the segment apparent viscosity, Q_{ij} is the simulated segment blood flow rate, D_{ij} is the segment diameter[4,6].

References

1. Ballermann, B. J., A. Dardik, E. Eng, and A. Liu. 1998. "Shear stress and the endothelium." *Kidney International* 54 (67): S-100-S-108. https://doi.org/10.1046/j.1523-1755.1998.06720.x.
2. Jain, R. K., J. D. Martin, and T. Stylianopoulos. 2014. "The role of mechanical forces in tumor growth and therapy." *Annual review of biomedical engineering* 16: 321-346. https://doi.org/10.1146/annurev-bioeng-071813-105259.
3. Huang, Q., X. Hu, W. He, Y. Zhao, S. Hao, Q. Wu, S. Li, S. Zhang, and M. Shi. 2018. "Fluid shear stress and tumor metastasis." *American journal of cancer research* 8 (5): 763-777.
4. Stamatelos, S. K., E. Kim, A. P. Pathak, and A. S. Popel. 2014. "A bioimage informatics based reconstruction of breast tumor microvasculature with computational blood flow predictions." *Microvascular research* 91: 8-21. https://doi.org/10.1016/j.mvr.2013.12.003.
5. Kamoun, W. S., S. S. Chae, D. A. Lacorre, J. A. Tyrell, M. Mitre, M. A. Gillissen, D. Fukumura, R. K. Jain, and L. L. Munn. 2010. "Simultaneous measurement of RBC velocity, flux, hematocrit and shear rate in tumor vascular networks." *Nature methods* 7 (8): 655–660. https://doi.org/10.1038/nmeth.1475.
6. Stamatelos, S. K., and A., Kim, E., Popel, A. S., Pathak, A. P Bhargava. 2019. "Tumor Ensemble-Based Modeling and Visualization of Emergent Angiogenic Heterogeneity in Breast Cancer." *Scientific reports* 9 (5276): 1-14. https://doi.org/10.1038/s41598-019-40888-w.

See also

Vessel diameter (D) | Blood flow rate (Q) | Hematocrit (Hemat)

Figure 25.10. Didactic window. Fluid shear stress illustration in window with accompanying text. *Text in image not intended to be read; full text included in Appendix A.*

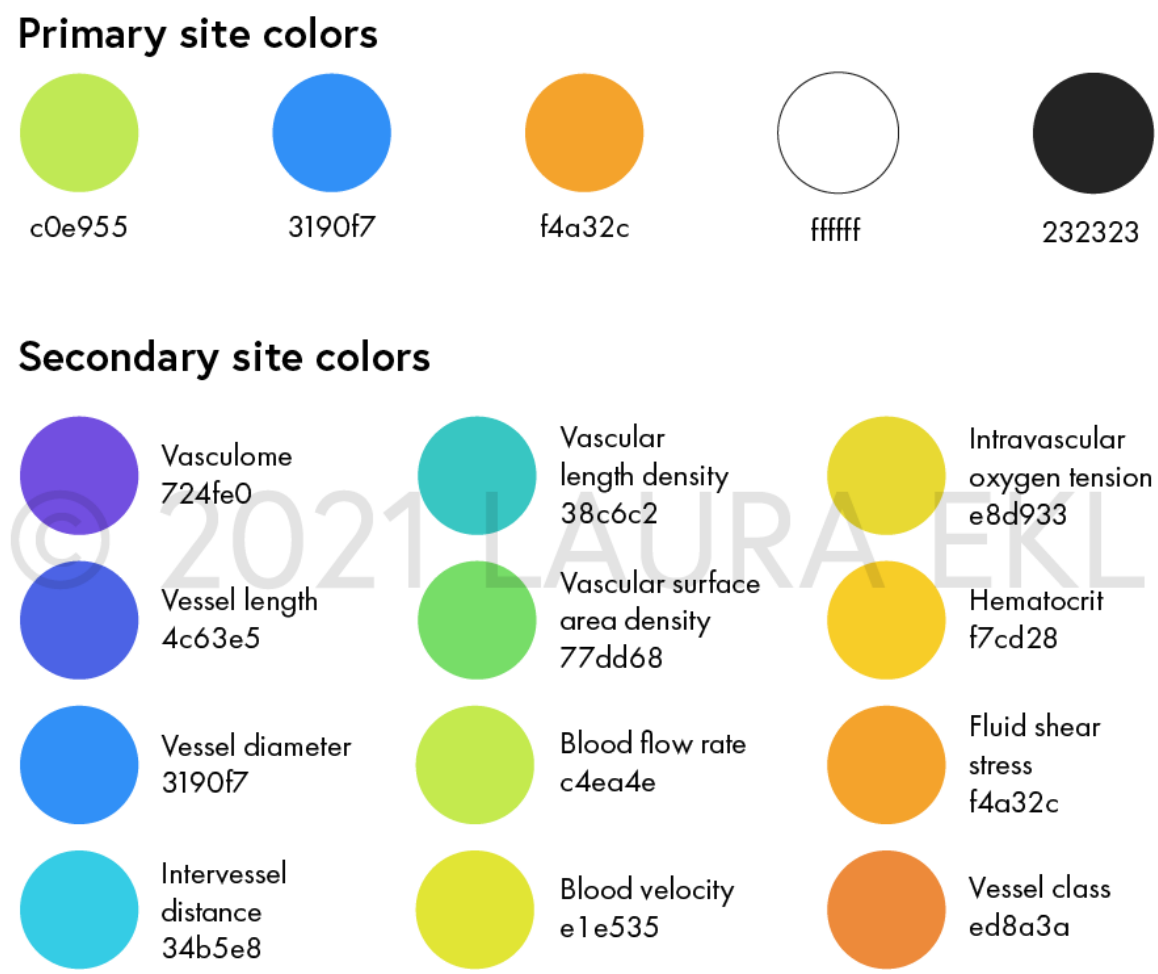

Figure 26.1. Style guide. Site colors.

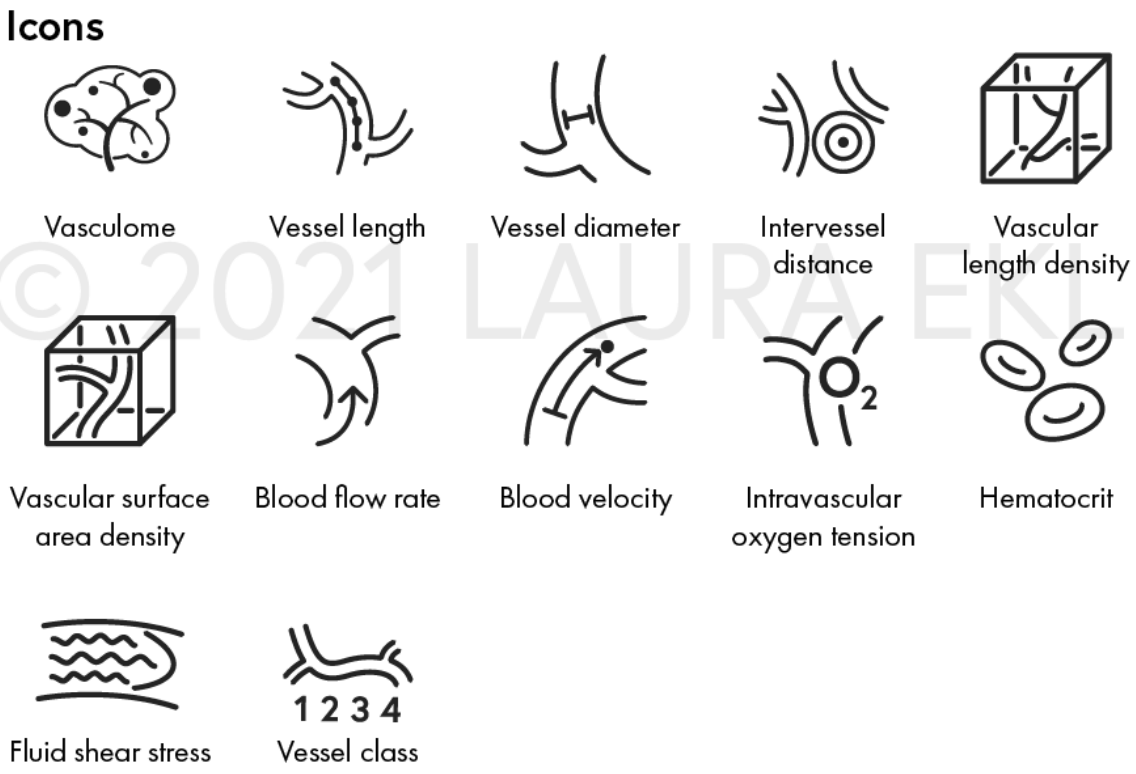

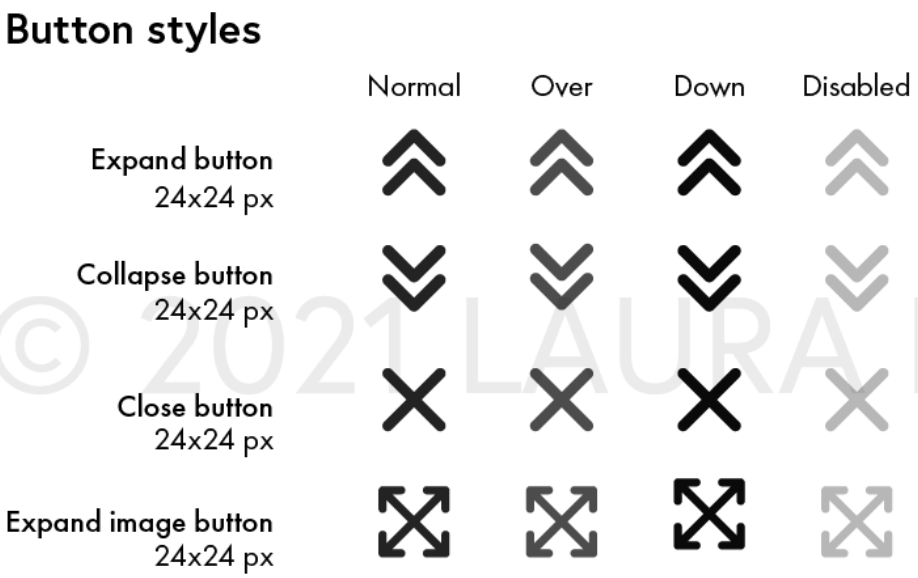

Figure 26.2. Style guide. Icon and button styles.

Button styles

Figure 26.3. Style guide. About and Contact button styles.

Typefaces

Europa

Regular	Sphinx of black quartz, judge my vow
Bold	**Sphinx of black quartz, judge my vow**

Futura PT

Book	Sphinx of black quartz, judge my vow
Book Oblique	Sphinx of black quartz, judge my vow
Demi	**Sphinx of black quartz, judge my vow**

Cambria Math

Regular	Sphinx of black quartz, judge my vow

Font styles

H1	**Europa Bold 24 pt**
H2	**Europa Bold 20 pt**
H3	**Futura PT Demi 16 pt**
Body & Illustration text	Futura PT Book 16 pt
Labels	Futura PT Book 12 pt
Button	Europa Regular 16 pt
Equation	Cambria Math 16 pt

Figure 26.4. Style guide. Typefaces and font styles.

Figure 26.5. Style guide. Didactic button states.

Figure 27. Full models. Soft tissue surface models in Zbrush. Top row: connective tissue surface (right: inferior view, left: superior view.) Bottom row: tumor surface model (right: inferior view, left: superior view).

Figure 28. Full models. Soft tissue (transparent) and tumor surface models aligned in Zbrush.

Access to Assets

The products created from this thesis can be viewed at www.pathaklab.org, www.eklmedicalillustrations.com, or by contacting the author at **lauramarieekl@gmail.com**. The author may also be contacted through the Department of Art as Applied to Medicine at Johns Hopkins University School of Medicine, **http://medicalart.johnshopkins.edu/**.

Discussion

Visualization of complex datasets

As imaging resolution increases and computers become more powerful, research datasets are becoming exponentially larger. The inherent size and complexity of research data is something that biomedical communicators must continue to grapple with while developing new visualization methods. In this case, the tumor vasculome dataset contained 70k+ points, each with multiple parameter values attached, resulting in hundreds of thousands cumulative points. Initially, the visualization was planned as a surface model that could be optimized. While Amira can export .obj files from a spatial graph, it is unable to remap the color-coding of the variables onto the .obj file. Unity was considered for the final visualization platform, but PlayCanvas was determined to offer more efficient web rendering.

In PlayCanvas, the size of the dataset still necessitated advanced optimization: the spatial graph data points were optimized for loading into the site by removing points that were close together, mapping the geometry on to the spatial graph points and rendering edges as cubes to reduce additional geometry as much as possible, and removing all lighting and shadows from the scene.

Interactive 3D visualization of high-resolution research datasets will be critical for faster and more effective learning by students and researchers. It is known that simulation is useful to assist students in developing a mental model of new content (Dunsworth, Murphy, and Wu 2020, Nowak and Borkowsku 2013). The best way to develop an accurate mental model is through interaction with the system (Dunsworth, Murphy, and Wu 2020, Norman 1983). As more and new types of data become prevalent, it is important to consider how these might be leveraged for more effective teaching.

Content development

The development of the didactic content for this project integrated best practices for teaching and learning hemodynamics. The variables were consistently included with their symbols and appropriate physical units because one of the first skills students must learn in bioengineering is the ability to precisely communicate quantities and variables with the correct units (Bellloni 1995). User cognitive load was reduced by minimizing text where possible (Sweller 1988, Sweller, Ayres, and Kalyuga 2011), and content was organized from most basic to most complex, i.e., starting

with the overarching term (e.g., vasculome) and the most fundamental definitions (e.g., length and diameter), and building upon these as other parameters were introduced (e.g., elaboration theory). Multiple tenets from the cognitive theory of multimedia learning were applied to foster generative processing (multimedia principle) and reduce extraneous processing (principles of coherence, signaling, and spatial contiguity) (Mayer 2001). The multimedia principle was heavily utilized (i.e., text with complementary illustrations and images from research papers) to enhance generative processing. When generating the didactic text and visual components, extraneous text and imagery were removed to reduce cognitive load (coherence principle). Key words and phrases were bolded (signaling principle), and labels were placed as close to the visual subject as possible (spatial contiguity principle).

The wireframes were developed in accordance with UI/UX best practices and underwent integrative rounds of review and revision. Initially, the wireframes had accordion menus, but these were swapped for buttons. The Apple usability guides (https://developer.apple.com/design/human-interface-guidelines/) and Nielsen Norma group (https://www.nngroup.com/) guidelines were followed for button size. A different typeface was used for mathematical formulas to improve legibility.

Future directions

This project developed a novel workflow for an interactive, 3D data-driven educational resource describing “the tumor vasculome”. Future development of the project could focus on coding and expanding additional interaction pathways laid out in the flowchart. The current visualizations are based on the data generated in Stamatelos and Bhargava et. al 2019, and a data set from a future publication on the murine brain vasculome. Since the code is extensible to any vasculome data supplied in the correct spatial graph format, the visualization can be adapted for any number of other tissue samples, both healthy and diseased, as well as for preclinical or human data.

In addition to adding more tissue samples, the didactic section could be expanded with the inclusion of additional morphological or functional parameters. For example, perfusion is another commonly measured functional parameter (defined as the blood flow rate in a unit volume of tissue). Viscosity, blood pressure, branchpoint density (Fenton and Zweifach 1981), tortuosity (Seaman, et al. 2011), lacunarity (Zudaire, et al. 2011), fractal dimension (Seaman, et al. 2011),

vessel segment partitioning (Corliss, et al. 2019), are other parameters that could also be represented.

The spatial graph data structure can be applied to other branching structures, namely lymphatic vessels or neurons. Lymphatic vessels play a crucial role in fluid transport and immune function within the tumor (Alitalo, et al. 2005). These vessels are structurally and functionally abnormal within tumors, leading to poor lymphatic function. The subsequently high interstitial pressure within tumors can cause blood and lymphatic vessels to collapse and decrease perfusion of oxygen, nutrients, and drugs, making lymphatic vessels another exciting area of cancer research (Paderal, et al. 2002). The spatial graph format could also be used to describe the lengths, diameters, length and surface area densities, and other variables to quantify abnormalities in the tumor lymphatic vessels and reveal new insights into the tumor vasculome.

Additional user functionality could be added to enhance the viewers experience:

- A tutorial mode when entering the site for first time.
- The ability to upload/attach a dataset to the contact form to share additional tissue data.
- A data orientation indicator.
- The ability to snap to orthogonal views.
- Cross section visualization.
- Split-screen comparison with other tissues.
- Further development of multimedia content (i.e., additional illustrations and animations).

Conclusion

The vasculome is an emerging concept in biology which encompasses the delicate interplay between morphological and functional characteristics of a vascular network, leading to the development of distinct microenvironments. In tumors, such microenvironments are known to impact progression, metastasis, and prognosis. The concept of the vasculome offers students and researchers a complex model for fully understanding how hemodynamic parameters affect each other, and the physiology of the tissue as a whole.

This thesis addresses the current lack of resources for interactive tumor vasculome visualization and depicts of the components of the tumor vasculome through an accessible, web-based visualization platform. Expected benefits of this platform include increased understanding of the morphological and functional hemodynamic concepts that characterize the vasculome, as well as the spatial arrangement of tumor blood vessels.

A didactic visualization resource will enhance understanding and contribute to discussions at the forefront of research in cancer biology. Such resources would also advance research efforts by highlighting the significance of fundamental vascular and hemodynamic properties of the tumor vasculome in cancer etiology. This web resource provides a novel platform to further enhance our understanding of the role of the vasculome in health and disease.

Works Cited

Alitalo, K., Tammela, T., Petrova, T. V. 2005. “Lymphangiogenesis in development and human disease.” Nature 438 (7070): 946-953.

American Cancer Society. 2019. *Cancer Facts & Figures 2019.* Annual publication, Atlanta: American Cancer Society.

Anderson, A. R. A., A. M. Weaver, P. T. Cummings, and V. Quaranta. 2006. “Tumor Morphology and Phenotypic Evolution Driven by Selective Pressure from the Microenvironment.” *Cell* 127 (5): 905-915.

Badeer, H. S. 2001. “Hemodynamics for Medical Students.” *Advances in Physiology Education* 25 (1): 44-52.

Baish, J W, T Stylianopoulos, R. M. Lanning, W. S. Kanoun, D. Fukumura, L. L. Munn, and R. K. Jain. 2011. “Scaling rules for diffusive drug delivery in tumor and normal tissues.” *Proceedings of the National Academy of Sciences of the United States of America* 108 (5): 1799-1803.

Ballermann, B. J., A. Dardik, E. Eng, and A. Liu. 1998. “Shear stress and the endothelium.” *Kidney International* 54 (67): S-100-S-108.

Baskurt, O. K., and H. J. Meiselman. 2003. “Blood Rheology and Hemodynamics.” *Seminars in Thrombosis and Hemostasis* 29 (5): 435-450.

Bedard, Phillippe L., Aaron R. Hansen, Mark J. Rataln, and Lillian L. Slu. 2013. “Tumor heterogeneity in the clinic.” *Nature* 501 (7467): 355-364.

Begum, R., A. G. Douglas-Jones, and J. M. Morgan. 2003. “Radial intratumoral increase and correlation of microvessels and proliferation in solid breast carcinoma.” *Histopathology* 43 (3): 244-253.

Belloni, F. L. 1999. “Teaching the Principles of Hemodynamics.” *The American Journal of Physiology* 277 (6 pt 6): S187-S202.

Bouck, N., V. Stellmach, and S. C. Hsu. 1996. “How Tumors Become Angiogenic.” *Advances in Cancer Research* 135-174.

Brizel, D. M., B. Klitzman, J. M. Cook, J. Edwards, G. Rosner, and M. W. Dewhirst. 1993. “A comparison of tumor and normal tissue microvascular hematocrits and red cell fluxes in a rat window chamber model.” *International Journal of Radiation Oncology Biology Physics*

25 (2): 269-276.

Carmeliet, P., and R. K. Jain. 2000. “Angiogenesis in cancer and other diseases.” *Nature* 407 (6801): 249-257.

Chien, Shu. 1987. “Red cell deformability and its relevance to blood flow.” *Annual Review of Physiology* 49: 177-192.

Clark, R. C., and R. E. Mayer. 2016. e-Learning and the Science of Instruction: Proven Guidelines for Consumers and Designers of Multimedia Learning. 4th Edition. San Francisco, CA: John Wiley & Sons.

Corliss, B. A., C. Matthews, R. Doty, G. Rohde, and S. M. Peirce. 2019. “Methods to label, image, and analyze the complex structural architectures of microvascular networks.” *Microcirculation* (Wiley) 26 (5): 1-24.

Costanzo, L. S. 2018. “Cardiovascular Physiology.” In *Physiology*, by L. S Costanzo, 117-188. Philadelphia, PA: Elsevier.

Dewhirst, M. W., E. T. Ong, B. Klitzman, T. W. Secomb, R. Z. Vinuya, R. Dodge, D. Brizel, and J. F. Gross. 1992. “Perivascular Oxygen Tensions in a Transplantable Mammary Tumor Growing in a Dorsal Flap Window Chamber.” *Radiation Research* 130 (2): 171-182.

Dunsworth, Q., B. Murphy, and Y. Wu. 2020. “Learning Circulation & Hemodynamics using an Interactive Simulation Package through a Graphic User Interface.” Paper, American Society for Engineering Education.

Fakhrejahani, E., and M. Toi. 2012. “Tumor Angiogenesis: Pericytes and Maturation Are Not to Be Ignored.” *Journal of Oncology* (Hindawi Publishing Corporation) 261750: 1-10.

Folarin, A. A., M. A. Konerding, J. Timonen, S. Nagl, and R. B. Pedley. 2010. “Three-dimensional analysis of tumour vascular corrosion casts using stereoimaging and micro-computed tomography.” *Microvascular Research* 80: 89-98.

Folkman, J. 2007. “Angiogenesis: an organizing principle for drug discovery?” *Nature Reviews* 6 (4): 273-286.

Folkman, J. 1971. “Tumor angiogenesis: therapeutic implications.” *The New England Journal of Medicine* 285 (21): 1182-1186.

Forster, J. C., W. M. Harriss-Phillips, M. J. J. Douglass, and E. Bezak. 2017. “A review of the development of tumor vasculature and its effects on the tumor microenvironment.” *Hypoxia*

5: 21-32.

Fukumura, D., D. G. Duda, and L. L., Jain, R. K. Munn. 2010. “Tumor Microvasculature and Microenvironment: Novel Insights Through Intravital Imaging in Pre-Clinical Models.” *Microcirculation* 17 (3): 206-225.

Gerlinger, M., J. Larkin, E. Gronroos, P. Martinez, C. Swanton, A. J. Rowan, S. Horswell, D. Endesfielder, N. Matthews, and A. et al Stewart. 2012. “Intratumor Heterogeneity and Branched Evolution Revealed by Multiregion Sequencing.” *The New England Journal of Medicine* 366 (10): 883-892.

Gould, I. G., and A. A. Linninger. 2015. “Hematocrit Distribution and Tissue Oxygenation in Large Microcirculatory Networks.” *Microcirculation* 22: 1-18.

Hanahan, D., and R. A. Weinberg. 2011. “Hallmarks of Cancer: The Next Generaton.” *Cell* 144: 646-674.

Hashizume, H., P. Baluk, S. Morikawa, J. W. McLean, G. Thurston, S. Roberge, R. K. Jain, and D. M McDonald. 2000. “Openings between Defective Endothelial Cells Explain Tumor Vessel Leakiness.” *American Journal of Pathology* 156 (4): 1363-1380.

Hessinger, M., A. Holzinger, D. Leitner, and S. Wassertheurer. 2008. “Hemodynamic models for education in physiology.” *Mathematics and Computers in Simulation* 79 (4): 1039-1047.

Hilmas, D. E., and E. L. Gillette. 1973. “Morphometric analyses of the microvasculature of tumors during growth and after x-irradiation.” *Cancer* 33: 103-110.

Huang, Q., X. Hu, W. He, Y. Zhao, S. Hao, Q. Wu, S. Li, S. Zhang, and M. Shi. 2018. “Fluid shear stress and tumor metastasis.” *American Journal of Cancer Research* 8 (5): 763-777.

Jackson, W. F. 2010. Microcirculation. Vol. 2, in Muscle, by J. A. Hill and E. N. Olson, 1197-1206. Philadelphia, PA: Academic Press.

Jain, R. K. 1988. “Determinants of Tumor Blood Flow: A Review.” *Cancer Research* 48 (10): 2641-2658.

Jain, R. K. 2005. “Normalization of Tumor Vasculature: An Emerging Concept in Antiangiogenic Therapy.” *Science* (AAAS) 307 (58): 58-62.

Jain, R. K. 2001. “Normalizing tumor vasculature with anti-angiogenic therapy: A new paradigm for combination therapy.” *Nature Medicine* (Nature Publishing Group) 7 (987-989).

Jain, R. K., J. D. Martin, and T. Stylianopoulos. 2014. “The role of mechanical forces in tumor

growth and therapy." *Annual Review of Biomedical Engineering* 16: 321-346.

Jain, R. K., J. D. Martin, V. P. Chaunhan, and D. G. Duda. 2020. "Tumor Microenvironment: Vascular and Extravascular Compartment." In Abeloff's Clinical Anatomy, by R. K. Jain, J. D. Martin, V. P. Chaunhan and D. G. Duda, 108-126. Philadelphia, PA: Elsevier.

Jeong, J. H., Y. Sugii, M. Minamiyama, and K. Okamoto. 2006. "Measurement of RBC deformation and velocity in capillaries in vivo." *Microvascular Research* (Elsevier) 71 (3): 212-217.

Junttila, M. R., and F. J de Sauvage. 2013. "Influence of tumour micro-environment heterogeneity on therapeutic response." *Nature* 501 (7467): 346-354.

Kamoun, W. S., S. S. Chae, D. A. Lacorre, J. A. Tyrell, M. Mitre, M. A. Gillissen, D. Fukumura, R. K. Jain, and L. L. Munn. 2010. "Simultaneous measurement of RBC velocity, flux, hematocrit and shear rate in tumor vascular networks." *Nature Methods* 7 (8): 655–660.

Kim, E., S. Stamatelos, J. Cebulla, Z. M. Bhujwalla, A. S. Popel, and A. P. Pathak. 2012. "Multiscale Imaging and Computational Modeling of Blood Flow in the Tumor Vasculature." *Annals of Biomedical Engineering* 40 (11): 2425-2441.

Konerding, M. A., C. van Ackern, E. Fait, F. Steinberg, and C. Streffer. 1998. "Morphological aspects of tumor angiogenesis and microcirculation." In Blood Perfusion and Microenvironment of Human Tumors: Implications for Clinical Radiooncology, by J. M. Brown, M. Molls and P. Vaupel, edited by M. Molls and P. Vaupel, 5-17. New York, NY: Springer.

Konerding, M.A., W. Malkusch, B. Klapthor, C. van Ackern, E. Fait, S. A. Hill, C. Parkins, D. J. Chaplin, M. Presta, and J. Denekamp. 1999. "Evidence for characteristic vascular patterns in solid tumours: quantitative studies using corrosion casts." *British Journal of Cancer* 80 (5/6): 724-732.

Kumar, V., A. K. Abbas, and J. C. Aster. 2018. "Blood Vessels." In Robbins Basic Pathology, by V. Kumar, A. K. Abbas and J. C. Aster, 361-398. Philadelphia, PA: Elsevier.

Kumar, Vinay, Abul K. Abbas, and Jon C. Aster. 2018. "Neoplasia." In Robbins Basic Pathology, by Vinay Kumar, Abul K. Abbas and Jon C. Aster, 189-242. Philadelphia, PA: Elseview.

Less, J. L., T. C. Skalak, E. M. Sevick, and R. K. Jain. 1991. "Microvascular Architecture in a Mammary Carcinoma: Branching Patterns and Vessel Dimensions." *Cancer Research* 51

(1): 265-273.

Less, J. R., M. C. Posner, T. C. Skalak, N. Wolmark, and R. K. Jain. 1997. “Geometric Resistance and Microvascular Network Architecture of Human Colorectal Carcinoma.” *Microcirculation* 4 (1): 25-33.

Leunig, M., F. Yuan, M. D. Menger, Y. Boucher, A. E. Goetz, K. Messmer, and R. K. Jain. 1992. “Angiogenesis, Microvascular Architecture, Microhemodynamics, and Interstitial Fluid Pressure during Early Growth of Human Adenocarcinoma LSI74T in SCID Mice.” *Cancer Research* 52 (23): 6553-6560.

Lowrie Jr., D. J. 2020. “Vessels.” In Histology: An Essential Textbook, by D. J. Lowrie Jr., 168-177. New York, NY: Thieme.

Marusyk, A., V. Almendro, and K. Polyak. 2012. “Intra-tumour heterogeneity: a looking glass for cancer?” *Nature Reviews*. Cancer (Macmillan Publishers Limited) 12 (5): 323-334.

Minnich, B., and A. Lametschwandtener. 2006. “Lengths Measurements in Microvascular Corrosion Castings: Two-Dimensional versus Three-Dimensional Morphometry.” *The Journal of Scanning Microscopies* 22 (3): 173-177.

Norwell, P. C. 1976. “The Clonal Evolution of Tumor Cell Populations.” *Science* (AAAS) 194 (4260): 23-28.

Padera, T. P., Kadambi, A., di Tomaso, E., Carriera, C. M., Brown, E. B., Boucher, Y., Choic, N. C., Mathisen, D., Wain, J., Mark, E. J., Munn, L. L., & Jain, R. K. 2002. “Lymphatic metastasis in the absence of functional intratumor lymphatics.” Science 296 (5574): 1883-1886.

Pathak, A. P., M. F. Penet, and Z. M. Bhujwalla. 2010. “MR Molecular Imaging of Tumor Vasculature and Vascular Targets.” *Advances in Genetics* (69): 1-30.

Popel, A. S., and P. C. Johnson. 2005. “Microcirculation and Hemorheology.” *Annual Reviwe of Fluid Mechanics* 37: 43-69.

Pries, A. R., A. J. M. Cornelissen, A. A. Sloot, M. Hinkelsey, M. R. Dreher, M. Höpfner, M. W. Dewhirst, and T. W. Secomb. 2009. “Structural Adaptation and Heterogeneity of Normal and Tumor Microvascular Networks.” *PLoS Computational Biology* 5 (5): 1-11.

Pries, A. R., and T. W. Secomb. 2008. “Origins of heterogeneity in tissue perfusion and metabolism.” *Cardiovascular Research* (European Society of Cardiology) 81 (2): 328-335.

Pries, A. R., and T. W. Secomb. 2003. “Rheology of the microcirculation.” *Clinical Hemorheology*

and Microcirculation (IOS Press) 29 (3-4): 143-148.

Pries, A. R., T. W. Secomb, and P. Gaehtgens. 1996. “Relationship between structural and hemodynamic heterogeneity in microvascular networks.” *The American Journal of Physiology* 2700 (2): 545-553.

Pries, A. R., T. W. Secomb, P. Gaehtgens, and J. F. Gross. 1990. “Blood flow in microvascular networks. Experiments and simulation.” *Circulation Research* 67 (4): 826-834.

Reigeluth, C. M. 1992. “Elaborating the Elaboration Theory.” *Educational Technology Research & Development* 40 (3): 80-86.

Reigeluth, C. M. 1979. “In search of a better way to organize instruction: The elabortion theory.” *Journal of Instructional Development* 2 (3): 8-15.

Reigeluth, C. M., and F. S. Stein. 1983. The Elaboration Theory of Instruction. Vol. I: An Overview of their Current Status, in Instructional-Design Theory, edited by C. M. Reigeluth, 335-381. Lawrence Erlbaum Associates.

Rozenblatt-Rosen, O. et al. 2020. “The Human Tumor Atlas Network:Charting Tumor Transitions acrossSpace and Time at Single-Cell Resolution.” *Cell* 181 (2): 236-249.

Sakai, T., and Y. Hosoyamada. 2013. “Are the precapillary sphincters and metarterioles universal components of the microcirculation? An historical review.” *The Journal of Physioloical Sciences* 63: 319-331.

Semenza, G. L. 2010. “Defining the Role of Hypoxia-Inducible Factor 1 in Cancer Biology and Therapeutics.” *Oncogene* 29 (5): 625-634.

Sevick, E. M., and R. K. Jain. 1989. “Geometric Resistance to Blood Flow in Solid Tumors Perfused ex Vivo: Effects of Tumor Size and Perfusion Pressure.” *Cancer Research* 49 (3): 3506-3512.

Sevick, E. M., and R. K. Jain. 1989. “Viscous Resistance to Blood Flow in Solid Tumors: Effect of Hematocrit on Intratumor Blood Viscosity.” *Cancer Research* 49 (13): 3513-3519.

Stamatelos, S. K., and A., Kim, E., Popel, A. S., Pathak, A. P Bhargava. 2019. “Tumor Ensemble-Based Modeling and Visualization of Emergent Angiogenic Heterogeneity in Breast Cancer.” *Scientific Reports* 9 (5276): 1-14.

Stamatelos, S. K., E. Kim, A. P. Pathak, and A. S. Popel. 2014. “A bioimage informatics based reconstruction of breast tumor microvasculature with computational blood flow predictions.”

Microvascular Research 91: 8-21.

Sweller, J. 1988. “Cognitive Load During Problem Solving: Effects on Learning.” *Cognitive Science* 12 (2): 257-285.

Sweller, J., P. Ayres, and S. Kalyuga. 2011. Cognitive Load Theory. Edited by M. J. Spector and S. P. Lajoie. New York, NY: Springer.

Torres Filho, I. P., M. Leung, F. Yuan, M. Intaglietta, and R. K. Jain. 1994. “Noninvasive measurement of microvascular and interstitial oxygen profiles in a human tumor in SCID mice.” P*roceedings of the National Academy of Sciences of the United States of America* 91 (6): 2081-2085.

Vaupel, P., A. Mayer, and M. Höckel. 2004. “Tumor Hypoxia and Malignant Progression.” *Methods in Enzymology* 381: 335-354.

Vaupel, P., F. Kallinowski, and P. Okunieff. 1989. “Blood Flow, Oxygen and Nutrient Supply, and Metabolic Microenvironment of Human Tumors - a Review.” *Cancer Research* 49: 6449-6465.

Vogel, A. W. 1965. “Intratumoral Vascular Changes With Increased Size of a Mammary Adenocarcinoma: New Method and Results.” *Journal of the National Cancer Institute 34* (5): 571-578.

Weidner, M. D., J. P. Semple, W. R. Welch, and J. Folkman. 1991. “Tumor Angiogenesis and Metastasis - Corelation in Invasive Breast Carcinoma.” *The New England Journal of Medicine* 324 (1): 1-8.

Wilson, D. F., and G. J. Cerniglia. 1992. “Localization of tumors and evaluation of their state of oxygenation by phosphorescence imaging.” *Cancer Research* 52 (14): 3988-3993.

Zawieja, D. C., P. Y. von der Weld, and A. A Gashev. 2011. “Microlymphatic Biology.” In *Comprehensive Physiology*, by D. C. Zawieja, P. Y. von der Weld and A. A Gashev.

Appendix A: Didactic content and sketches

Full text, formulas, and citations for didactic content included in web application. Sketches for final illustrations included.

Vasculome

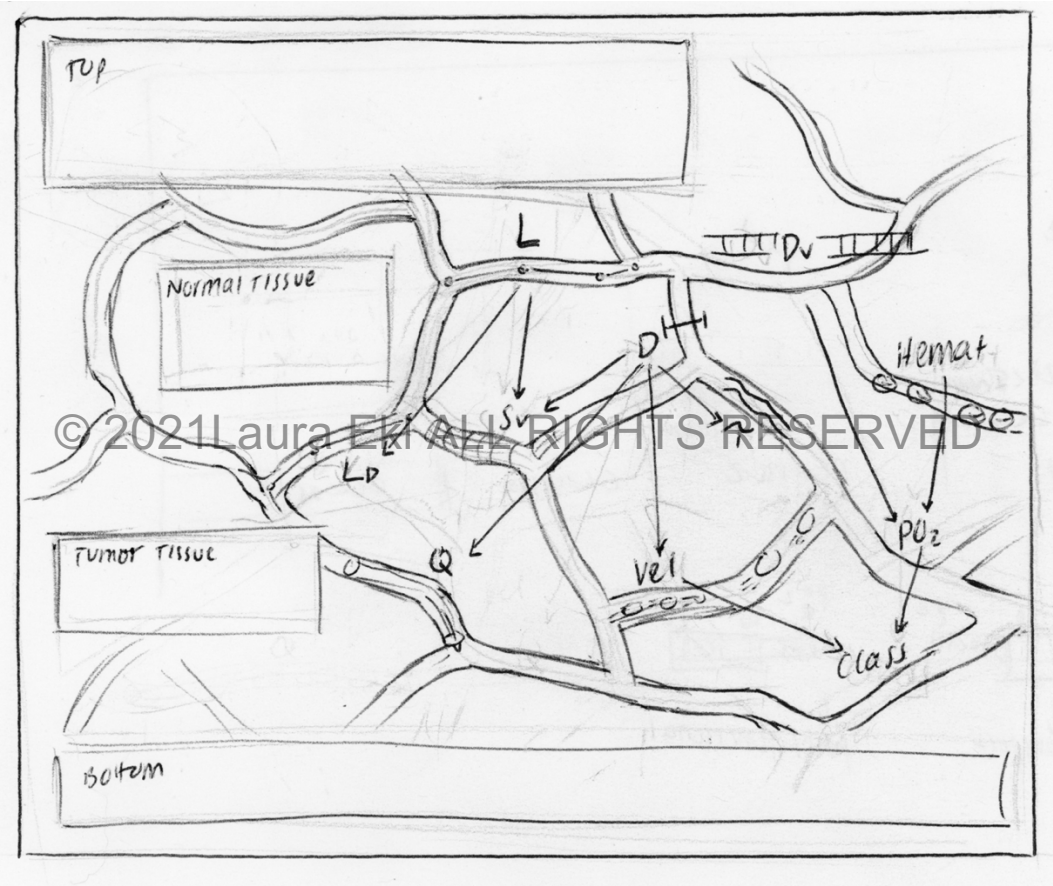

Figure 29.1. Illustration sketch. Initial sketch for vasculome illustration.

Definition

‘Vasculome’ refers to the complete set of characteristics that define the microvascular components of a tissue.

The vasculome includes both morphological parameters of the blood vessels, such as vessel length, diameter, and distance to the nearest vessel, as well as functional characteristics, like blood flow velocity, hematocrit, oxygenation, and shear stress.

The morphological and functional characteristics of the vasculome are tightly interrelated. Not included here, the vasculome can also include genomic and metabolic data obtained from complementary assays or techniques.

Normal tissue

In healthy tissue, the vasculome is well-regulated and follows predictable physiological mechanisms[1,2].

Tumor tissue

In tumor tissue, the vasculome becomes irregular, heterogenous and is regulated by the aberrant pathophysiology of cancer[3-6].

Studying the vasculome offers valuable insights into the **tumor microenvironment (TME)**, which may inform new cancer therapies, and help develop novel biomarkers of relapse, progression, or treatment response[3,4,6,7].

Learn more about the morphological and functional parameters included in the tumor vasculome by clicking on the variable buttons above.

References

1. Popel, A. S., and P. C. Johnson. 2005. "Microcirculation and Hemorheology." *Annual Review of Fluid Mechanics* 37: 43-69. https://doi.org/10.1146/annurev.fluid.37.042604.133933.

2. Pries, A. R., T. W. Secomb, P. Gaehtgens, and J. F. Gross. 1990. "Blood flow in microvascular networks. Experiments and simulation." *Circulation research* 67 (4): 826-834. https://doi.org/10.1161/01.res.67.4.826.
3. Jain, R. K. 1988. "Determinants of Tumor Blood Flow: A Review." *Cancer Research* 48 (10): 2641-2658. https://pubmed.ncbi.nlm.nih.gov/3282647/.
4. Vaupel, P., F. Kallinowski, and P. Okunieff. 1989. "Blood Flow, Oxygen and Nutrient Supply, and Metabolic Microenvironment of Human Tumors - a Review." *Cancer Research* 49: 6449-6465. *https://pubmed.ncbi.nlm.nih.gov/2684393/*.
5. Konerding, M.A., W. Malkusch, B. Klapthor, C. van Ackern, E. Fait, S. A. Hill, C. Parkins, D. J. Chaplin, M. Presta, and J. Denekamp. 1999. "Evidence for characteristic vascular patterns in solid tumours: quantitative studies using corrosion casts." *British Journal of Cancer* 80 (5/6): 724-732. *https://doi.org/10.1038/sj.bjc.6690416*.
6. Stamatelos, S. K., and A., Kim, E., Popel, A. S., Pathak, A. P Bhargava. 2019. "Tumor Ensemble-Based Modeling and Visualization of Emergent Angiogenic Heterogeneity in Breast Cancer." *Scientific reports* 9 (5276): 1-14. https://doi.org/10.1038/s41598-019-40888-w.
7. Pathak, A. P., M. F. Penet, and Z. M. Bhujwalla. 2010. "MR Molecular Imaging of Tumor Vasculature and Vascular Targets." *Advances in Genetics* (69): 1-30. https://doi.org/10.1016/S0065-2660(10)69010-4.
8. Stamatelos, S. K., E. Kim, A. P. Pathak, and A. S. Popel. 2014. "A bioimage informatics based reconstruction of breast tumor microvasculature with computational blood flow predictions." *Microvascular research* 91: 8-21. https://doi.org/10.1016/j.mvr.2013.12.003.

Morphological parameters

Vessel length (L)

Unit: mm, μm

Definition

Vessel length (L) is defined as the distance between the end points of a blood vessel.

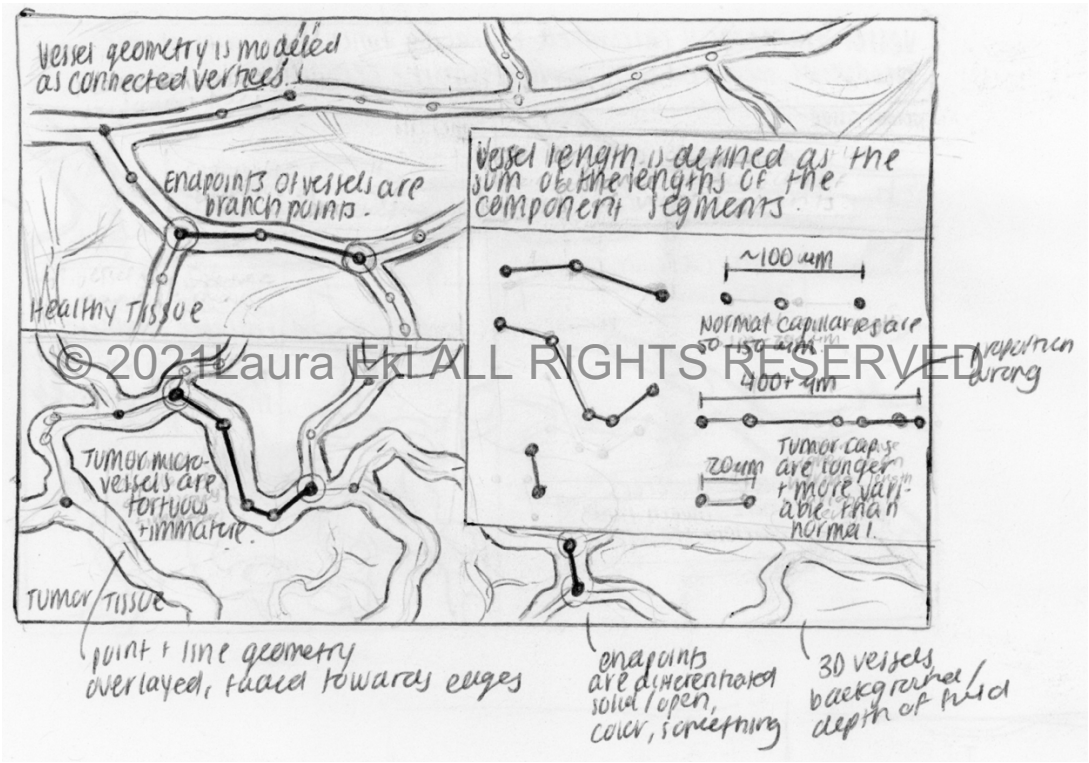

Figure 29.2. Illustration sketch. Initial sketch for vessel length illustration.

Prior to computing the metrics used in this study, each blood vessel segment was reduced to its “skeleton” or “centerline” representation that is series of connected vertices[1].

In this representation, each blood vessel segment is defined by a series of points bounded from **node i** to **node j** as shown in the diagram.

The length along the series of points corresponding to each blood vessel segment results in the "**total segment length**".

Normal tissue

For example, in healthy microvascular networks, capillaries are typically a few hundred microns long[2], which allows delivery and exchange of oxygen and nutrients.

Tumor tissue

Tumor blood vessels are less organized and more tortuous than their normal tissue counterparts. Increased tortuosity signifies longer total vessel length. Increased length and tortuosity also affect flow resistance, which impacts the delivery of oxygen, nutrients, and therapeutics to tumor tissues[3,4].

Formula

$$L_{ij} = \sum_{k=i}^{j} \sqrt{(x_{k+1} - x_k)^2 + (y_{k+1} - y_k)^2 + (z_{k+1} - z_k)^2}$$

where L_{ij} is the length of the segment from nodes i to j, and node i and j are defined by the Cartesian points (x_i, y_i, z_i), (x_j, y_j, z_j).

References

1. Stamatelos, S. K., E. Kim, A. P. Pathak, and A. S. Popel. 2014. "A bioimage informatics based reconstruction of breast tumor microvasculature with computational blood flow predictions." *Microvascular research* 91: 8-21. https://doi.org/10.1016/j.mvr.2013.12.003.
2. Pries, A. R., and T. W. Secomb. 2003. "Rheology of the microcirculation." *Clinical Hemorheology and Microcirculation* (IOS Press) 29 (3-4): 143-148. https://europepmc.org/article/med/14724335.
3. Hilmas, D. E., and E. L. Gillette. 1974. "Morphometric analyses of the microvasculature of tumors during growth and after x-irradiation." *Cancer* 33: 103-110. https://doi.org/10.1002/1097-0142(197401)33:1<103::AID-CNCR2820330116>3.0.CO;2-7.
4. Stamatelos, S. K., and A., Kim, E., Popel, A. S., Pathak, A. P Bhargava. 2019. "Tumor Ensemble-Based Modeling and Visualization of Emergent Angiogenic Heterogeneity in Breast Cancer." *Scientific reports* 9 (5276): 1-14. https://doi.org/10.1038/s41598-019-40888-w.

See also

- Intervessel distance (D_V)
- Length density (L_V)
- Surface area density (S_V)

Vessel diameter (D)

Unit: μm

Definition

Vessel diameter (D) is calculated by doubling the radius of the blood vessel, measured orthogonally from the centerline to either side of the vessel lumen.

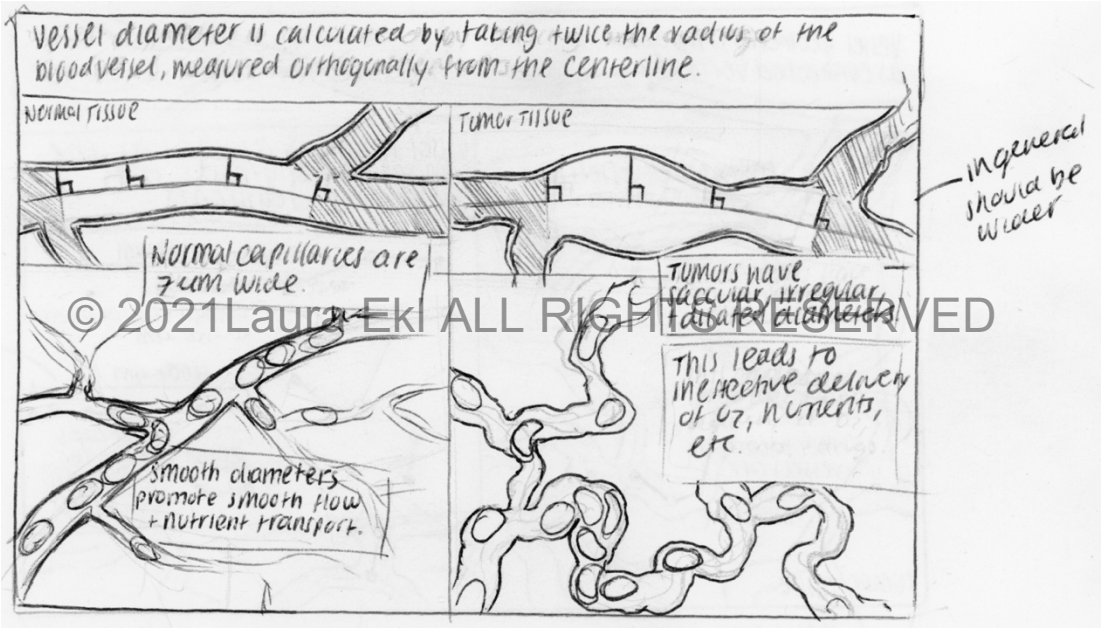

Figure 29.3. Illustration sketch. Initial sketch for vessel diameter illustration.

Normal tissue

Blood vessels present in normal tissues follow predictable growth patterns that generate uniform vessel diameters. The average diameter of a capillary in healthy tissue (e.g. murine brain) is 3-4 μm.

Smooth and uniform diameter changes enhance the delivery of oxygen and nutrients[1].

Tumor tissue

Tumor microvessels are sinusoidal, tortuous, and often have irregular diameters. In general, tumor microvessels are larger than their normal counterparts.

The larger diameters and abrupt caliber changes of tumor vessels result in irregular flow rates, which can disrupt distribution of oxygen and nutrients[2,3].

Formula

$$D_{ij} = \frac{2}{j - i + 1} \sum_{k=i}^{j} r_k$$

where D_{ij} is blood vessel diameter, r_k is the radius at a point k within the segment bounded from nodes i to j[3,4].

References

1. Quintana, D. D., S. E. Lewis, Y. Anantula, J. A. Garcia, S. N. Sarkar, J. Z. Cavendish, C. M. Brown, and J. W. Simpkins. 2019. "The cerebral angiome: High resolution MicroCT imaging of the whole brain cerebrovasculature in female and male mice." *Neuroimage* 202 (116109): 1-17. https://doi.org/10.1016/j.neuroimage.2019.116109.
2. Leunig, M., F. Yuan, M. D. Menger, Y. Boucher, A. E. Goetz, K. Messmer, and R. K. Jain. 1992. "Angiogenesis, Microvascular Architecture, Microhemodynamics, and Interstitial Fluid Pressure during Early Growth of Human Adenocarcinoma LSI74T in SCID Mice." *Cancer Research* 52 (23): 6553-6560. https://pubmed.ncbi.nlm.nih.gov/1384965/.
3. Stamatelos, S. K., and A., Kim, E., Popel, A. S., Pathak, A. P Bhargava. 2019. "Tumor Ensemble-Based Modeling and Visualization of Emergent Angiogenic

Heterogeneity in Breast Cancer." *Scientific reports* 9 (5276): 1-14. https://doi.org/10.1038/s41598-019-40888-w.

4. Stamatelos, S. K., E. Kim, A. P. Pathak, and A. S. Popel. 2014. "A bioimage informatics based reconstruction of breast tumor microvasculature with computational blood flow predictions." *Microvascular research* 91: 8-21. https://doi.org/10.1016/j.mvr.2013.12.003.

See also:

- Intervessel distance (D_V)
- Surface area density (S_V)
- Blood flow rate (Q)
- Blood velocity (Vel)
- Fluid shear stress (t)
- Vessel class

Intervessel distance (D_V)

Unit: μm

Definition

Intervessel distance or the **distance to the nearest blood vessel (D_V)** is the 3D Euclidian distance (μm) between a point in the tissue to the nearest blood vessel. Intervessel distance is an indirect measure of the efficacy of extravascular transport of nutrients.

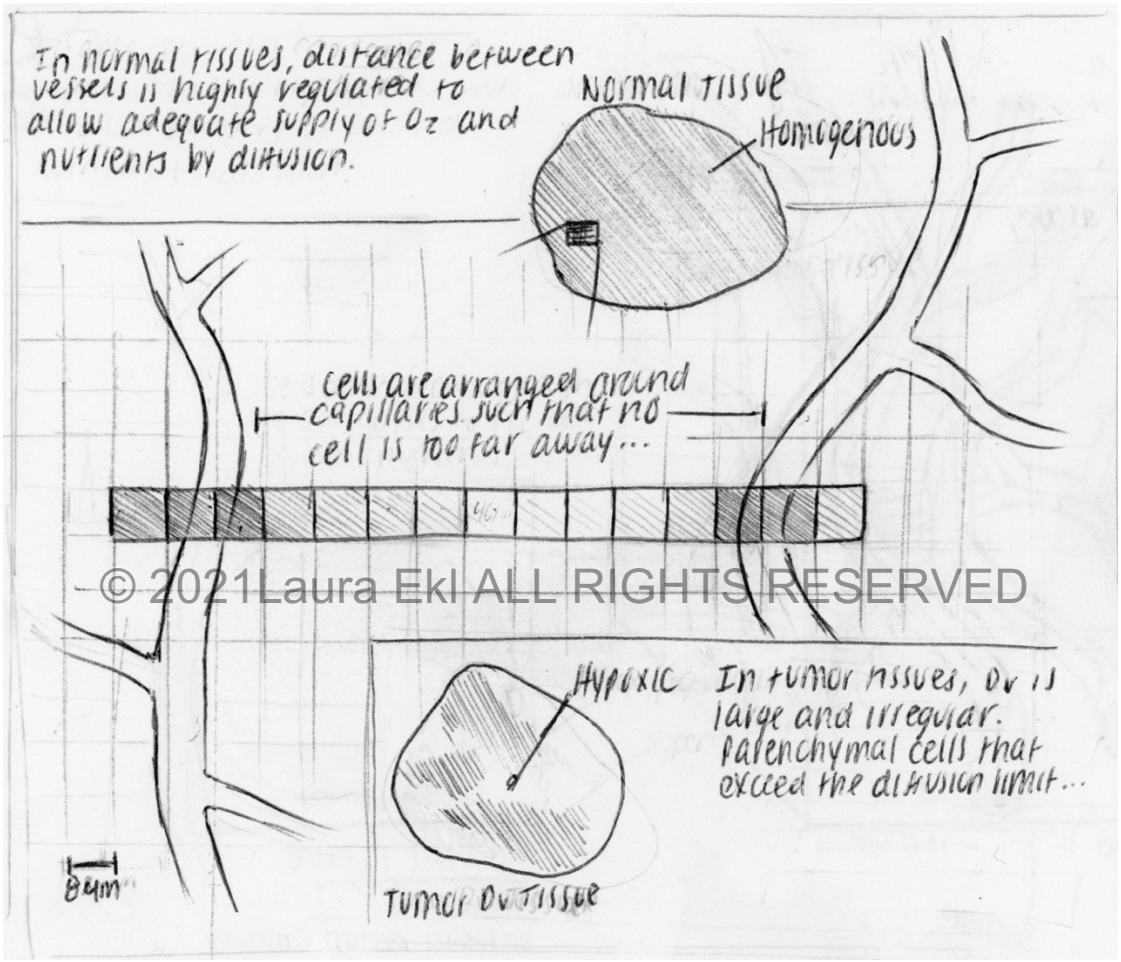

Figure 29.4. Illustration sketch. Initial sketch for intervessel distance illustration.

In normal tissue, the intervessel distance is high due to the elevated density of blood vessels, which results in an efficient supply of oxygen and nutrients via both perfusion and diffusion[1].

Normal tissue

Due to the presence of a dense network of capillaries, most cells have access to oxygen and nutrients delivered by diffusion and perfusion via blood vessels. The intervessel distance is small (less than 150 μm) to facilitate adequate supply of oxygen and nutrients.

Cells are arranged around capillaries such that no cell is too far away to receive oxygen by diffusive transport. If cells experience a lack of oxygen. i.e. hypoxia, it can trigger angiogenesis.

Tumor tissue

In tumor tissues, intervessel distances tend to be greater and irregular. Cells that are located beyond the typical diffusion distance of oxygen and nutrients may therefore experience hypoxia, which can lead to tissue necrosis[1,2].

Formula

$$R = \frac{1}{\sqrt{\pi \cdot L_D}}$$

where R is the extravascular diffusion distance and L_D is the vascular length density as described in the next section[1,2].

References:

1. Konerding, M.A., W. Malkusch, B. Klapthor, C. van Ackern, E. Fait, S. A. Hill, C. Parkins, D. J. Chaplin, M. Presta, and J. Denekamp. 1999. "Evidence for characteristic vascular patterns in solid tumours: quantitative studies using corrosion casts." British Journal of Cancer 80 (5/6): 724-732. https://doi.org/10.1038/sj.bjc.6690416.
2. Baish, J W, T Stylianopoulos, R. M. Lanning, W. S. Kanoun, D. Fukumura, L. L. Munn, and R. K. Jain. 2011. "Scaling rules for diffusive drug delivery in tumor and normal tissues." *Proceedings of the National Academy of Sciences of the United States of America* 108 (5): 1799-1803. https://doi.org/10.1073/pnas.1018154108.
3. Stamatelos, S. K., E. Kim, A. P. Pathak, and A. S. Popel. 2014. "A bioimage informatics based reconstruction of breast tumor microvasculature with computational blood flow predictions." *Microvascular research* 91: 8-21. https://doi.org/10.1016/j.mvr.2013.12.003.
4. Stamatelos, S. K., and A., Kim, E., Popel, A. S., Pathak, A. P Bhargava. 2019. "Tumor Ensemble-Based Modeling and Visualization of Emergent Angiogenic Heterogeneity in Breast Cancer." *Scientific reports* 9 (5276): 1-14. https://doi.org/10.1038/s41598-019-40888-w.

See also:

- Vessel length (L)
- Vessel diameter (D)
- Length density (L_V)
- Intravascular oxygen tension (PO_2)

Vascular length density (L_V)

Unit: mm/mm^3

Definition

Vascular length density (L_V) is defined as the average length of blood vessels within a unit volume of tissue. Therefore, vascular length density has units of mm/mm^3.

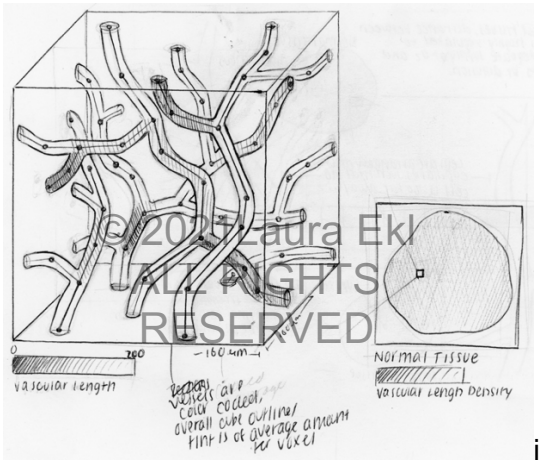

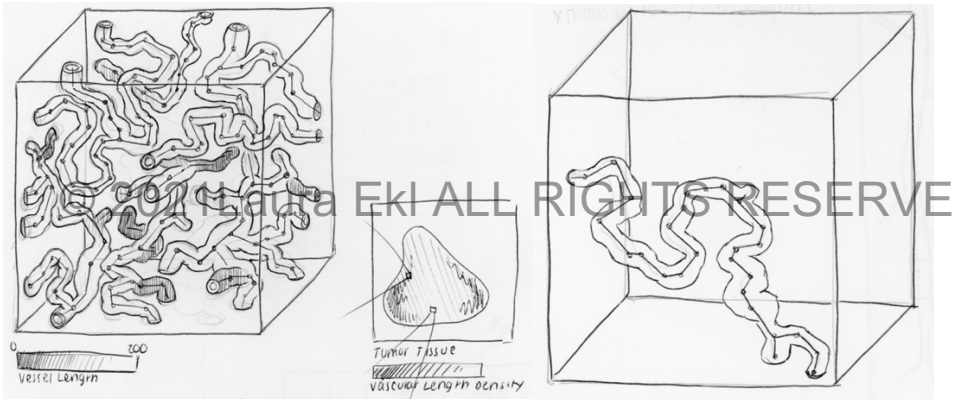

Figure 29.5. Illustration sketch. Initial sketch for vascular length density illustration.

Vascular length density is a measure of overall microvessel density.

Tumor tissue

Microvascular length density is elevated in solid tumors relative to healthy tissue[1-3]. Microvascular length density affects the delivery of oxygen, nutrients, and drugs. For example, low microvessel density in a tissue can lead to hypoxia or ischemia[4]. Increased microvessel length density in breast cancer is often correlated with an increased likelihood of metastasis.

Formula

$$L_D = \frac{1}{V_{tissue}} \sum_{i,j=1}^{N} L_{ij}$$

where L_D is vascular length density (mm/mm^3), V_{tissue} is volume of the tissue (mm^3), N is the number of vessels, and L_{ij} is the vessel segment length (mm)[3,5].

References

1. Hilmas, D. E., and E. L. Gillette. 1974. "Morphometric analyses of the microvasculature of tumors during growth and after x-irradiation." *Cancer* 33: 103-110. https://doi.org/10.1002/1097-0142(197401)33:1<103::AID-CNCR2820330116>3.0.CO;2-7.
2. Forster, J. C., W. M. Harriss-Phillips, M. J. J. Douglass, and E. Bezak. 2017. "A review of the development of tumor vasculature and its effects on the tumor microenvironment." *Hypoxia* 5: 21-32. https://doi.org/10.2147/HP.S133231.
3. Stamatelos, S. K., and A., Kim, E., Popel, A. S., Pathak, A. P Bhargava. 2019. "Tumor Ensemble-Based Modeling and Visualization of Emergent Angiogenic Heterogeneity in Breast Cancer." *Scientific reports* 9 (5276): 1-14. https://doi.org/10.1038/s41598-019-40888-w.

4. Hasan, J., R. Byers, and G. C. Jayson. 2002. "Intra-tumoural microvessel density in human solid tumours." *British Journal of Cancer* 86 (10): 1566 – 1577. https://doi.org/10.1038/sj.bjc.6600315.
5. Stamatelos, S. K., E. Kim, A. P. Pathak, and A. S. Popel. 2014. "A bioimage informatics based reconstruction of breast tumor microvasculature with computational blood flow predictions." *Microvascular research* 91: 8-21. https://doi.org/10.1016/j.mvr.2013.12.003.

See also

- Length (L)
- Intervessel distance (D_V)
- Surface area density (S_V)

Vascular surface area density (S_V)

Unit: mm^2/mm^3

Definition

Vascular surface area density (S_V) is the average surface area of the blood vessel in a unit volume of tissue. Therefore, the units for vascular surface area density are mm^2 per mm^3.

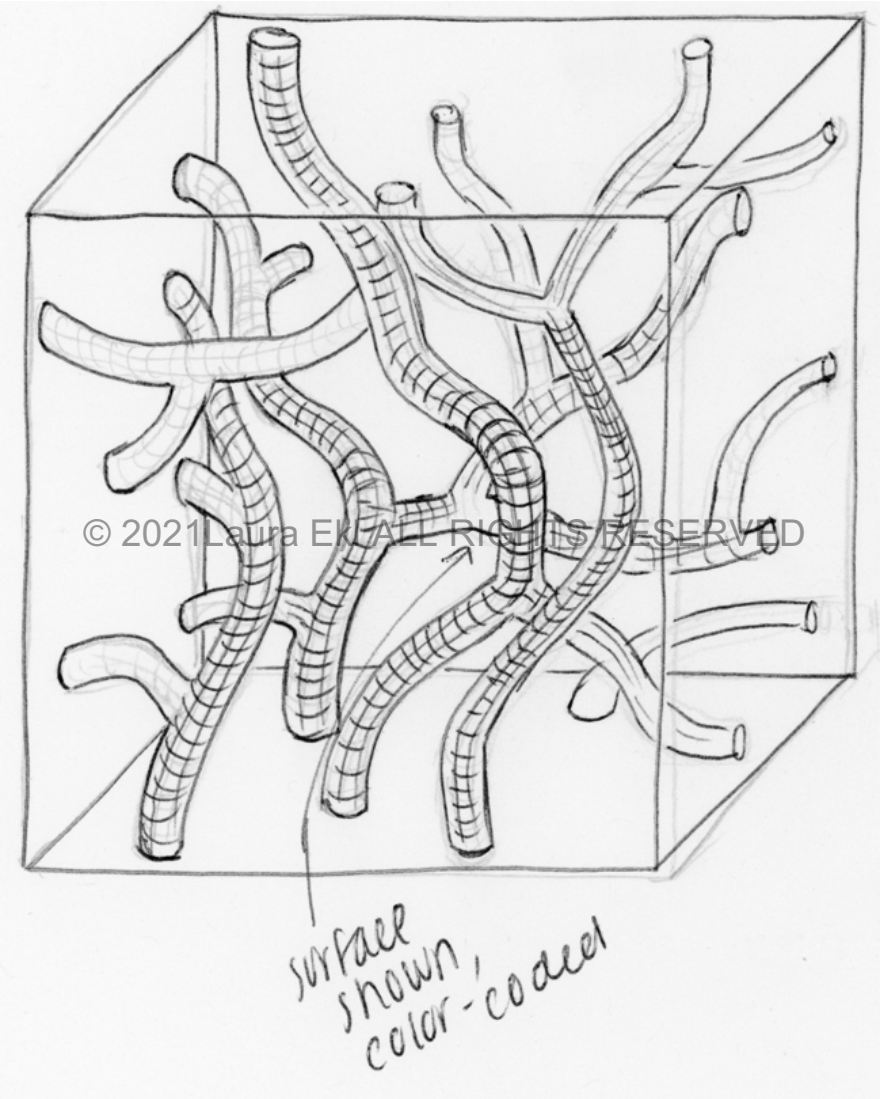

Figure 29.6. Illustration sketch. Initial sketch for vascular surface area density illustration.

Normal tissue

Vascular surface area density is a similar measure to vessel length density, but it also accounts for the diameter of the vessel, making it a more accurate measurement of vascularity per unit volume of tissue[1,2].

Vascular surface area density affects the delivery of oxygen, nutrients, and drugs. For example, low vascular surface area density in a tissue can lead to hypoxia or ischemia[3].

Formula

$$S_D = \frac{1}{V_{tissue}} \sum_{i,j=1}^{N} \pi \cdot D_{ij} \cdot L_{ij}$$

where S_D is vascular surface density (mm^2/mm^3), V_{tissue} is volume of the tissue (mm^3), N is the total number of vessels, D_{ij} is the diameter of the segment between nodes i and j, L_{ij} is the length of the segment between nodes i and j (mm)[2,4].

References

1. Forster, J. C., W. M. Harriss-Phillips, M. J. J. Douglass, and E. Bezak. 2017. "A review of the development of tumor vasculature and its effects on the tumor microenvironment." *Hypoxia* 5: 21-32. https://doi.org/10.2147/HP.S133231.
2. Stamatelos, S. K., and A., Kim, E., Popel, A. S., Pathak, A. P Bhargava. 2019. "Tumor Ensemble-Based Modeling and Visualization of Emergent Angiogenic Heterogeneity in Breast Cancer." *Scientific reports* 9 (5276): 1-14. https://doi.org/10.1038/s41598-019-40888-w.

3. Hasan, J., R. Byers, and G. C. Jayson. 2002. "Intra-tumoural microvessel density in human solid tumours." *British Journal of Cancer* 86 (10): 1566 – 1577. https://doi.org/10.1038/sj.bjc.6600315.
4. Stamatelos, S. K., E. Kim, A. P. Pathak, and A. S. Popel. 2014. "A bioimage informatics based reconstruction of breast tumor microvasculature with computational blood flow predictions." *Microvascular research* 91: 8-21. https://doi.org/10.1016/j.mvr.2013.12.003.

See also

- Vessel length (L)
- Vessel diameter (D)
- Vascular length density (L_V)

Blood flow rate (Q)

Unit: ml/s

Definition

Blood flow rate (Q) is a measure of the **volume** of blood flowing per unit time (e.g. measured in ml/s) within a blood vessel segment.

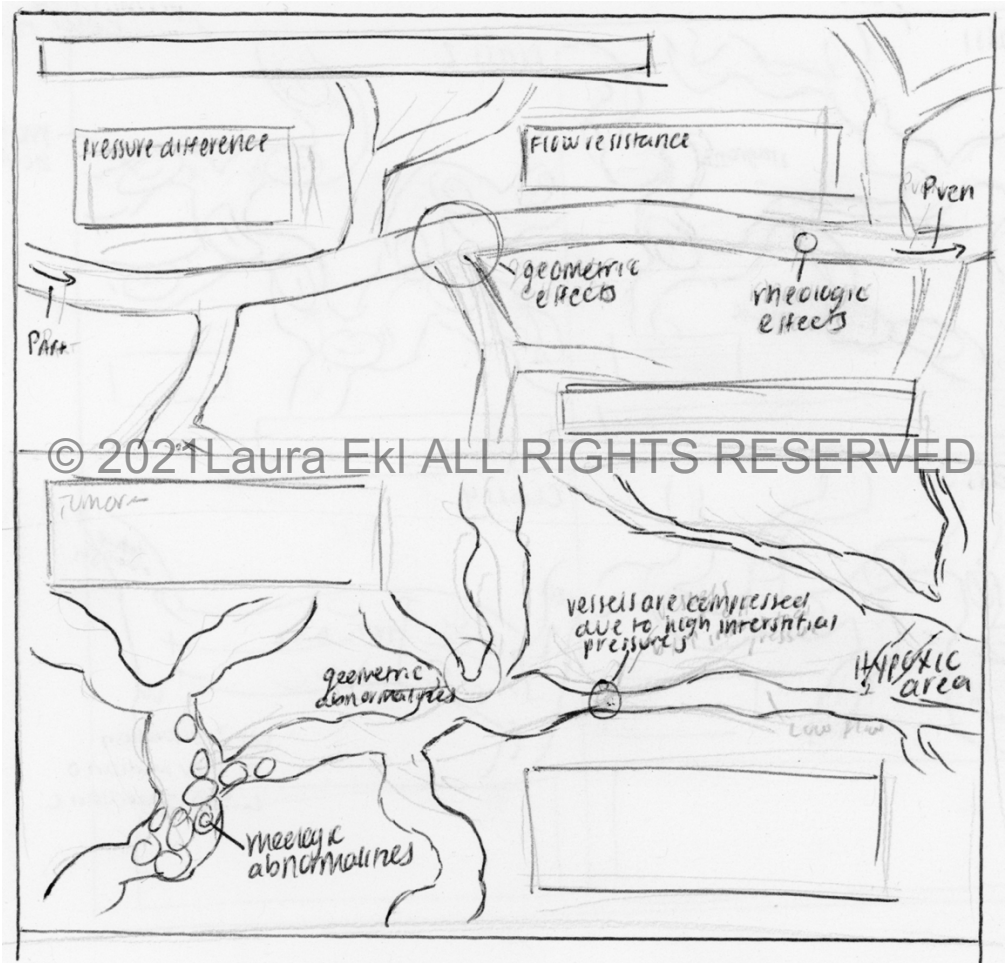

Figure 29.7. Illustration sketch. Initial sketch for blood flow rate illustration.

The range of blood flow rates affects nutrient and drug availability within a tissue. In a vascular network, the flow rate is governed by the pressure difference between the arterial and venous ends, as well as by the vascular resistance[1].

Vascular resistance arises from the combination of the vascular architecture (i.e. geometric factors) and the viscosity of blood (i.e. rheologic or mechanical factors)[2].

Tumor tissue

Tumor vascular networks are characterized by morphological irregularities that result in an abnormal range of blood flow rates. Additionally, within tumors, the blood flow to certain areas may be temporarily cut off, resulting is acute hypoxia. Poor or irregular blood flow also results in the poor delivery of therapeutic agents within tumors[3-6].

Abnormalities in the vascular geometry as well as the blood viscosity within tumors results in an elevated resistance to flow. Moreover, blood flow is generally lower in tumor blood vessels relative to healthy tissues[2,3].

Formula

The distribution of blood flow rate follows mass conservation, as shown by the following equation:

$$\sum_{i,j=1}^{N} Q_{ij} = 0$$

where N is the number of vessel segments, and Q_{ij} is the flow rate between nodes i and j.

$$Q_{ij} = G_{ij} \cdot \left(P_i - P_j\right)$$

where Q_{ij} is the blood flow rate of the segment between nodes *i* and *j*, G_{ij} is the hydraulic conductance of a segment, and $(P_i\text{-}P_j)$ is the pressure drop from nodes *i* to *j*.

$$G_{ij} = \frac{\pi \cdot {D_{ij}}^4}{128 \cdot \mu_{ij} \cdot L_{ij}}$$

G_{ij} can be further defined, where D_{ij} is the diameter of the segment from nodes *i* to *j*, μ_{ij} is the apparent viscosity of the segment from nodes *i* to *j*, and L_{ij} is the length of the segment from nodes *i* to *j*.

References

1. Gagnon, L., A. F. Smith, D. A. Boas, A. Devor, T. W. Secomb, and S. Sakadžić. 2016. "Modeling of Cerebral Oxygen Transport Based on In vivo Microscopic Imaging of Microvascular Network Structure, Blood Flow, and Oxygenation." *Frontiers in Computations Neuroscience* 10 (82): 1-20. https://doi.org/10.3389/fncom.2016.00082.
2. Jain, R. K. 1999. "Transport of Molecules, Particles, and Cells in Solid Tumors." *Annual review of biomedical engineering* 1 (1): 241-263. https://doi.org/10.1146/annurev.bioeng.1.1.241.
3. Leunig, M., F. Yuan, M. D. Menger, Y. Boucher, A. E. Goetz, K. Messmer, and R. K. Jain. 1992. "Angiogenesis, Microvascular Architecture, Microhemodynamics, and Interstitial Fluid Pressure during Early Growth of Human Adenocarcinoma LSI74T in SCID Mice." *Cancer Research* 52 (23): 6553-6560. https://pubmed.ncbi.nlm.nih.gov/1384965/.
4. Jain, R. K. 1988. "Determinants of Tumor Blood Flow: A Review." *Cancer Research* 48 (10): 2641-2658. https://pubmed.ncbi.nlm.nih.gov/3282647/.

5. Torres Filho, I. P., M. Leung, F. Yuan, M. Intaglietta, and R. K. Jain. 1994. "Noninvasive measurement of microvascular and interstitial oxygen profiles in a human tumor in SCID mice." *Proceedings of the National Academy of Sciences of the United States of America* 91 (6): 2081-2085. https://doi.org/10.1073/pnas.91.6.208.
6. Stamatelos, S. K., and A., Kim, E., Popel, A. S., Pathak, A. P Bhargava. 2019. "Tumor Ensemble-Based Modeling and Visualization of Emergent Angiogenic Heterogeneity in Breast Cancer." *Scientific reports* 9 (5276): 1-14. https://doi.org/10.1038/s41598-019-40888-w.
7. Stamatelos, S. K., E. Kim, A. P. Pathak, and A. S. Popel. 2014. "A bioimage informatics based reconstruction of breast tumor microvasculature with computational blood flow predictions." *Microvascular research* 91: 8-21. https://doi.org/10.1016/j.mvr.2013.12.003.

See also

- Vessel length (L)
- Vessel diameter (D)

Blood flow velocity (Vel)

Unit: mm/s

Definition:

Fluid flow velocity (Vel) is a measure of the **distance** (mm) traveled by the fluid per second (i.e. mm/s).

Normal tissue

In normal tissues, blood flow velocity is inversely proportional to the cross sectional area of a blood vessel. This means that if we assume the blood flow rate (i.e. ml/min) remains constant, when a blood vessel vasodilates by a factor of 2, the flow velocity decreases by a factor of 4.

Tumor tissue

Tumor microvascular networks are characterized by abnormal blood flow velocities. Flow velocity in tumors does not have a proportional relationship to cross sectional area or vessel diameter[1-4].

Blood velocity in tumors is usually an order of magnitude lower than the blood flow velocity through comparably 'normal' vessels[5].

Formula

$$u_{ij} = \frac{4 \cdot Q_{ij}}{\pi \cdot {D_{ij}}^2}$$

where u_{ij} is the mean blood velocity in the segment from nodes *i* to *j*, Q_{ij} is the blood flow rate from nodes *i* to *j*, and D_{ij} is the diameter of the segment from nodes *i* to *j* [3,6].

References

1. Jain, R. K. 1988. "Determinants of Tumor Blood Flow: A Review." *Cancer Research* 48 (10): 2641-2658. https://pubmed.ncbi.nlm.nih.gov/3282647/.
2. Leunig, M., F. Yuan, M. D. Menger, Y. Boucher, A. E. Goetz, K. Messmer, and R. K. Jain. 1992. "Angiogenesis, Microvascular Architecture, Microhemodynamics, and Interstitial Fluid Pressure during Early Growth of Human Adenocarcinoma LSI74T in SCID Mice." *Cancer Research* 52 (23): 6553-6560. https://pubmed.ncbi.nlm.nih.gov/1384965/.
3. Stamatelos, S. K., and A., Kim, E., Popel, A. S., Pathak, A. P Bhargava. 2019. "Tumor Ensemble-Based Modeling and Visualization of Emergent Angiogenic Heterogeneity in Breast Cancer." *Scientific reports* 9 (5276): 1-14. https://doi.org/10.1038/s41598-019-40888-w.
4. Torres Filho, I. P., M. Leung, F. Yuan, M. Intaglietta, and R. K. Jain. 1994. "Noninvasive measurement of microvascular and interstitial oxygen profiles in a human tumor in SCID mice." *Proceedings of the National Academy of Sciences of the United States of America* 91 (6): 2081-2085. https://doi.org/10.1073/pnas.91.6.2081.
5. Jain, et al. 2010
6. Gagnon, L., A. F. Smith, D. A. Boas, A. Devor, T. W. Secomb, and S. Sakadžić. 2016. "Modeling of Cerebral Oxygen Transport Based on In vivo Microscopic Imaging of Microvascular Network Structure, Blood Flow, and Oxygenation." *Frontiers in Computations Neuroscience* 10 (82): 1-20. https://doi.org/10.3389/fncom.2016.00082.

7. Stamatelos, S. K., E. Kim, A. P. Pathak, and A. S. Popel. 2014. "A bioimage informatics based reconstruction of breast tumor microvasculature with computational blood flow predictions." *Microvascular research* 91: 8-21. https://doi.org/10.1016/j.mvr.2013.12.003.

See also

- Vessel diameter (D)
- Blood flow rate (Q)
- Fluid shear stress (t)

Intravascular oxygen tension (PO_2)

Unit: mmHg

Definition

Intravascular oxygen tension (PO_2) is the partial pressure of oxygen (measured in mmHg) inside blood vessels.

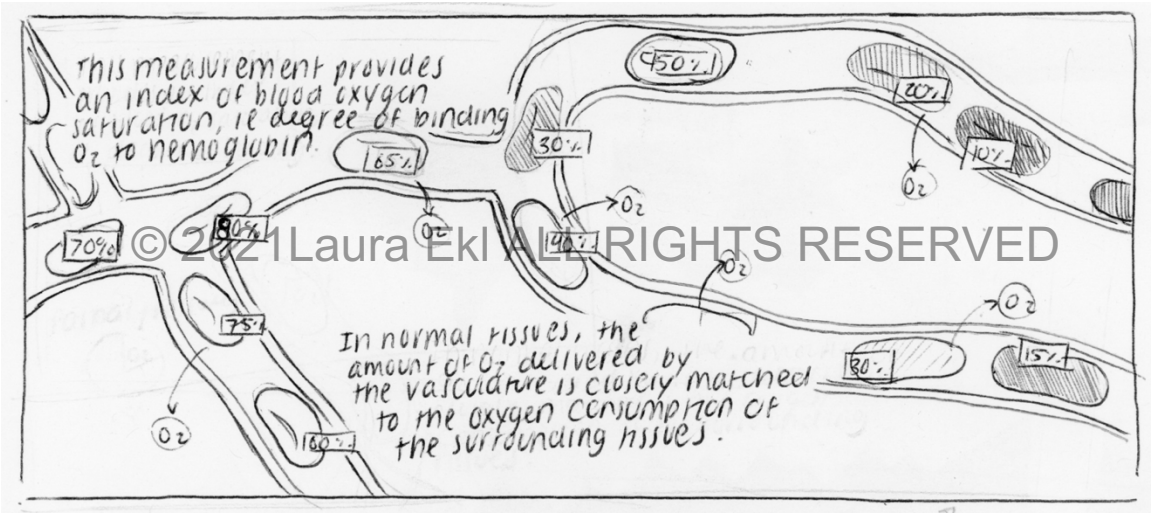

Figure 29.8. Illustration sketch. Initial sketch for intravascular oxygen tension illustration.

This measurement provides an index of the blood oxygen saturation i.e. the degree of oxygen binding to hemoglobin inside a blood vessel.

Normal tissue

In normal tissues, the amount of oxygen delivered by the vasculature is closely matched to the oxygen consumption of the surrounding tissues[1].

Tumor tissue

In tumor tissues, the demands of rapidly dividing tumor cells and supporting stromal cells exceed the available supply of oxygen. Therefore, tumors are often characterized by low intravascular oxygen tension (< 10 mmHg). Tumor hypoxia is a negative

prognostic indicator in many cancers and associated with a likelihood of metastasis and poor patient outcomes. Chronic hypoxia can also lead to tissue necrosis[2-5].

Formula

$$Q_{b_{i,j}} \cdot \left(\alpha_{b_{i,j}} \cdot \Delta P_{i,j} + H_{D_{i,j}} \cdot C_{bind} \cdot \Delta S_{Hb}\right) = J_{wall_{i,j}} \qquad (1)$$

where

$$J_{wall_{i,j}} = M_c \cdot m_{tissue} \cdot \frac{L_{ij}}{\sum_{i,j=1}^{N} L_{ij}} \qquad (2)$$

$$\alpha_{b_{i,j}} = H_{T_{i,j}} \cdot \alpha_{RBC} + \left(1 - H_{T_{i,j}}\right) \cdot \alpha_{pl} \qquad (3)$$

$$S_{Hb_{i,j}}(P_{i,j}) = \frac{P_{ij}^{n_{hill}}}{P_{ij}^{n_{hill}} + P_{50}^{n_{hill}}} \qquad (4)$$

Here, values of blood flow $Q_{b_{i,j}}$, discharge hematocrit $H_{D_{i,j}}$, and tube hematocrit $H_{T_{i,j}}$ in the individual vessels segments ij of length L_{ij} (where i and j represent branching or boundary nodes) are estimated from the blood flow model. $P_{i,j}$ is the oxygen tension in the blood, C_{bind} and $S_{Hb_{i,j}}$ are reb blood cells' binding capacity and oxygen saturation respectively; $J_{wall_{i,j}}$ is the total oxygen flux across the vessel wall for vessel segment of length $L_{ij} \cdot M_c$ is the oxygen consumption rate for breast cancer xenografts derived from Vaupel et al[2], m_{tissue} is the tissue mass; n_{hill} is the Hill coefficient for hemoglobin binding cooperativity (2.7)[7], $P_{50}$is the constant for 50% hemoglobin oxygen saturation (37 mmHg)[7], and $\propto_{pl}$ is the oxygen solubility in plasma (2.82x10^{-5}ml O_2/ml tissue/mmHg)[7].

With the application of appropriate boundary conditions, Equation 1 can be transformed to the following system of equations:

$$(D_{int} + S_{int}) \cdot P_{int} = (D_{bound} + S_{bound}) \cdot P_{bound} + J_{wall} \qquad (5)$$

References

1. Gagnon, L., A. F. Smith, D. A. Boas, A. Devor, T. W. Secomb, and S. Sakadžić. 2016. "Modeling of Cerebral Oxygen Transport Based on In vivo Microscopic Imaging of Microvascular Network Structure, Blood Flow, and Oxygenation." *Frontiers in Computations Neuroscience* 10 (82): 1-20. https://doi.org/10.3389/fncom.2016.00082.
2. Vaupel, P., F. Kallinowski, and P. Okunieff. 1989. "Blood Flow, Oxygen and Nutrient Supply, and Metabolic Microenvironment of Human Tumors - a Review." *Cancer Research* 49: 6449-6465. https://pubmed.ncbi.nlm.nih.gov/2684393/.
3. Dewhirst, M. W., E. T. Ong, B. Klitzman, T. W. Secomb, R. Z. Vinuya, R. Dodge, D. Brizel, and J. F. Gross. 1992. "Perivascular Oxygen Tensions in a Transplantable Mammary Tumor Growing in a Dorsal Flap Window Chamber." *Radiation Research* 130 (2): 171-182. https://doi.org/10.2307/3578274.
4. Torres Filho, I. P., M. Leung, F. Yuan, M. Intaglietta, and R. K. Jain. 1994. "Noninvasive measurement of microvascular and interstitial oxygen profiles in a human tumor in SCID mice." *Proceedings of the National Academy of Sciences of the United States of America* 91 (6): 2081-2085. https://doi.org/10.1073/pnas.91.6.2081.
5. Stamatelos, S. K., and A., Kim, E., Popel, A. S., Pathak, A. P Bhargava. 2019. "Tumor Ensemble-Based Modeling and Visualization of Emergent Angiogenic Heterogeneity in Breast Cancer." *Scientific reports* 9 (5276): 1-14. https://doi.org/10.1038/s41598-019-40888-w.
6. Stamatelos, S. K., E. Kim, A. P. Pathak, and A. S. Popel. 2014. "A bioimage informatics based reconstruction of breast tumor microvasculature with computational blood flow predictions." *Microvascular research* 91: 8-21. https://doi.org/10.1016/j.mvr.2013.12.003.

7. Ji, J. W., Tsoukias, N. M., Goldman, D. & Popel, A. S. A computational model of oxygen transport in skeletal muscle for sprouting and splitting modes of angiogenesis. *Journal of Theoretical Biology* 241(1), 94–108 (2006). https://doi.org/10.1016/j.jtbi.2005.11.019.

See also

- Length (L)
- Flow rate (Q)
- Hematocrit (Hemat)

Hematocrit (Hemat)

Unit: Percentage

Definition

Hematocrit (Hemat) is the volume of red blood cells (erythrocytes) in a given volume of blood expressed as a percentage.

Figure 29.9. Illustration sketch. Initial sketch for hematocrit illustration.

Systemic hematocrit is usually 40-45% in humans, depending on gender.

The distribution of hematocrit at a vascular bifurcation depends on many factors including the diameter of parent and daughter vessels, their blood flow levels and hematocrit in the parent vessel[1].

Formula

$$\text{logit}(FQ_{E1}) = A + B \cdot \text{logit}(\frac{FQ_{B1} - X_0}{1 - 2 \cdot X_0})$$

$$A = -\frac{6.96 \cdot \ln\left(\frac{D_1}{D_2}\right)}{D_P}$$

$$B = 1 + 6.98 \cdot \left(\frac{1 - H_{DP}}{D_P}\right)$$

$$X_0 = \frac{0.4}{D_P}$$

Logit is the inverse of the sigmoidal logistic function (log(p)-log(1-p)), where 0<p<1. FQ_{E1} and FQ_{B1} are the fractional flows of erythrocytes and blood in daughter branch 1. D_1, D_2, and D_P are the diameters of the daughter branches and parent segment, respectively. H_{DP} is the discharge hematocrit in the parent segment. A, B, and X_0 are empirically measured constants.

Consequently, the hematocrit in daughter branch 1 is calculated according to:

$$H_{D1} = \frac{FQ_{E1} \cdot H_{DP} \cdot Q_P}{Q_1}$$

In a converging bifurcation, downstream hematocrit (H_{DP}) is estimated by downstream flow rate (Q) as well as the hematocrits (H_{D1}, H_{D2}) and flow rates (Q_1, Q_2) in the two parent segments:

$$H_{DP} \cdot Q_P = H_{D1} \cdot Q_1 + H_{D2} \cdot Q_2$$

References

1. Popel, A. S., and P. C. Johnson. 2005. "Microcirculation and Hemorheology." *Annual Review of Fluid Mechanics* 37: 43-69. https://doi.org/10.1146/annurev.fluid.37.042604.133933.
2. Stamatelos, S. K., and A., Kim, E., Popel, A. S., Pathak, A. P Bhargava. 2019. "Tumor Ensemble-Based Modeling and Visualization of Emergent Angiogenic Heterogeneity in Breast Cancer." *Scientific reports* 9 (5276): 1-14. https://doi.org/10.1038/s41598-019-40888-w.
3. Stamatelos, S. K., E. Kim, A. P. Pathak, and A. S. Popel. 2014. "A bioimage informatics based reconstruction of breast tumor microvasculature with computational blood flow predictions." *Microvascular research* 91: 8-21. https://doi.org/10.1016/j.mvr.2013.12.003.

See also

- Vessel diameter (D)
- Blood flow rate (Q)
- Intravascular oxygen tension (PO_2)
- Shear

Fluid shear stress (τ)

Unit: dyne/cm^2

Definition

Shear stress (τ) is the frictional force experienced by adjacent layers of a fluid due to its motion, expressed in dyne/cm^2.

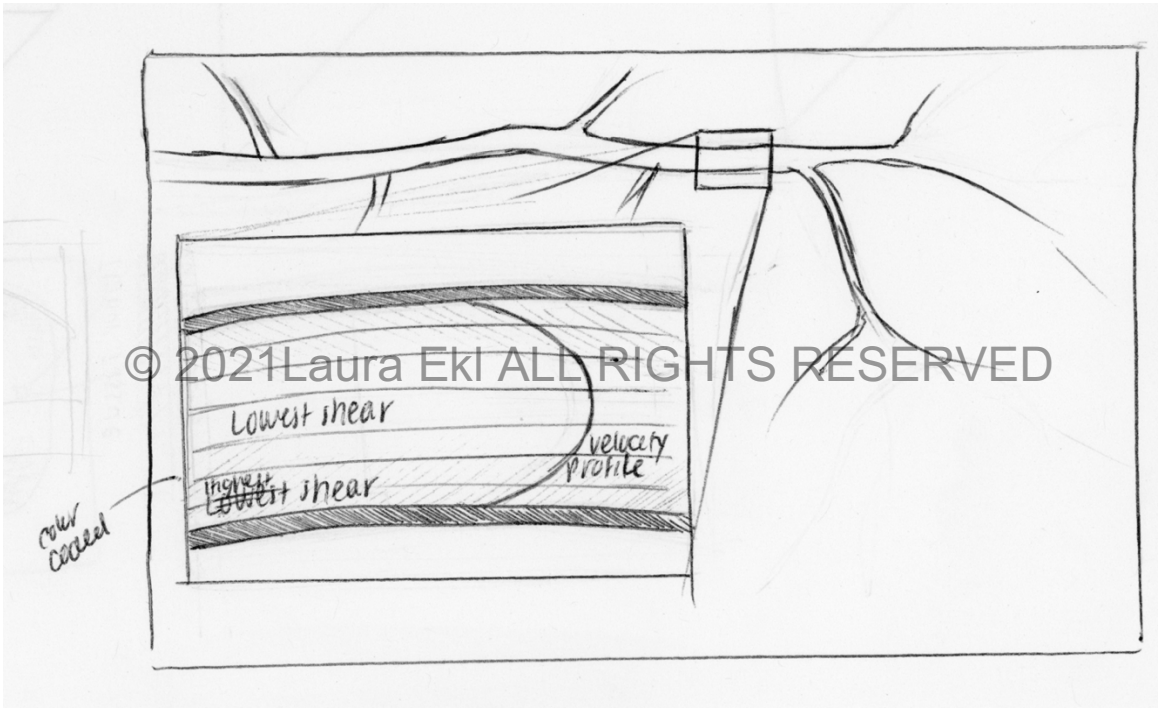

Figure 29.10. Illustration sketch. Initial sketch for fluid shear stress illustration.

Within vessels, shear is greatest at the vessel walls, and lowest at the center of the vessel.

Shear is inversely proportional to the third power (i.e. cube) of the blood vessel diameter, so small changes in blood vessel diameter can drastically affect the shear.

Normal tissue

Shear stress tends to be highest in arterioles and smallest in veins[1].

Arterioles~60-80 dyne/cm^2

Veins~1 dyne/cm^2

Tumor tissue

In cancer, the fluid shear stress plays a crucial role in multiple processes, including proliferation, apoptosis, invasion, and metastasis and vessel remodeling[2-3].

Formula

$$\tau_{ij} = \frac{32 \cdot \mu_{ij} \cdot Q_{ij}}{\pi \cdot {D_{ij}}^3}$$

where τ_{ij} is the wall shear stress, μ_{ij} is the segment apparent viscosity, Q_{ij} is the simulated segment blood flow rate, D_{ij} is the segment diameter[4,6].

References:

1. Ballermann, B. J., A. Dardik, E. Eng, and A. Liu. 1998. "Shear stress and the endothelium." *Kidney International* 54 (67): S-100-S-108. https://doi.org/10.1046/j.1523-1755.1998.06720.x.
2. Jain, R. K., J. D. Martin, and T. Stylianopoulos. 2014. "The role of mechanical forces in tumor growth and therapy." *Annual review of biomedical engineering* 16: 321-346. https://doi.org/10.1146/annurev-bioeng-071813-105259.
3. Huang, Q., X. Hu, W. He, Y. Zhao, S. Hao, Q. Wu, S. Li, S. Zhang, and M. Shi. 2018. "Fluid shear stress and tumor metastasis." *American journal of cancer research* 8 (5): 763-777. https://www.ncbi.nlm.nih.gov/pmc/articles/PMC5992512/.
4. Stamatelos, S. K., E. Kim, A. P. Pathak, and A. S. Popel. 2014. "A bioimage informatics based reconstruction of breast tumor microvasculature with

computational blood flow predictions." *Microvascular research* 91: 8-21. https://doi.org/10.1016/j.mvr.2013.12.003.

5. Kamoun, W. S., S. S. Chae, D. A. Lacorre, J. A. Tyrell, M. Mitre, M. A. Gillissen, D. Fukumura, R. K. Jain, and L. L. Munn. 2010. "Simultaneous measurement of RBC velocity, flux, hematocrit and shear rate in tumor vascular networks." *Nature methods* 7 (8): 655–660. https://doi.org/10.1038/nmeth.1475.
6. Stamatelos, S. K., and A., Kim, E., Popel, A. S., Pathak, A. P Bhargava. 2019. "Tumor Ensemble-Based Modeling and Visualization of Emergent Angiogenic Heterogeneity in Breast Cancer." *Scientific reports* 9 (5276): 1-14. https://doi.org/10.1038/s41598-019-40888-w.

See also

- Diameter (D)
- Flow rate (Q)
- Hematocrit (Hemat)

Vessel Class

Definition

Every blood vessel within an ensemble of tumors can be categorized into a **vessel class** based upon its physical and functional properties[1].

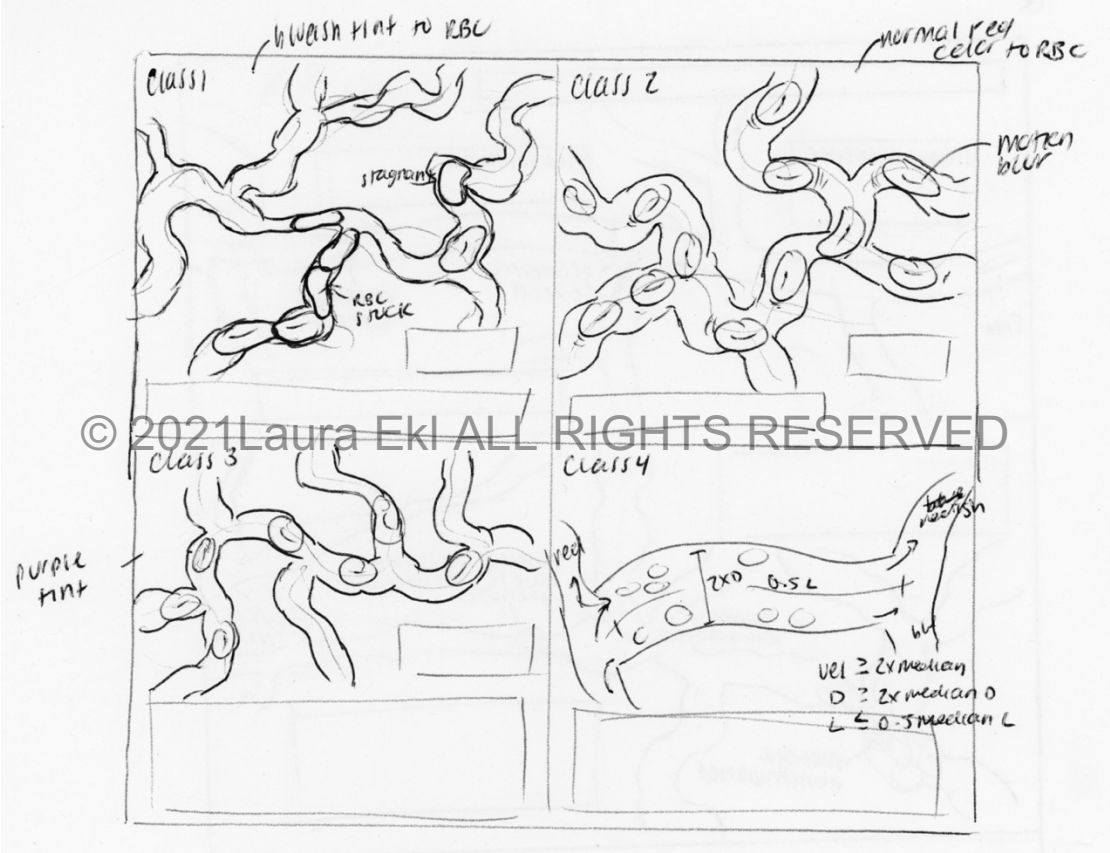

Figure 29.11. Illustration sketch. Initial sketch for vessel class illustration.

Class 1

For the purposes of this study, Class 1 blood vessels were those that were hypoperfused and hypoxic.

Vel < 50 μm/s and PO2 < 10 mmHg

Class 2

Class 2 blood vessels were those that were hyperperfused and normoxic.

Vel ≥ 50 μm/s and PO2 ≥ 10 mmHg

Class 3

Class 3 blood vessels were those that were hypoperfused and normoxic (i.e. low velocity and normal oxygenation), or hyperperfused and hypoxic (i.e. normal velocity but low oxygenation). Class 3 vessels lack the full functionality of Class 2 vessels yet are capable of maintaining blood transport better than Class 1 vessels.

Vel < 50 μm/s and PO2 ≥ 10 mmHg, or norm velocity and PO2 < 10 mmHg

Class 4

Class 4 vessels were those that were considered functional 'shunts'. In tumors, functional shunting occurs as a result of abnormal vascular remodeling and causes blood flow to bypass long pathways leading to regions of impaired microcirculation[2]. Here, these shunts are defined as blood vessels in which the blood velocity is at least two times greater than the median blood flow velocity of the tissue, and the vessel diameter at least twice as great as the median diameter of the tissue, and the vascular length smaller than the median length of the tissue by a factor of 0.5[1].

References

1. Stamatelos, S. K., and A., Kim, E., Popel, A. S., Pathak, A. P Bhargava. 2019. "Tumor Ensemble-Based Modeling and Visualization of Emergent Angiogenic Heterogeneity in Breast Cancer." *Scientific reports* 9 (5276): 1-14. https://doi.org/10.1038/s41598-019-40888-w.
2. Pries, A. R., M. Höpfner, F. le Noble, M. W. Dewhirst, and T. W. Secomb. 2010. "The shunt problem: control of functional shunting in normal and tumour

vasculature." *Nature reviews. Cancer* 10 (8): 587-593. https://doi.org/10.1038/nrc2895.

3. Stamatelos, S. K., E. Kim, A. P. Pathak, and A. S. Popel. 2014. "A bioimage informatics based reconstruction of breast tumor microvasculature with computational blood flow predictions." *Microvascular research* 91: 8-21. https://doi.org/10.1016/j.mvr.2013.12.003.

See also

- Diameter (D)
- Velocity (Vel)
- Intravascular oxygen tension (PO_2)

Vita

Laura Ekl was born in 1994 in the Chicago suburbs. She grew up in Lake Zurich, Illinois, where she was first introduced to the field of medical illustration during high school.

Laura attended Iowa State University (ISU) in Ames, Iowa, and graduated *cum laude* in 2015 with a Bachelor of Arts in Biological and Pre-Medical Illustration (BPMI) and minors in Biology and Mathematics. While studying at ISU, she was involved in several mentorship roles for younger students in the BPMI program.

After graduation from ISU, Laura took a position as the lead content creator at BodyViz, a medical visualization software company based in Clive, Iowa. She spent several years diving into radiological imaging, 3D visualization, and anatomy education while developing an interactive content platform. She had the pleasure of working online and onsite with numerous domestic and international higher education clients.

In August 2019, Laura continued her education in the Medical and Biological Illustration graduate program in the Department of Art as Applied to Medicine at the Johns Hopkins University School of Medicine. During her time at Johns Hopkins, she continued engaging in mentorship opportunities, and she was named a Vesalian Scholar for her thesis work. In the future, she hopes to continue to develop new workflows for novel data visualization. Laura will be receiving her Master of Arts degree in May of 2021.